

**MANUFACTURING OF BULK METALLIC GLASS**

**& GLASS FORMING ABILITY**

**NET SHAPE MANUFACTURING OF BULK  
METALLIC GLASS AND PREDICTION OF  
GLASS FORMING ABILITY**

By

**YUELU LI, B.Eng.**

A Thesis

Submitted to the School of Graduate Studies

in Partial Fulfillment of the Requirements

for the Degree

**Master of Applied Science**

McMaster University

© Copyright by Yuelu Li, January 2007

MASTER OF APPLIED SCIENCE (2007)  
(Mechanical Engineering)

McMaster University  
Hamilton, Ontario

TITLE: Net Shape Manufacturing of Bulk Metallic Glass  
and Prediction of Glass Forming Ability

AUTHOR: Yuelu Li, B.Eng. (Xi'an Jiaotong University)

SUPERVISOR: Dr. Sumanth Shankar

NUMBER OF PAGES: xiv, 121

## Abstract

Bulk Metallic Glass (BMG) possesses a variety of extraordinary properties including ultra high elastic limit and strength and has been applied in diverse fields such as industrial coatings, sporting goods, medical devices, defense and aerospace sectors. The cross-section thickness of a few millimeters for cast BMG alloy components limits their application to manufacturing structural components. However, continuing global efforts are underway to increase the critical part size cast with BMG alloys.

There are two phases to this project. Phase 1 investigates the feasibility of using suitable BMG alloys to manufacture a pivot assembly in an Airborne Gravity Gradiometer (AGG) via net shape manufacturing techniques. Success of Phase 1 will enable a quantum leap in the capabilities of the present day AGG devices to successfully and accurately scope the vast untapped mineral and petroleum resources globally. Requirements of high tolerances in the pivot assembly with very specific material properties and a net shape manufacturing route coupled with the lack of any database for BMG alloys were the inherent challenges. Suitable BMG alloys have been identified for this purpose and continued efforts are underway to manufacture the pivot assembly.

Phase 2 of this project lays the foundation for a much needed tool to predict the Glass forming Ability of BMG alloys. This will enable to scientifically develop novel BMG alloys to suite specific application in lieu of the current ad-hoc development trends. A viable thermal model to understand the relationship between growth rate of solid phase and melt undercooling during uni-directional solidification coupled with a solidification model based on competitive growth principles have been developed. Novel experiment program and setup have been developed to verify these models.

## Acknowledgements

The author wishes to be deeply grateful to her supervisor, Dr. Sumanth Shankar from McMaster University, for his patient and instructive supervision throughout the thesis work.

The author would like to thank Dr. Barry French and Dr. Kieran A. Carroll from GEDEX Corporation, Mississauga, ON, Canada; Mr. Harvey Pellegrini at the Ontario Centre of Excellence (OCE) – CAMM, Mississauga, ON, Canada; Dr. Steve Thorpe and Paul Borges at University of Toronto, Toronto, ON, Canada; Dr. Ping Wen at Institute of Physics, Chinese Academy of Science and Jim Garrett at McMaster University for their instructive discussions and advice.

Very special thanks must be given to Ron Lodewyks, Jim McLaren, Mark MacKenzie, Dave Schick, Joe Verhaeghe, Frank Gibbs, Ed McCaffery, Doug Culley, Rob Lemmon, Connie Barry and John Rodda at McMaster University for their collaboration on experiments, demonstrations of equipment, and general companionship.

The author would like to thank her colleagues at the department of Mechanical Engineering, namely, Hongda Wang, Dr. Xiaochun Zeng, Prakash V. Srirangam, Mohammad Minhajuddin Malik, Ahmed M. T. Omar and Salam Ali for their helpful advice and assistance with this project.

The author wishes to thank her family members and friends for their constant support and encouragement.

The financial support from OCE (CAMM), GEDEX Corporation and McMaster University is greatly appreciated.

# Table of Contents

Contents	Page
<b>Descriptive Note</b> .....	ii
<b>Abstract</b> .....	iii
<b>Acknowledgements</b> .....	iv
<b>Table of Contents</b> .....	v
<b>List of Figures</b> .....	ix
<b>List of Tables</b> .....	xii
<b>List of Symbols</b> .....	xiii
<b>Chapter 1 Introduction</b> .....	1
1.1 Work in Thesis .....	1
1.2 Metallic Glass and Property Characteristics .....	1
1.3 Fundamentals.....	3
1.3.1 Glass transition.....	3
1.3.2 Glass formation.....	4
1.4 Bulk Metallic Glasses and Current Applications.....	4
References.....	6
<b>Chapter 2 Bulk Metallic Glass (BMG) Material Selection and Net Shape Manufacturing for Air Borne Gravity Gradiometer (AGG) Application</b> .....	7
2.1 Background.....	7
2.1.1 Airborne gravity gradiometer utilizing orthogonal quadrupole responder design.....	8
2.1.2 Improving spatial resolution of OQR design.....	10
2.2 Selection of Bulk Metallic Glasses .....	11
2.2.1 Definition of critical properties of pivot in an airborne gravity gradiometer.....	11
2.2.2 Comparison of critical material properties of titanium, niobium and BMGs.....	14

2.2.3 Bulk metallic glass material properties database.....	16
2.2.4 Criteria for selecting BMGs for further study.....	18
2.3 Manufacturing of AGG Pivot with a Suitable BMG.....	23
2.3.1 Pivot geometry of AGG gradiometer.....	23
2.3.2 BMG material for AGG pivot.....	23
2.3.2.1 Vacuum arc melting (VAM).....	24
2.3.2.2 Vacuum sealed quartz tube casting.....	25
2.3.2.3 Melt spinning of $\text{Cu}_{43}\text{Zr}_{43}\text{Al}_7\text{Ag}_7$ .....	26
2.3.2.4 X-ray diffraction results of as melt spun and ground ribbons...	26
2.3.2.5 Differential Scanning Calorimetry (DSC) results of $\text{Cu}_{43}\text{Zr}_{43}\text{Al}_7\text{Ag}_7$ .....	28
2.3.3 Net shape manufacturing of AGG pivot with BMG.....	30
2.3.3.1 Casting.....	30
2.3.3.2 Superplastic forming (SPF).....	31
2.3.4 Casting of AGG pivot sample .....	33
2.3.4.1 Selection of mold and coating materials for casting.....	33
2.3.4.2 Mold design and machining .....	37
2.3.4.3 Casting of Vit1 alloy.....	41
2.3.4.3.1 Inert sealing process.....	41
2.3.4.3.2 Casting of the AGG pivot.....	43
2.3.4.4 Summary.....	44
2.3.5 Superplastic forming (Hot pressing) of BMG.....	45
2.3.5.1 Hot pressing of $\text{Cu}_{43}\text{Zr}_{43}\text{Al}_7\text{Ag}_7$ amorphous ribbons.....	45
2.3.5.1.1 Hot pressing conditions.....	45
2.3.5.1.2 Selection of mold materials for hot pressing.....	47
2.3.5.1.3 Hot pressing of $\text{Cu}_{43}\text{Zr}_{43}\text{Al}_7\text{Ag}_7$ amorphous ribbons.....	49
2.3.5.2 SPF of Vit1 and Vit4.....	50
2.3.5.3 Summary.....	51
References.....	52
<b>Chapter 3 Theoretical Model for Predicting Glass Forming Ability of Metallic Glasses</b>	<b>54</b>

3.1 Glass Forming Ability (GFA).....	54
3.1.1 Summary of popular parameters used to indicate the GFA of a BMG.....	55
3.1.2 Review of prior art - Identifying the best GFA alloys by competitive growth principle approach.....	56
3.2 Objective of the Present Model.....	57
3.3 Development of Theoretical Model to Predict GFA.....	57
3.3.1 Competitive growth principle.....	57
3.3.1.1 Concepts.....	57
3.3.1.2 Applications.....	58
3.3.2 Strategy of developing the model.....	60
3.3.3 Developing tip temperature $T_g$ -growth rate $V_g$ relationship for solidified amorphous structure .....	64
3.3.4 Developing undercooling-growth rate relationship of crystalline phases ( single phase & eutectic, equations).....	65
3.3.4.1 Quasi-steady state directional solidification of primary phases $\alpha$ and $\beta$ .....	65
3.3.4.2 Unsteady-state directional solidification of primary phases $\alpha$ and $\beta$ .....	67
3.3.4.3 Quasi-steady state directional solidification of lamellar eutectic phase.....	67
3.3.4.4 Unsteady state directional solidification of lamellar eutectic phase.....	68
3.3.5 Apply competitive growth principle and find the instant critical cooling rate and critical size .....	69
3.5 Summary.....	69
References .....	71
<b>Chapter 4 Critical Heat Flux and Instant Critical Cooling Rate of Bulk Metallic Glass under Uni-Directional Heat Conduction Conditions</b>	<b>72</b>
4.1 Introduction.....	72
4.2 Experiment Setup.....	72

4.2.1 Crucible and thermocouples.....	73
4.2.2 Aluminum cooling block.....	75
4.3 Exploratory Experiments on Al-7.45 wt%Si Alloy.....	77
4.3.1 Equipments and experiment procedure.....	77
4.3.2 Results and discussion.....	79
4.4 Summary .....	82
<b>Chapter 5 Summary and Future Work</b>	<b>83</b>
<b>Appendices</b> .....	<b>86</b>
Appendix A: Bulk Metallic Glass Properties Database.....	86
Appendix B: Bulk Metallic Glass Systems Literature Review Based on Castability.....	111

# List of Figures

Figure 1.1 Strength vs elastic limit plot for various conventional materials.....	3
Figure 2.1 Airborne Gravity Gradiometer (AGG) based on Orthogonal Quadrupole Responder (OQR) design.....	8
Figure 2.2 Comparison of various AGG capabilities. (a) Simulation with zero detection noise, (b) Present industry standard and (c) GEDEX's OQR design.....	9
Figure 2.3 Principle of a superconducting accelerometer.....	10
Figure 2.4 Elastic limit plotted against Young's modulus for various BMGs.....	15
Figure 2.5 Resilience plotted against loss coefficient for various BMGs.....	16
Figure 2.6 Selection criteria, identification and testing of suitable BMG materials for AGG pivot application.....	22
Figure 2.7 Drawing of AGG gradiometer pivot.....	23
Figure 2.8 Ingot of $\text{Cu}_{43}\text{Zr}_{43}\text{Al}_7\text{Ag}_7$ alloy.....	24
Figure 2.9 Quenched $\text{Cu}_{43}\text{Zr}_{43}\text{Al}_7\text{Ag}_7$ alloy with quartz on its surface.....	25
Figure 2.10 Optical microscopy (OM) of $\text{Cu}_{43}\text{Zr}_{43}\text{Al}_7\text{Ag}_7$ alloy. (a) Center, (b) Edge.....	25
Figure 2.11 Melt spun ribbon of $\text{Cu}_{43}\text{Zr}_{43}\text{Al}_7\text{Ag}_7$ .....	26
Figure 2.12 X-ray diffraction pattern of the melt-spun $\text{Cu}_{43}\text{Zr}_{43}\text{Al}_7\text{Ag}_7$ alloy ribbons.....	27
Figure 2.13 X-ray diffraction pattern of melt-spun $\text{Cu}_{43}\text{Zr}_{43}\text{Al}_7\text{Ag}_7$ alloy ribbons which were subsequently ground mechanically for size reduction to less than 0.105mm.....	27
Figure 2.14 Typical DSC curves of $\text{Cu}_{43}\text{Zr}_{43}\text{Al}_7\text{Ag}_7$ melt spun ribbons obtained at different heating rates to show the glass transition and crystallization behavior. (a) to (e) shows the heating rates of 1, 5, 10 20, 50 and 100 K/min, respectively.....	29
Figure 2.15 Schematic of injection casting technique.....	31
Figure 2.16 A schematic TTT diagram showing the processing methods. (1) Die casting and (2) Superplastic casting.....	33

Figure 2.17 Compression stress (indicated by arrows) applied on cast piece if coefficient of mold material is less than that of mold material .....	34
Figure 2.18 Candidate mold material for die casting BMG. From left to right: BN mold, ceramic 902(fired), white silk aerosol BN coated ceramic 902, grey BN lubricoat coated stainless steel and white silk aerosol BN coated stainless steel.....	36
Figure 2.19 Experimental mold materials stacked inside the Zr-gettered He rich quartz tube. The coating used was a combination of white silk BN and grey BN lubricoat. Top to bottom: BN, Cotronics 902, white silk aerosol BN coated Cotronics 902, aerosol (white) BN coated stainless steel 304, grey BN lubricoat coated stainless steel 304 .....	37
Figure 2.20 Exploded view of assembled mold used for die casting BMG.....	38
Figure 2.21 Components of the mold shown in Figure 2.20.....	39
Figure 2.22 Stainless steel components of the mold shown in Figure 2.20.....	40
Figure 2.23 Assembled stainless steel mold for die casting BMG.....	40
Figure 2.24 Schematic top view of mold within quartz tube.....	41
Figure 2.25 Assembled mold with Vit1 solid pieces inside sealed quartz tube.....	42
Figure 2.26 Quartz tube containing the metal mold is held inside an electric furnace.....	43
Figure 2.27 As-quenched mold with Vit1 part in it. (a) Top view and (b) bottom view.....	44
Figure 2.28 DSC curves for $\text{Cu}_{43}\text{Zr}_{43}\text{Al}_7\text{Ag}_7$ alloy heated at constant heating rate of 10K/min and maintained at different isothermal temperatures: (a) 738K, (b) 750K and (c) 756K.....	47
Figure 2.29 Hot pressing molds. Left: stainless steel and right: fired ceramic 902).....	48
Figure 2.30 $\text{Cu}_{43}\text{Zr}_{43}\text{Al}_7\text{Ag}_7$ alloy ribbons after hot pressing operation.....	50
Figure 3.1 Two type of coupled zone in a binary eutectic reaction: (a) Skewed zone (b) Symmetric zone.....	59

Figure 3.2 Coupled zone (V-C diagram) and growth rate relationship of various competing phases.....	60
Figure 3.3 Process flow for predicting GFA of BMG.....	62
Figure 3.4 Uni-directional heat conduction.....	63
Figure 3.5 Uni-directional heat conduction from liquid bottom. (a) Solid is glassy phase; (b) Solid is crystalline phase.....	64
Figure 4.1 Schematic of instant critical cooling rate setup under 1-D heat condition.....	73
Figure 4.2 Thermocouple positions within mold cavity.....	75
Figure 4.3 Drawing of aluminum cooling block consisting of two parts: (a) block with cavity for cooling water flow and (b) top plate to seal the cooling channel.....	76
Figure 4.4 Ceramic mold with thermocouples and coil.....	77
Figure 4.5 Aluminum cooling block used for uni-directional heat extraction.....	77
Figure 4.6 Assembled equipments for uni-directional solidification.....	78
Figure 4.7 Mold dimension and thermocouple positions within mold cavity.....	79
Figure 4.8 Temperature-time curves at different thermocouple positions during solidification process.....	81
Figure 4.9 Temperature gradient curves during solidification process.....	81

## List of Tables

Table 2.1 Critical material properties of pivot used in the AGG.....	12
Table 2.2 Comparison of material properties of Niobium, Titanium and BMGs....	14
Table 2.3 Bulk metallic glass systems in database.....	17
Table 2.4 Criteria for BMGs used for the AGG pivot application.....	18
Table 2.5 Bulk metallic glasses satisfying initial criteria for AGG application.....	19
Table 2.6 LCTE of Niobium, Ti and a few potential BMG alloys for the AGG application.....	20
Table 2.7 Properties of trial materials: $\text{Cu}_{43}\text{Zr}_{43}\text{Al}_7\text{Ag}_7$ and Vitreloy 1(Vit1).....	21
Table 2.8 Chemical composition of $\text{Cu}_{43}\text{Zr}_{43}\text{Al}_7\text{Ag}_7$ alloy tested by ICP.....	24
Table 2.9 Average transformation temperatures in DSC experiments as a function of heating rate for $\text{Cu}_{43}\text{Zr}_{43}\text{Al}_7\text{Ag}_7$ . melt spun ribbons.....	29
Table 2.10 Continuous service temperature and coefficient of thermal expansion at room temperature of candidate mold materials for die casting application.....	35
Table 2.11 Dimensions of molds and plungers for hot pressing.....	48

## List of Symbols

- C Concentration, wt%, at%
- $C_E$  Eutectic composition
- $C_I$  Composition at the tip or interface
- $C_p$  Heat capacity
- $C_x^I$  Concentration of crystalline phases,  $x = \alpha, \beta$  and eutectic phase
- $\bar{C}$  Composition averaged across the interface
- $C_S^*$  Solid and compositions at the interface
- $C_L^*$  Liquid compositions at the interface
- $C_0$  Liquid concentration at infinity
- $C_\infty$  Alloy composition
- D Diffusion coefficient
- G Temperature gradient
- h Heat transfer coefficient
- k Equilibrium partition ratio
- $K_e$   $4m^2 a^L Q^L$ , constant
- m Liquidus slope
- R Radius of curvature
- $q_y$  Heat flux in y axis direction
- t Time
- T Temperature
- $T_D$  Dendrite tip temperature
- $T_g$  Glass transition temperature
- $T_{eut}^I$  Eutectic tip temperature
- $T_l$  Liquidus temperature
- $T_{rg}$  Reduced glass transition temperature

- $T_w$  Substrate temperature
- $T_x$  Crystallization onset temperature
- $T_x^I$  Tip temperature of crystalline phases,  $x = \alpha, \beta$  and eutectic phase
- $\Delta T$  Undercooling
- $\Delta T_D$  undercooling due to the local concentration in the liquid at Liquid/solid
- $\Delta T_E$  Eutectic undercooling
- $\Delta T_K$  Kinetic undercooling
- $\Delta T_x$  Supercooled liquid region
- $\Delta T_\sigma$  undercooling due to the Gibbs-Thompson effect acting at curved interfaces
- $V$  Growth rate
- $V_c$  Growth rate of crystalline phase
- $V_g$  Growth rate of glassy phase
- $V_x^I$   $V_\alpha^I, V_\beta^I, V_{eut}^I$  (tip growth rate of  $\alpha, \beta$  and eutectic phase, respectively)
- $\alpha$  Thermal diffusivity Redrawn cup depth or punch displacement
- $\kappa$  Thermal conductivity
- $\rho$  Density
- $\tau$  Time in coordinates moving with the dendrite tip
- $\theta$  Gibbs-Thompson coefficient

## **Chapter 1 Introduction**

### **1.1 Work in Thesis**

There are five chapters in this thesis document.

*Chapter 1.* Introduction to Metallic Glasses and their unique properties.

*Chapter 2.* Work carried out for Gedex Corporation, Ontario, Canada on Bulk Metallic Glass (BMG) material selection and net shape manufacturing for Air Borne Gravity Gradiometer (AGG) application.

*Chapter 3.* Development of theoretical model to predict the Glass Forming Ability (GFA) of BMG.

*Chapter 4.* Setup of experiments to quantify relationship between heat flux, cooling rate and GFA of BMG in uni-directional solidification.

*Chapter 5.* Summary of work in this project.

### **1.2 Metallic Glass and Property Characteristics**

Metallic glasses or amorphous metals are primarily composed of metallic elements. Some amount of metalloid elements may also be included though it may lead to brittleness and not a complete metallic glass system [1]. The primary distinguishing feature of metallic glasses is that they lack the long atomic periodicity predominantly observed in the more common crystalline materials. The lack of crystallinity results in

superior mechanical and performance properties such as high tensile strength and high elastic strain, unique performance properties in electrical, magnetic and corrosion aspects. Moreover, the amorphous nature of the material results in negligible shrinkage during solidification thus eliminating defects arising from the same. In addition, the surface finish and the dimensional consistency (manufactured tolerance limits) are superior to crystalline materials.

Theoretically, all metallic materials can form metallic glass when subjected to a high cooling rate during transformation from a gas or liquid state by preventing crystallization [2]. During solidification, from the liquid state, metallic glasses maintain liquid state well past the crystalline solidification temperature as predicted by conventional phase diagrams and reaches a temperature (high under-cooling) called the glass transition temperature,  $T_g$ , wherein, the liquid transforms to a solid structure with a short range periodicity (nanometer scale) and hence, have no discernable grain boundaries (crystallinity). In conventional polycrystalline materials, grain boundaries are where defects initiate from fracture and corrosion and subsequently results in the failure of the component. The lack of discernable grain boundaries in metallic glasses results in superior mechanical and performance properties such as strength, hardness, toughness, elasticity, corrosion and wear resistance. Figure 1.1 [3] shows as graph wherein many popular conventional materials are plotted with respect to their strength and elastic limits. It can be seen that metallic glass systems can possess a high strength of the magnitude of 2 GPa while maintaining their elastic limit at about 2 %, which is unattainable in any other conventional material.

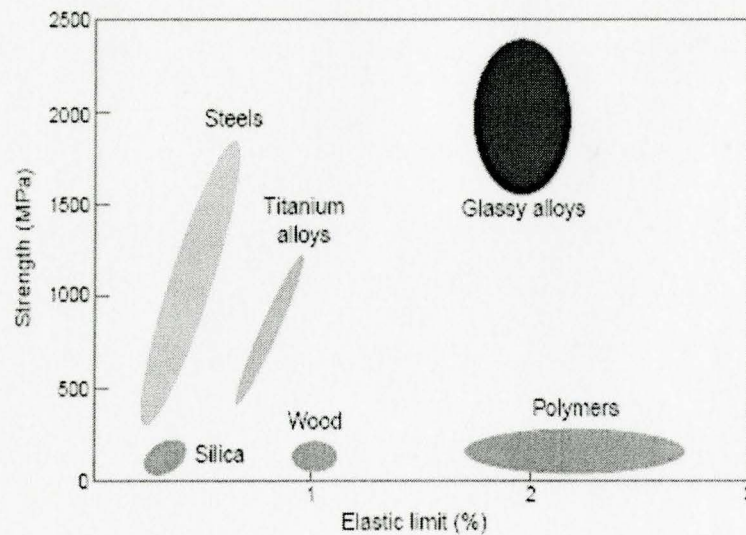


Figure 1.1 Strength vs elastic limit plot for various conventional materials.

### 1.3 Fundamentals

#### 1.3.1 Glass transition

When a material is quenched from gas or liquid state (phases) at a high cooling rate, the crystallization process may be bypassed and an amorphous solid forms by undergoing glass transition at a temperature called the glass transition temperature,  $T_g$ . At temperature range between liquidus temperature  $T_L$  and  $T_g$ , the material behaves like a supercooled liquid with a structure akin to a liquid. At  $T_g$ , extensive properties such as entropy ( $S$ ), enthalpy ( $H$ ) and volume show an abrupt change in their rate of decrease and their rate of decrease above and below the  $T_g$  is different from each other. This variation in properties is utilized in identifying  $T_g$ . Concomitance with this glass transition is an abrupt change in the intensive variables such as heat capacity, coefficient of thermal expansion and compressibility, which suggests that glass transition might be a second-order phase transition. It is found that the temperature,  $T_g$  of a particular material is dependant on its thermal history during solidification. A higher cooling rate will result in a lower value of  $T_g$ . The reason is that the structural relaxation of the glass is a kinetic process and hence, at higher cooling rates, liquid configuration can be retained to a lower temperature before glass transition occurs. Viscosity of the liquid and supercooled liquid

continuously increases as the material is cooled to lower temperatures. Another frequently used identification marker for  $T_g$ , is that  $T_g$  is the temperature at which the liquid attains a viscosity of  $10^{12}$  Pa s which is characteristic of solids. No firm rules for predicting  $T_g$  and no ready prescriptions with which to calculate  $T_g$  for a given glassy material is available in the literature.

### **1.3.2 Glass formation**

Liquid and solid are in equilibrium at melting temperature,  $T_m$ . At temperatures below  $T_m$ , the liquid either transforms to a crystalline solid or suppressed into a state of supercooled (undercooled) liquid. This process depends on the crystallization kinetics of the liquid. If crystallization is prevented, liquid becomes more viscous with decreasing temperature and ultimately form a glass when temperature reaches  $T_g$ , which is achieved by rapid extraction of heat. Thermodynamically, undercooled liquid is at a metastable state since at any temperature below  $T_m$ , the free energy of the solid is less than that of the liquid. Therefore, transition from liquid to solid is a spontaneous process and the rate of transformation can be instantaneous or very slow resulting in a long transformation time. In liquids with a slow transformation kinetics, a rapid extraction of heat from the solidifying system will undercool the melt and result in a morphologically refined solidified structure. In extreme cases, if the rate of transformation is slow enough and the heat extraction fast enough such that the solidified structure forms grain boundaries in the scale of a few angstroms or nanometers, the crystallinity of the resultant solid will not be discernable by any conventional instrumentation. Such solid are termed amorphous materials or metallic glasses. Hence, an investigation of the glass formation ability (GFA) of a particular metallic glass system will be akin to evaluating the kinetics of crystallization, especially in the early stages of crystal nucleation and growth.

### **1.4 Bulk Metallic Glasses and Current Applications**

In earlier years, fabrication techniques such as thermal evaporation, sputtering, glow-discharge decomposition, chemical vapor deposition, melt quenching, chill block

casting and free jet spinning had been used to manufacture metallic glasses with the part thickness usually in the range of a few micrometers. The size limitation precluded a wide spread application of such materials, especially as structural materials. However, in recent years, metallic alloy systems have been identified wherein; the rate of crystallization is so slow that cooling rates of the order of a few tens or hundreds of Kelvin per minute result in an amorphous solid. These systems are termed Bulk Metallic Glass (BMG) due to their ability to form amorphous solids with dimensions ranging in the tens of millimeter scale. In general, alloy systems forming BMG solids have deep eutectic regions in their phase diagrams and the elemental compositions lie around these deep eutectic regions. Typically, amorphous solids obtained by solidifying with cooling rates less than 500 K/min are termed BMG. These low cooling rates makes BMG systems applicable in manufacturing bulk components with a near net shape process while retaining the unique properties of amorphous materials. Appendix A and B of this report presents a comprehensive list of the current BMG systems available globally along with their mechanical and casting properties, respectively.

The first BMG developed was a ternary Pd–Cu–Si alloy prepared by Chen in 1974 [4]. Later, Pd–Ni–P alloys with thickness of up to 10mm were developed by David Turnbull et al in the early 1980s[5,6]. Since then, innumerable alloy systems such as Zr-based [7] (Zr–Cu–Ni, Zr–Cu–Ni–Al), Mg-based [8] (Mg–Y–Cu, Mg–Y–Ni), La-based [9] (La–Al–Ni and La–Al–Cu), Au-based[ 10], Cu-based[ 11, 12, 13, 14] etc., have been developed by different near net shape fabrication techniques. Among them, Vit1 ( $Zr_{41.2}Ti_{13.8}Cu_{12.5}Ni_{10}Be_{22.5}$ ) [15,16] has the largest critical size exceeding 10 cm. Some of these materials have been successfully applied in various commercial applications such as die materials (PdCuNiP), sporting equipment (ZrTiCuNiBe and ZrTiNiCu) and electrode materials (PdCuSiP). Further development of BMG systems will witness extensive applications in the medical, defense, automotive and aerospace sectors.

## References

- [1] A.L. Greer, *Nature* **366**, 303 (1993).
- [2] D. Turnbull, *Contemp. Phys.* **10**, 437 (1969).
- [3] M. Telford, *Materials Today*, 36, March (2004).
- [4] H.S. Chen, *Acta Metall.* **22**, 1505 (1974).
- [5] A.L. Drehman, A.L. Greer, D. Turnbull, *Appl. Phys. Lett.* **41**, 716 (1982).
- [6] W.H. Kui, A.L. Greer, D. Turnbull, *Appl. Phys. Lett.* **45**, 615 (1984).
- [7] A. Inoue, T. Zhang, T. Masumoto, *Mater. Trans. JIM* **34**, 1234 (1993).
- [8] A. Inoue, *Mater. Trans. JIM* **36**, 866 (1995).
- [9] A. Inoue, T. Zhang, T. Masumoto, *Mater. Trans. JIM* **30**, 965 (1989).
- [10] Jan Schroers, *Appl. Phys. Lett.* **87**, 061912 (2005).
- [11] X. H. Lin and W. L. Johnson, *J. Appl. Phys.* **78** (11), 6514 (1995).
- [12] D. Wang and Y. Li, *Appl. Phys. Lett.* **84**, 4029 (2004).
- [13] Qingping Cao, Jinfi Li and Yaohe Zhou, *Appl. Phys. Lett.* **86**, 081913 (2005).
- [14] Gang Duan, Donghua Xu, and William L. Johnson, *Metall. Mater. Trans. A*, **36A**, 455 (2005).
- [15] A. Peker, W.L. Johnson, *Appl. Phys. Lett.* **63**, 2342 (1993).
- [16] Wei-Hua Wang, Hai Yang Bai, *J. Appl. Phys.* **84** (11), 5961 (1998).

## **Chapter 2 Bulk Metallic Glass (BMG) Material Selection and Net Shape Manufacturing for Air Borne Gravity Gradiometer (AGG) Application**

In this chapter, the following topics will be discussed in detail:

- Background on Airborne Gravity Gradiometer (AGG).
- Selection criteria of BMG for AGG application.
- Manufacturing of BMG alloy sample and Net shape manufacturing of the AGG pivot sample.

### **2.1 Background**

GEDEX Corporation is currently developing a superior AGG for use in the mineral and petroleum exploration industry. This device is to be used to map out the anomalies in the earth's gravitational field that can be related to the anomalies in the subsurface density arising from a variation in localized geological formations. For example, a 3D map of the subsurface density could be used to indicate the location of kimberlite pipes and hydrocarbon deposits. An AGG working as a sensor with a high-resolution gravity gradient (tensor) to a level up to  $1 \text{ Eotvos/Hz}^{1/2}$  would provide the necessary spatial resolution to resolve such features. An AGG is significantly more cost effective compared to time consuming land based devices that are commonly used to measure subsurface density.

### 2.1.1 Airborne gravity gradiometer utilizing orthogonal quadrupole responder design

One possible design of the airborne gravity gradiometer is known as the Orthogonal Quadrupole Responder (OQR) as shown in Figure. 2.1 [1]. The simplistic principle of this device involves the rotation of two beams, each incorporating a pivot, about a common axis. The two orthogonal beams rotate either in the same directions due to rotations of the housing caused by aircraft motion or in opposite directions due to the gravity gradient produced by the mass anomaly. As the differential rotation is caused by properties of the gravity gradient tensor, the sensor can then distinguish between base rotations and gravity gradients. To eliminate the rotational response of the beams, the center of rotation about the supporting pivots should be right at the center of mass of the beams. Thus the OQR is inherently insensitive to both rotational and linear accelerations of the support [2]. An integral part of this system is the GeoMIM - an isolation platform that will provide the sensor with an ultra-quiet platform in an aircraft environment, even in moderate turbulence.

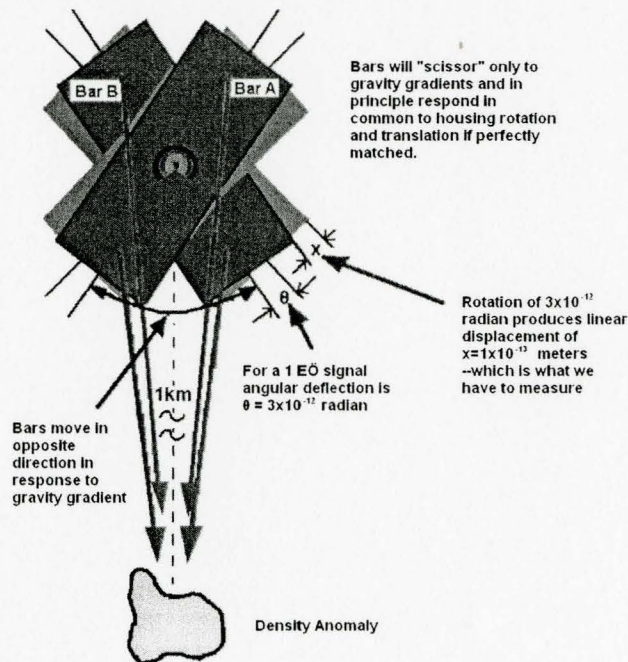


Figure 2.1 Airborne Gravity Gradiometer (AGG) based on Orthogonal Quadrupole Responder (OQR) Design.

The advantage of the OQR design compared to other AGGs in the industry is best illustrated in Figure 2.2 [3]. Figure 2.2(a) shows a simulation of the detection of a kimberlite pipe, shown in the top right corner, if there was zero measurement noise. The current industry detection capability is shown in Figure 2.2(b). GEDEX's OQR design, which has the potential of achieving  $1 \text{ Eotvos/Hz}^{1/2}$  resolution, can more clearly define the location of the kimberlite pipe compared to the industry standard as shown in Figure 2.2(c).

Currently, the beams and pivots in the OQR are made of niobium, which becomes a superconductor at cryogenic temperatures below 4K and exhibits perfect diamagnetic properties. Figure 2.3 [4] shows a superconducting accelerometer in its simplest form. The displacement of the proof mass relative to the sensing coil is caused by the accelerated movement of the platform and leads to induction modulation in the circuit part. Thus, a time-varying current is generated and the Superconducting quantum interference device (SQUID) converts the induced current into an output voltage signal.

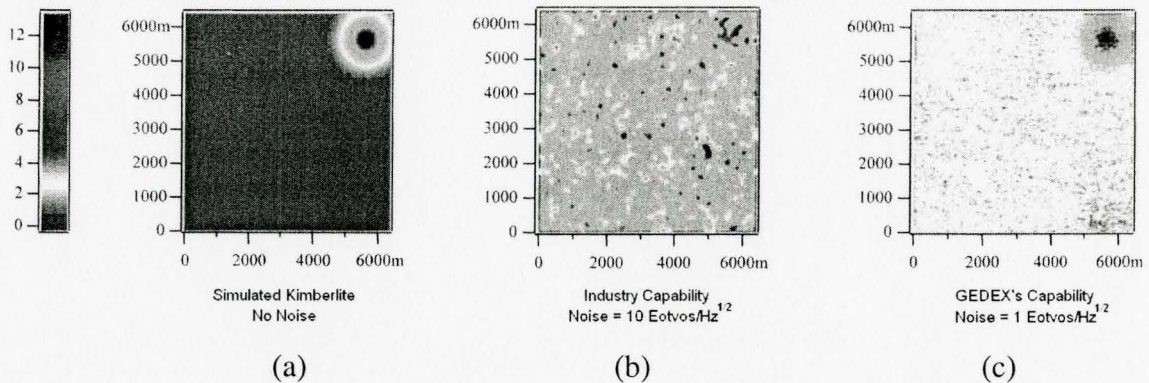


Figure 2.2 Comparison of various AGG capabilities. (a) Simulation with zero detection noise, (b) Present industry standard and (c) GEDEX's OQR design.

The advantage of the newly proposed AGG in this project is its ability to effectively function at ambient temperature. This achievement will provide economic advantages and simpler operating procedures by eliminating the use of the sophisticated cryogenic chamber containing liquid helium. However, challenges lie in designing and

manufacturing materials for the pivot to meet the ambient temperature operating requirements and in providing the necessary resolution in linear transduction.

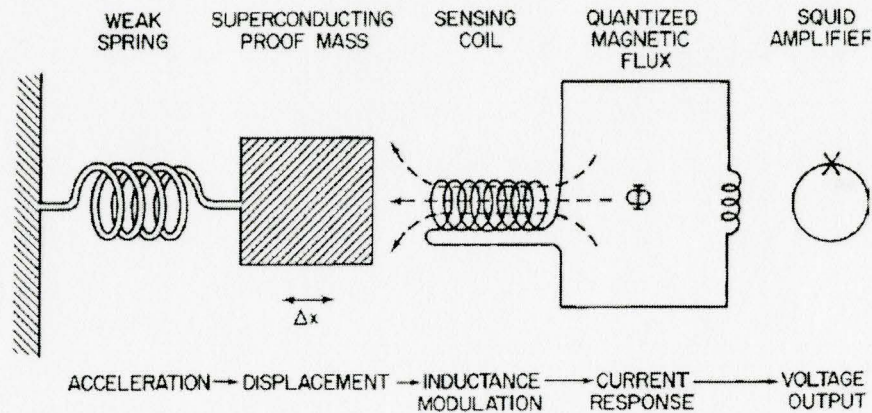


Figure 2.3 Principle of a superconducting accelerometer.

### 2.1.2 Improving spatial resolution of OQR design

The design of the OQR has been successfully prototyped, but changes are required to achieve the target spatial resolution of 1 Eotvos/Hz<sup>1/2</sup> during surveying. The maximum achievable spatial resolution depends on the signal to noise ratio of the recorded data. The signal to noise(S/N) ratio takes the following form [5]:

$$\frac{\theta_{sig}}{\theta_{RMS, \omega_{BW}}} = \frac{G_{xy}}{2} \sqrt{\frac{QI}{k_B T \omega_{BW} \varpi_n}}$$

Where,  $\theta_{sig}$  is the rotational displacement arising from the local gravity gradient  $G_{xy}$ ,  $Q$  is quality-factor,  $k_B$  is Boltzman's constant, and  $T$  is the temperature of the dipole. Here  $T$  is the ambient temperature.  $I$  is second moment of inertia about its sensitive axis, which is restrained by a rotational stiffness of  $k_r$ . Once the value of  $\omega_n$  is chosen, the S/N ratio can only vary with the second moment of inertia,  $I$  of the dipole and increasing  $I$  will increase the S/N ratio.

The noise value is governed by how effectively the aircraft accelerations are isolated from the gravity gradiometer, and by how well it is compensated during data processing. Noise also increases as hysteresis in the material increases. Hysteresis is related to loss coefficient which is a property of the material. The signal value is

dependent on how much the pivot can deflect elastically while still having a high Young's modulus value. Up to this point, the pivot materials used have been either titanium or niobium metal. Selecting a pivot material that has a higher maximum elastic deflection value than and a Young's modulus that is close to niobium and titanium would increase the signal/noise ratio and consequently improve the spatial resolution of the OQR. As discussed in chapter 1, bulk metallic glass is a promising pivot material because of high elastic limit and strength. In the following sections, selection of suitable bulk metallic glasses will be discussed in detail.

## **2.2 Selection of Bulk Metallic Glasses**

### **2.2.1 Definition of critical properties of pivot in an airborne gravity gradiometer**

Table 2.1 contains a list of the critical properties for the design of a pivot, the property values desired and a relative importance scale for each property. The Young's modulus corresponds to the stiffness of a material. The stiffness must be high in order for the pivot and beam system to have a low natural frequency and to maintain geometric stability of the pivot while the AGG is in operation. A low natural frequency is desired because the signal to noise ratio of the measurements increases as the natural frequency of the pivot and beam in the sensing mode decreases.

The elastic limit and the ultimate tensile strength (UTS) must be high because the pivot undergoes high stresses and strains due to its small size (thickness of  $130\mu\text{m}$ ). The maximum elastic deflection may be the most important property. The higher it is, the higher the allowable deflection of the pivot without mechanical hysteresis, the better the signal to noise ratio of the gravity field measurements.

The loss coefficient, or internal friction, relates to the hysteresis characteristics of a material. When the gradiometer is in operation, the pivot must return as close as possible to the starting point, i.e. origin, when a gravity field is not being detected. This is necessary in order to maintain a high signal to noise ratio in the measurements and to prevent drift of the gradiometer. Hysteresis effects in a material make it impossible for a material to return to its exact starting point when a load is applied and then removed. The

lower the loss coefficient, the lower the hysteresis in a material, and the closer the pivot returns to the origin when no gravity field is being detected.

Table 2.1 Critical material properties of pivot used in the AGG

<b>Material Property</b>	<b>Value of Property</b>	<b>Importance (0 – 10 Scale)</b>
Maximum Elastic Deflection (%)	> 1.2	10
Near Net Shape Manufacturability	Castability, bonding, EDM and ion beam milling, niobium plating. Essential that we develop a solution.	10
Magnetic Susceptibility	Low	9
Yield Strength (MPa)	> 1150	8
UTS (MPa)	> 1175	8
Young's Modulus (GPa)	> 125	7
Loss Coefficient / Internal Friction ( $Q^{-1}$ )	< 9.0E-09	7
Creep	Low	7
Fatigue Limit (MPa)	>75	5
Linear Coefficient of Thermal Expansion (m/m/°C)	~ 2.0E-07	3
Electrical Conductivity	High	-

The linear coefficient of thermal expansion (LCTE) value of the pivot should be as similar as possible to the niobium value. This is necessary because the beam that is attached to the pivot is made out of niobium. If the values do not match closely, high thermal stresses and strains can be introduced in the pivot when the OQR is cooled to

cryogenic temperatures necessary for displacement measurements using the SQUID transducers. High thermal stresses and strains can introduce significant measurement errors.

For most applications, creep of high melting point metals is not a factor when the temperature of operation is room temperature or below. In the case of the AGG, extremely precise measurements in the nanometer range are required and creep cannot be ignored. Creep of the pivot can introduce drift measurement errors. Although drift can be zeroed periodically, it is desirable for the creep to be as small as possible in order to maximize the amount of time the gradiometer can be used prior to recalibration. The fatigue limit should be as high as possible so that the pivot can operate for as long a time as possible without fracturing and needing replacement.

The magnetic susceptibility of the pivot is a very important factor for the successful operation of the gradiometer. If the pivot is magnetic, this can cause interference with the gravity field measurements and may cause errors. For this reason, the pivot material must be non-magnetic, which corresponds to it having a low magnetic susceptibility value. In order for the SQUID transducers in the gradiometer to operate properly, electric current must easily travel through the beam and pivot. This requires that the pivot material have a high enough electrical conductivity value.

It is also of critical importance to evaluate the manufacturability of the material being considered for the pivot. The material must be cast to a specific size and shape, may require additional processing such as EDM and ion beam milling to obtain final dimensional tolerances, and may also need to be bonded to a niobium part. It must be possible to do any/all of these processes without degrading the core pivot material properties.

Materials that show favorable values for these critical material properties, and can be manufactured without property degradation, may be good candidates to be used as a pivot in the AGG.

### 2.2.2 Comparison of critical material properties of titanium, niobium and BMGs

Bulk metallic glasses rate very favorably with regards to many of the material properties that are needed for the pivot in an airborne gravity gradiometer. Table 2.2 compares the values for some of these material properties for niobium, titanium and bulk metallic glass. Titanium was also added to the list in Table 2.2 because a few AGG devices currently in application use Ti instead of Nb. The BMG property values shown in Table 2.2 where obtained from literature.

Table 2.2 Comparison of material properties of Niobium, Titanium and BMGs

Material Property	Ti at 77 K	Nb at 20 K	BMGs at RT
Young's Modulus (GPa)	115	125	146
Yield strength (MPa)	637	1150	2420
UTS (MPa)	810	1175	2500
Maximum Elastic Deflection (%)	0.55	1.2	2.0
Loss Coefficient / Internal Friction ( $Q^{-1}$ )	1E-06	9E-09	2E-04
Linear Coefficient of Thermal Expansion (m/m/°C)	3.2E-06	2.0E-07	8.0E-06
Fatigue Limit (MPa)	54 at RT	75 at RT	1100

The Young's moduli of some BMGs are somewhat higher than that of titanium or niobium. The elastic limit, UTS and maximum elastic deflection of some BMGs can be over two times greater than that of titanium or niobium. The increased strength and maximum elastic deflection capabilities of BMGs are two of the key reasons why they may be a superior choice for use as the pivot material. Figure 2.4 [6] contains a diagram that plots the elastic limit of various types of materials versus Young's modulus. The  $\sigma_y/E$  contour corresponds to the maximum elastic deflection of the material. One can see that BMGs, which are indicated by the filled in circles, have mechanical properties that are superior to conventional metals.

Preliminary data obtained from journal sources show that BMGs at room temperature may have loss coefficients higher than that of cryogenic high purity titanium and niobium. This may not be a favorable property of BMG for AGG pivot application, but more study needs to be done to verify the accuracy of the data. Figure 2.5 [6] contains a diagram that plots the resilience of various types of materials versus loss coefficient. The BMGs are indicated in the diagram by the circles that are filled in. When comparing with conventional metallic alloys, it can be seen that BMGs have loss coefficients that are at least one order of magnitude lower. This implies that BMGs have lower hysteresis effects, which means a pivot made out of a BMG, would spring back closer to the origin when no gravity field is detected.

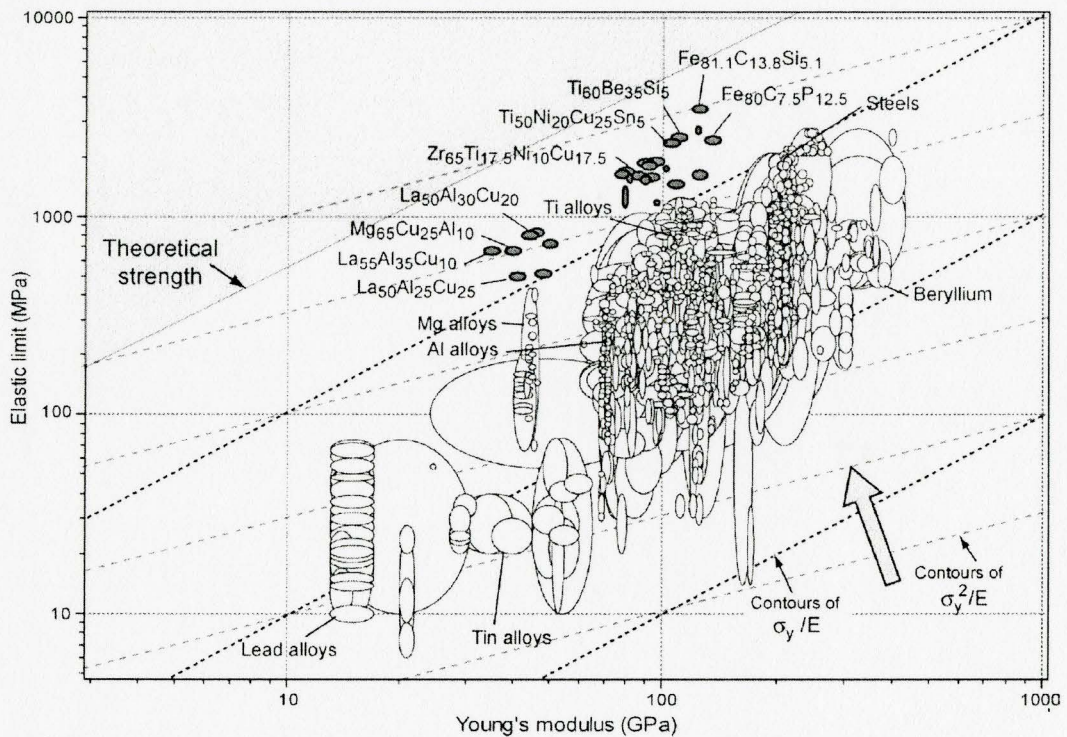


Figure 2.4 Elastic limit plotted against Young's modulus for various BMGs [6].

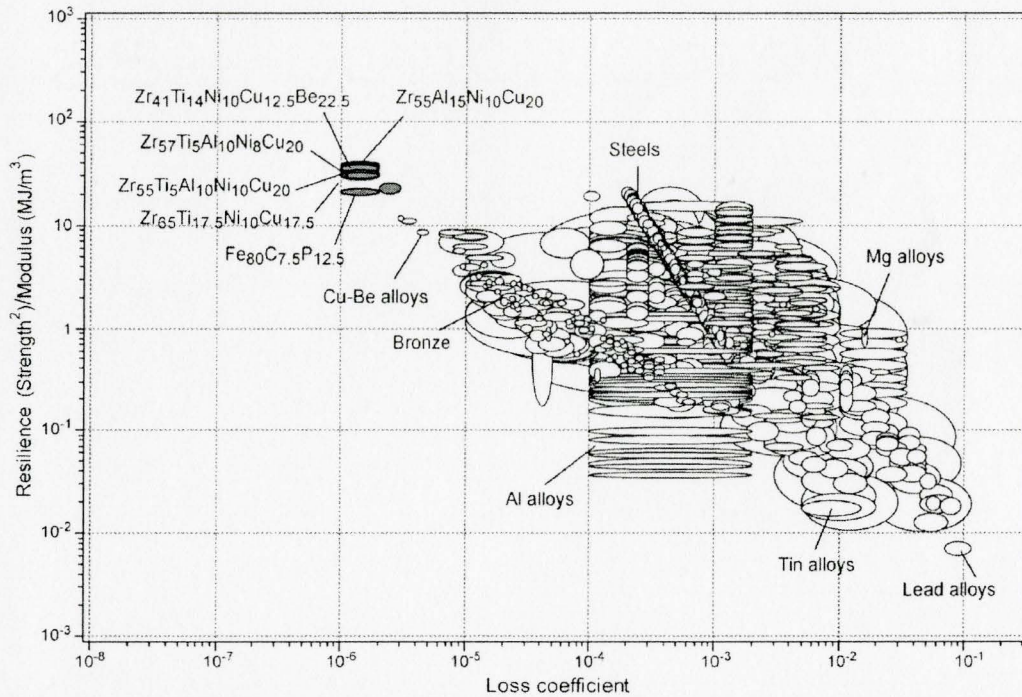


Figure 2.5 Resilience plotted against loss coefficient for various BMGs [6].

The LCTE of BMGs appears to be at least one to two orders of magnitude greater than that of niobium. It is important to point out that the coefficient values were taken at different temperatures. It is believed that the LCTE of BMGs could drop between one to two orders of magnitude if measured at 20 K, which would match more favorably with the coefficient values of niobium. Fatigue limit data for BMGs are preliminary, but can be significantly better than that of titanium and niobium.

Bulk metallic glasses generally have sufficient electrical conductivities to be used in the pivot application and can be designed with numerous metals that have very low magnetic susceptibilities. Unfortunately, few journal studies have investigated creep of BMGs at room temperature or below. At this time, the creep of BMGs cannot be compared with the creep properties of titanium or niobium.

### 2.2.3 Bulk metallic glass material properties database

Over the last 15 years, numerous bulk metallic glasses have been manufactured. Unfortunately, property data is contained in numerous journal articles and is not readily

available in one universal database. Hence, a database of bulk metallic glass material properties has been developed. The database compiles nonmagnetic BMGs and their material properties crucial to this application. As of now, data from 172 journal and conference articles have been obtained in hardcopy format and are referenced in the database. A total of 30 distinct BMG systems have been identified (see Table 2.3) and a total of 250 distinct alloys with properties have been added. The entire database and the list of references from where the data was extracted are included in Appendix A. Bulk metallic glasses systems literature review based on castability are given in Appendix B. Many other distinct alloys have been developed, but the required material property data could not be found and were not added to the database.

At this time, the process of searching and adding BMGs to the database has been completed. It is believed that the vast majority of data that is available to the public has been analyzed.

Table 2.3 Bulk Metallic Glass systems in database.

Mg-LN-(Ni, Cu, Zn)	Cu-(Zr, Hf, Nb)-Ti
Mg-LN-(Ni, Cu, Zn)-(Ag, Pd)	Cu-(Zr, Hf, Nb)-Ti-Ta
Ln-Al-TM	Cu-(Zr, Hf)-Ti-(Y, Be)
Ln-Y-Al-TM	Cu-(Zr, Hf, Nb)-Ti-TM
Ti-(Zr, Hf)-TM	Cu-(Zr, Hf)-(Al, Ga)
Ti-Zr-TM-Be	Cu-(Zr, Hf)-Ti-(Ag, Au, Pd, Pt)
Ti-Zr-TM-Al-Si-B	Cu-(Zr, Hf)-Ti-Al-(Ag, Au, Pd, Pt)
Ti-Ni-Cu-Sn	Cu-(Zr, Hf)
Ti-Ni-Cu-Sn-Be	Au-Cu-Si-(Ag, Pd)
Zr-Al-TM	Pt-TM-P
Zr-(Ti, Nb)-TM-Be	Pd-TM-P
Zr-Al-(Ti, Nb)-TM-Be	Pd-Cu-Si
Zr-(Ti, Nb, Pd)-Al-TM	Pd-Cu-Si-P
(Hf, Zr)-Ti-(Al, Ga)-TM	Ca-Mg-(Ni, Cu, Zn)
(Y, Sc)-Al-TM	Ca-Al-Mg-(Ni, Cu, Zn)

### 2.2.4 Criteria for selecting BMGs for further study

The initial criteria for narrowing down the list of BMGs in the database are outlined in Table 2.4. The minimum Young's modulus, UTS and maximum elastic deflection values were set to 100 GPa, 2000 MPa and 2.0 % respectively. With these criteria, the La and Mg-based systems are not suitable for the present application because their tensile strengths are below 1000MPa and the elastic modulus is less than 70 GPa. Also the required properties of non-ferromagnetism and diamagnetism eliminate the Fe-, Ni-, Co-, Nd-, Pr-based alloys. The LCTE had to be within an order of magnitude of the niobium value. At this time, the criterion for loss coefficient is being discussed and yet to be determined.

The systems that contain BMGs that satisfy this initial criteria are: Zr-Al-TM, (Hf, Zr)-Ti-(Al, Ga)-TM, Cu-(Zr, Hf, Nb)-Ti-TM and Cu-(Zr, Hf, Nb)-Ti-Ta. The room temperature properties of specific BMGs from all four of these systems are shown in Table 2.5. Property values of niobium at 20 K are also included for comparison. It can be seen that the strength and maximum elastic deflection values of BMGs are significantly higher than that for niobium, while the Young's Modulus values are similar.

Table 2.4 Criteria for BMG used for the AGG Pivot application.

Material Property	Property Criteria
Young's Modulus (GPa)	$\geq 100$
UTS (MPa)	$\geq 2000$
Maximum Elastic Deflection (%)	$\geq 2.0$
Linear Coefficient of Thermal Expansion (m/m/°C)	Within order of magnitude of Nb value
Loss Coefficient / Internal Friction ( $Q^{-1}$ )	To Be Determined

Table 2.5 Bulk Metallic Glasses satisfying initial criteria for AGG application.

Material Property	Nb at 20 K	Zr <sub>55</sub> Co <sub>25</sub> Al <sub>20</sub>	Hf <sub>50</sub> Cu <sub>30</sub> Ni <sub>10</sub> Al <sub>10</sub>	Cu <sub>47</sub> Ti <sub>34</sub> Zr <sub>11</sub> Ni <sub>8</sub>	(Cu <sub>0.6</sub> Zr <sub>0.3</sub> Ti <sub>0.1</sub> ) <sub>98</sub> Ta <sub>2</sub>
Young's Modulus (GPa)	125	114	118	109	123
UTS (MPa)	1175	2200	2420	2186	2250
Maximum Elastic Deflection (%)	1.2	2.1	2.1	2.1	2.1

The LCTE of Zr-, Cu- and Hf-based BMG systems and pure Ti and Nb are shown in Table 2.6. Since the thermal expansion data for the BMGs in Figure 11 is not available, alloys having similar compositions are referenced to estimate LCTE for the desired alloys. The LCTE of Zr-, Cu-, and Hf-based BMG alloys and pure Nb are comparable at room temperature and they all can be potentially used as materials for the AGG application.

Further filtering of these alloy systems will have to be carried out based on their castability to successfully make the final component. Based on castability of the alloys discussed in Appendix B, Zr- and Cu-based BMG alloys are better choices for candidate materials due to the rapid oxidation characteristics of Ti - based alloys, which will impede successful melt preparation and casting.

Table 2.6 LCTE of Niobium, Ti and a few potential BMG alloys for the AGG application.

Material	LCTE (m/m/°C)		
	25 °C	-196 °C	-253 °C
Pure Nb	7.10E-06	4E-06	2.0E-07
Pure Ti	8.60E-06	3.2E-06	–
Cu <sub>55</sub> Zr <sub>30</sub> Ti <sub>10</sub> Pd <sub>5</sub>	1.1E-05	–	–
Cu <sub>55</sub> Zr <sub>30</sub> Ti <sub>10</sub> Ni <sub>5</sub>	1.3E-05	–	–
Zr Based BMG alloys	8.0E-06 – 1.5E-05	–	–
Hf <sub>50</sub> Cu <sub>24</sub> Al <sub>10</sub> Ni <sub>8</sub> Zr <sub>3</sub> Ga <sub>3</sub> Ti <sub>2</sub>	9.0E-06	–	–

It is expected that these criteria will be continually modified until the exact design requirements of the pivot are determined. This will lead to an increase or decrease of BMG systems that can be considered for the pivot application.

Finally, Cu<sub>43</sub>Zr<sub>43</sub>Al<sub>7</sub>Ag<sub>7</sub> and Vitreloy 1: Zr<sub>41.2</sub>Be<sub>22.5</sub>Ti<sub>13.8</sub>Cu<sub>12.5</sub>Ni<sub>10.0</sub> were selected as trial materials for AGG pivot application considering their comparable properties shown in Table 2.7.

Figure 2.6 shows a flow chart of the selection process, identification and testing of the ideal BMG trial material for the AGG pivot application. In Figure 2.6, the Cu<sub>43</sub>Zr<sub>43</sub>Al<sub>7</sub>Ag<sub>7</sub> alloy is as an example.

Table 2.7 Properties of trial materials:  $\text{Cu}_{43}\text{Zr}_{43}\text{Al}_7\text{Ag}_7$  and Vitreloy 1(Vit1).

<b>Material Property</b>	<b>Vitreloy 1(Vit1):</b>	
	<b><math>\text{Zr}_{41.2}\text{Ti}_{13.8}\text{Cu}_{12.5}\text{Ni}_{10.0}\text{Be}_{22.5}</math></b>	<b><math>\text{Cu}_{43}\text{Zr}_{43}\text{Al}_7\text{Ag}_7</math></b>
Density( $\text{g}/\text{cm}^3$ )	6.11[9]	7.56
Young's Modulus (GPa)	96 [9]	103[43]
Yield Strength (MPa)	1900 [9]	1850[43]
Ultimate Tensile Strength (MPa)	1900 [9]	1850[43]
- Poisson's ratio (and/or shear modulus)	0.36[9]	0.35
Elastic Limit (%)	2[9]	1.8[43]
critical size in diameter (mm)	100	8[43]
Linear Coefficient Of Thermal Expansion ( $\text{m}/\text{m}/^\circ\text{C}$ )	9.26E-06	N/A

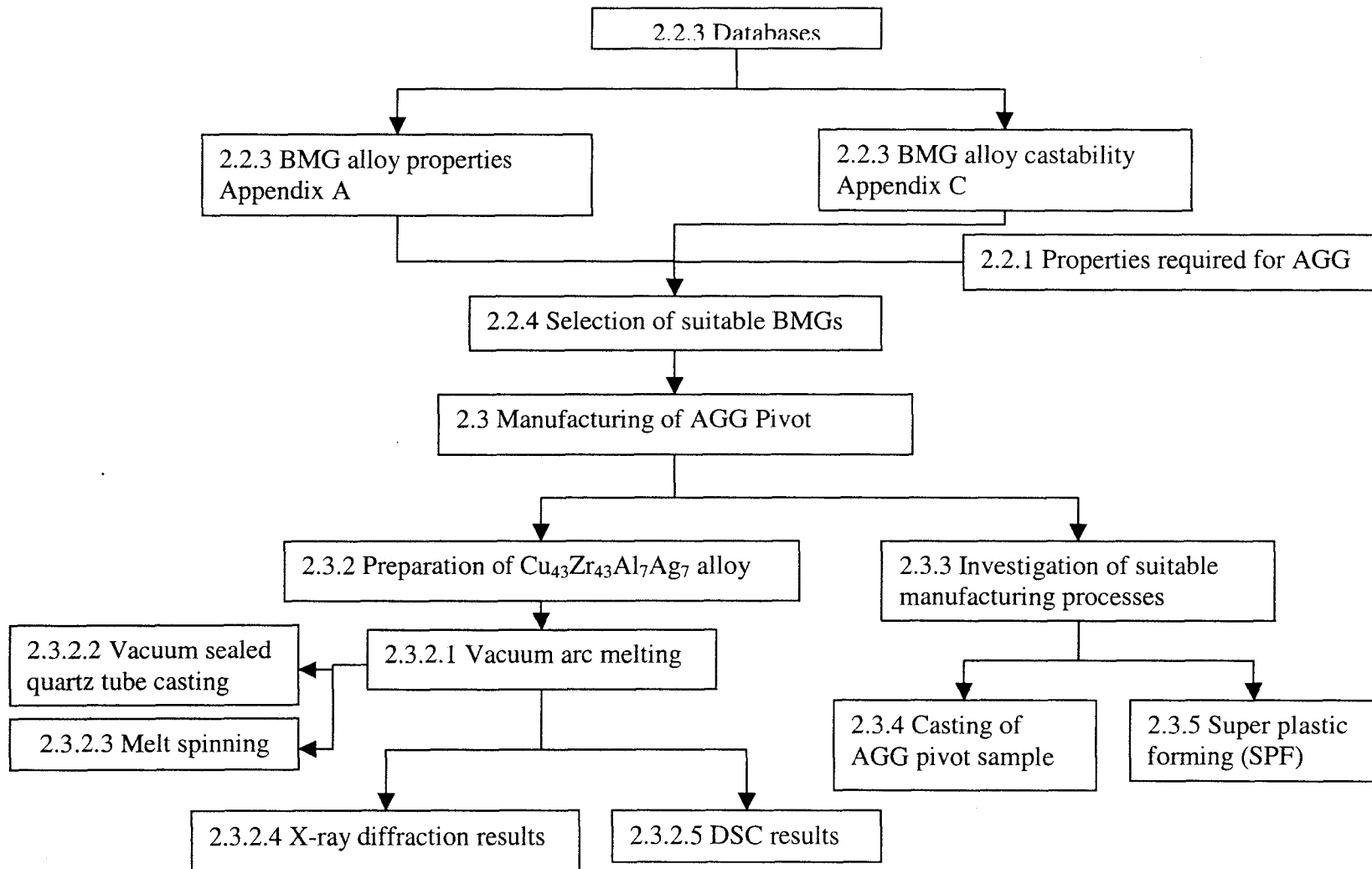


Figure 2.6 Selection criteria, identification and testing of suitable BMG materials for AGG pivot application.

## 2.3 Manufacturing of AGG Pivot with a Suitable BMG

### 2.3.1 Pivot geometry of AGG gradiometer

The proposed AGG gradiometer web with the pivot is shown in Figure 2.7. The piece consists of two small rectangular blocks of 20mm×5mm×4.34mm each connected by a centrally placed flexure of 0.13mm thickness through the entire length.

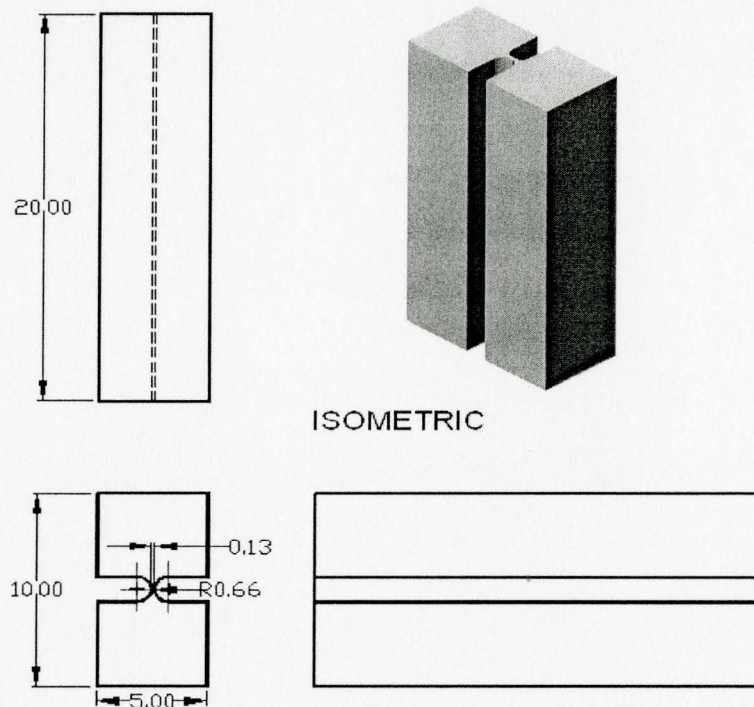


Figure 2.7 Drawing of AGG gradiometer pivot.

### 2.3.2 BMG material for AGG pivot

In this section I will consider the preparation of the Cu<sub>43</sub>Zr<sub>43</sub>Al<sub>7</sub>Ag<sub>7</sub> BMG alloy as an example. The other material used to make the same web piece was Vit1 (Zr<sub>41.2</sub>Ti<sub>13.8</sub>Cu<sub>12.5</sub>Ni<sub>10.0</sub>Be<sub>22.5</sub>). The alloy and sample preparation techniques for both these BMG candidates are identical except that the amorphous Cu based alloy was obtained by melt spinning technique and amorphous the Vit 1 was obtained by vacuum suction casting method.

### 2.3.2.1 Vacuum arc melting (VAM)

The ingot of the  $\text{Cu}_{43}\text{Zr}_{43}\text{Al}_7\text{Ag}_7$  alloy was obtained by arc melting mixture of ultrasonically-cleansed elemental metals in high purity argon atmosphere. The melting process was repeated for five times to guarantee chemical homogeneity in the final alloy sample. The elemental metals Cu, Zr, Al and Ag with purity of 99.9%, 99.95% (metal basis excluding Hf and Hf nominal 3%), 99.9999% and 99.9%, respectively were used as raw materials. The arc melting furnace chamber was evacuated to 200 millitorr then backfilled with high purity argon (HP +) to a pressure of 0.5 atmosphere. The ingot mass after vacuum arc melting was 45.6682 g with mass loss of 0.0057 g. Figure 2.8 shows the as-cast ingot.

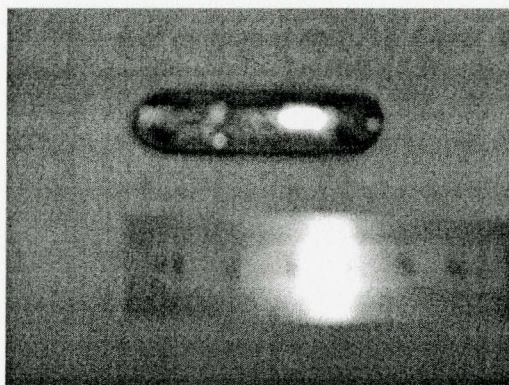


Figure 2.8 Ingot of  $\text{Cu}_{43}\text{Zr}_{43}\text{Al}_7\text{Ag}_7$  alloy.

The composition of the alloy was tested by Inductively Coupled Plasma-Mass Spectrometry (ICP) chemical analysis. The oxygen and nitrogen content were examined by LECO TC-136 Nitrogen/Oxygen determinator. The difference between the nominal and actual composition is shown in Table 2.8.

Table 2.8 Chemical composition of  $\text{Cu}_{43}\text{Zr}_{43}\text{Al}_7\text{Ag}_7$  alloy tested by ICP

Weight (%)	Zr	Cu	Al	Ag	Oxygen	Nitrogen
Nominal	51.62	35.96	2.49	9.94	-	-
Actual	51.64	36.50	2.40	9.46	.0110	.01121

### 2.3.2.2 Vacuum sealed quartz tube casting

2.8955g of the ingot was obtained by cutting and remelting in VAM chamber. The small piece of  $\text{Cu}_{43}\text{Zr}_{43}\text{Al}_7\text{Ag}_7$  alloy was then vacuum sealed within a quartz tube with inner diameter (ID) of 4mm, outer diameter (OD) of 6mm at a pressure of  $2 \times 10^{-5}$  torr. The quartz tube was put into a resistance furnace and heated to  $920^\circ\text{C}$  for about 30 min. Subsequently, the quartz tube was taken from the furnace and quenched in water at room temperature. Figure 2.9 shows the quenched  $\text{Cu}_{43}\text{Zr}_{43}\text{Al}_7\text{Ag}_7$  sample piece with length of 35mm. The sample was cut along the cross section by ISOMET 11-1180 low speed diamond saw cooled with kerosene, which guaranteed minimal heating of the sample during cutting. The sample was polished and etched using 0.5% HF solution. The microstructure shown in Figure 2.10 indicates that there is no difference of the microstructure in the center and on the edge of alloy rod. The alloy layer adjacent to the quartz tube shows crystallized microstructure, which indicates negligible amorphous layer of  $\text{Cu}_{43}\text{Zr}_{43}\text{Al}_7\text{Ag}_7$  was formed by this method with alloy diameter of 4mm.

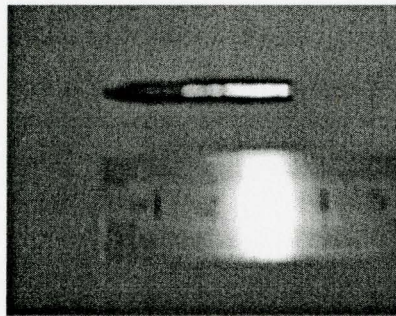


Figure 2.9 Quenched  $\text{Cu}_{43}\text{Zr}_{43}\text{Al}_7\text{Ag}_7$  alloy with quartz on its surface.

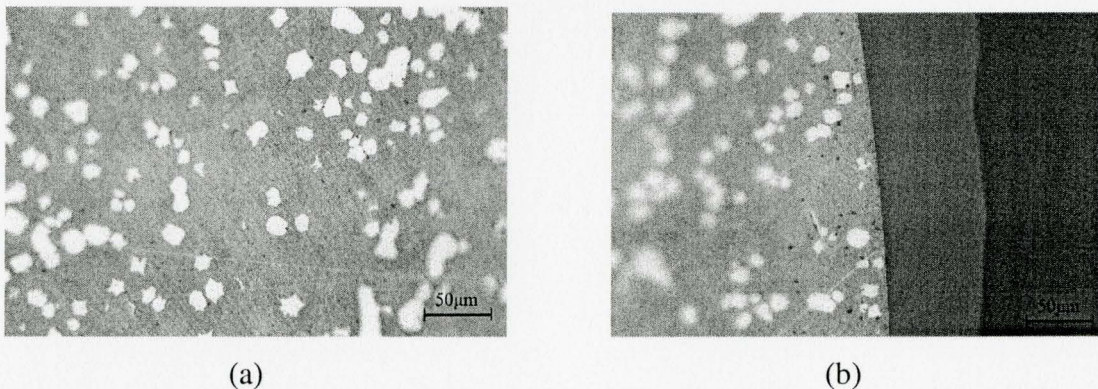


Figure 2.10 Optical microscopy (OM) of  $\text{Cu}_{43}\text{Zr}_{43}\text{Al}_7\text{Ag}_7$  alloy: (a) Center and (b) Edge.

### 2.3.2.3 Melt spinning of $\text{Cu}_{43}\text{Zr}_{43}\text{Al}_7\text{Ag}_7$

The amorphous ribbon with thickness of  $30\mu\text{m}$  and width of  $1\text{mm}$  was obtained by melt spinning the ingot under an over-pressure of  $2.5\text{atm}$  Argon onto a copper wheel rotating at a speed about  $35\text{ m/s}$ . Figure 2.11 shows the pieces of amorphous ribbons. Small chips with size below  $0.210\text{mm}$  and  $0.105\text{mm}$  were prepared by mechanically breaking ribbon using mortar/pestle.



Figure 2.11 Melt spun ribbon of  $\text{Cu}_{43}\text{Zr}_{43}\text{Al}_7\text{Ag}_7$ .

### 2.3.2.4 X-ray diffraction results of as melt spun and ground ribbons

X-ray diffraction (XRD; Nicolet I2,  $\text{Cu K}\alpha$  radiation) were performed to examine if the melt spun ribbon and ground ribbon pieces were amorphous. The results are showed in Figure 2.12 and Figure 2.13. The broad peak in the diffraction pattern in Figure 2.12 indicates the formation of an amorphous single phase, while sharp peaks in Figure 2.13 represent crystallized phases. The melt spun ribbons were amorphous, but ground ribbon pieces were not, which shows that mechanical force produced by grinding induced crystallization process.

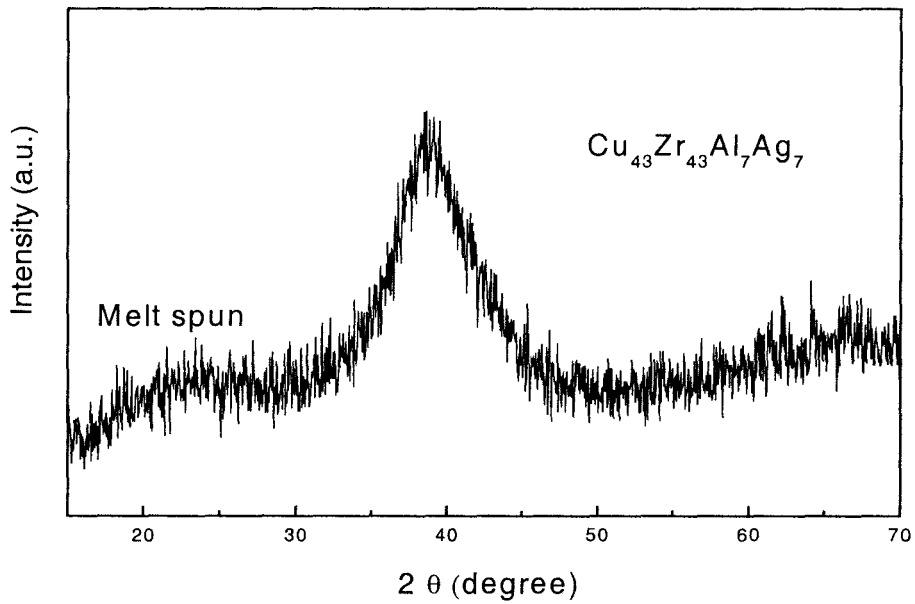


Figure 2.12 X-ray diffraction pattern of the melt-spun  $\text{Cu}_{43}\text{Zr}_{43}\text{Al}_7\text{Ag}_7$  alloy ribbons.

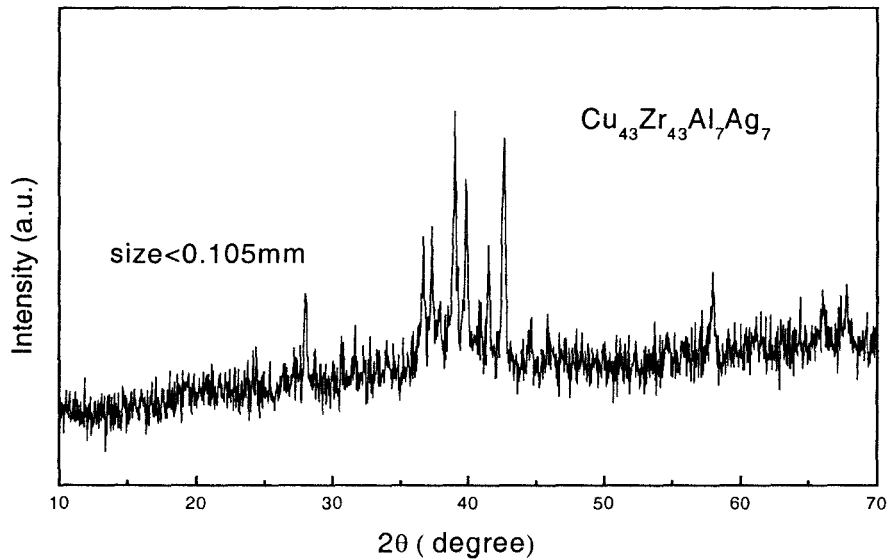
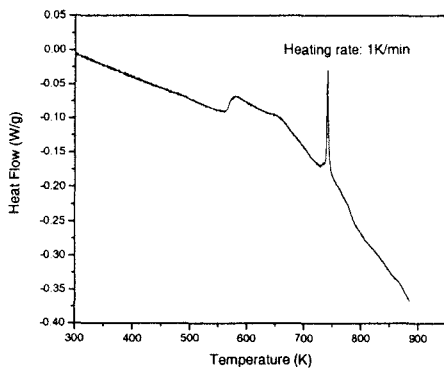


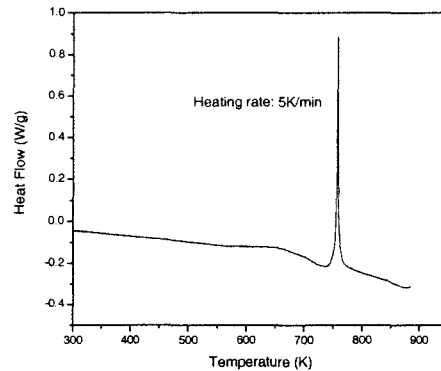
Figure 2.13 X-ray diffraction pattern of melt-spun  $\text{Cu}_{43}\text{Zr}_{43}\text{Al}_7\text{Ag}_7$  alloy ribbons which were subsequently ground mechanically for size reduction to less than 0.105mm.

### 2.3.2.5 Differential Scanning Calorimetry (DSC) results of $\text{Cu}_{43}\text{Zr}_{43}\text{Al}_7\text{Ag}_7$

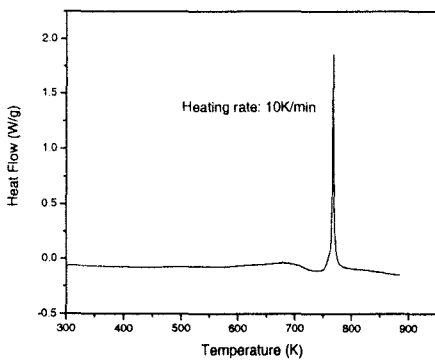
The thermal properties associated with the glass transition and crystallization for the melt-spun  $\text{Cu}_{43}\text{Zr}_{43}\text{Al}_7\text{Ag}_7$  alloy were determined by TA Instrument DSC 910 differential scanning calorimeter at constant heating rates of 1, 5, 10, 20, 50, 100K/s respectively in the temperature range of 293 to 900 K as shown in Figure 2.14. Three typical DSC curves were obtained from three separate DSC runs for each of the six selected heating rates. The summarized data is shown in Table 2.9, where  $T_g$ ,  $T_x$  and  $T_p$  represent glass transition temperature, crystallization onset temperature and crystallization peak temperature, respectively. All the three observed temperatures increased with the heating rate.



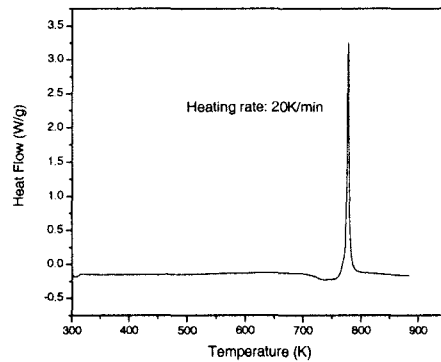
(a)



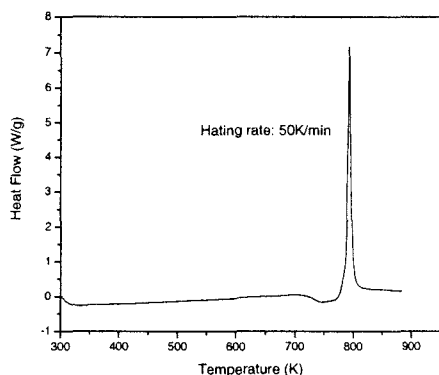
(b)



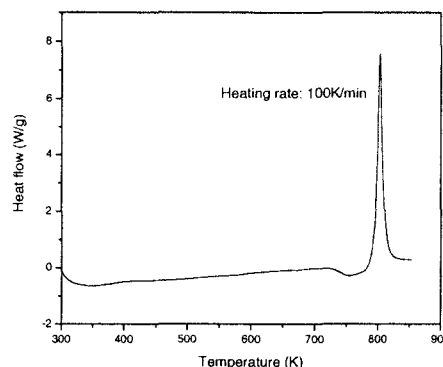
(c)



(d)



(e)



(f)

Figure 2.14 Typical DSC curves of  $\text{Cu}_{43}\text{Zr}_{43}\text{Al}_7\text{Ag}_7$  melt spun ribbons obtained at different heating rates to show the glass transition and crystallization behavior. (a) to (e) shows the heating rates of 1, 5, 10, 20, 50 and 100 K/min, respectively.

Table 2.9 Average\* transformation temperatures in DSC experiments as a function of heating rate for  $\text{Cu}_{43}\text{Zr}_{43}\text{Al}_7\text{Ag}_7$  melt spun ribbons.

Heating Rate (K/min)	Glass transition temperature $T_g$ (K)	Crystallization onset temperature $T_x$ (K)	Crystallization peak temperature $T_p$ (K)
1	691	739	741
5	708	756	759
10	715	764	767
20	721	772	776
50	728	785	790
100	734	791	798

\* Average data for three DSC experiments at each heating rate shown in the table.

### **2.3.3 Net shape manufacturing of AGG pivot with BMG**

#### **2.3.3.1 Casting**

Currently, for commercial applications, die casting is used as a viable net-shape manufacturing technique. Due to the metastable nature of most amorphous structures, BMGs must be solidified rapidly to avoid crystallization. To achieve this, the liquid mass has to be thin and remain in complete thermal contact with an efficient heat sink, i.e., a highly conducting material, like copper. Injection casting is a common and convenient rapid solidification processing to obtain metallic glasses in bulk form and examine their critical thickness. Figure 2.15 is a schematic of the injection casting process devised to obtain a near net shape part of the micro-flexure pivot test piece using a BMG alloy. A quartz tube with an inner diameter of 0.8 mm is placed on top of the water cooled copper mold. The quartz tube contains solid chips of the BMG alloy. One end of the quartz tube is secured into the copper mold by a high temperature ceramic putty seal. The other end of the tube is sealed with a ceramic plug with two holes on top for Ar gas purging and gas venting. A vent is also machined into the copper mold. The mold is machined to the final component dimensions. The quartz tube is heated by an induction furnace to melt the solid BMG alloys in an argon atmosphere. The outlet hole of the quartz tube between the tube and the copper mold is in the order of 1 mm and surface tension forces of the melt will prevent it from entering the mold. Once the liquid metal reaches the required superheat for casting, the vent on top of the quartz tube is shut off enabling a pressure buildup in the quartz tube due to the Ar gas purge. The pressure buildup will enable the molten metal to be injected into the cavity of the copper mold. The vent in the mold will ensure that the gas in the mold is purged out ahead of the molten metal interface. Due to the extraordinary thermal conductivity of copper, the liquid alloy can solidify with a high enough cooling rate to form a BMG alloy component. If the desired alloy requires a higher cooling rate, the copper mold can be water chilled.

The common defects for injection casting are trapped air bubbles, fine scale porosity and non-fill. Solidification time has a parabolic relationship with thickness of casting. Hence, solidification of the 0.13mm thickness connector (refer to Figure 2.7) in

the center of the pivot can be more than one thousand times faster than the rectangular block with thickness of 5mm. It is possible that the thin section (0.13 mm) of the pivot will solidify prematurely and prevent further flow of liquid to attain a sound casting.

For Vit1( $Zr_{41.2}Ti_{13.8}Cu_{12.5}Ni_{10.0}Be_{22.5}$ ), because the critical cooling rate is as low as 1K/s, it is possible to achieve a cast piece with complete amorphous structure by melting the alloy in a metal die within a vacuum sealed quartz tube and subsequently quenching the quartz tube with the mould in agitated water.

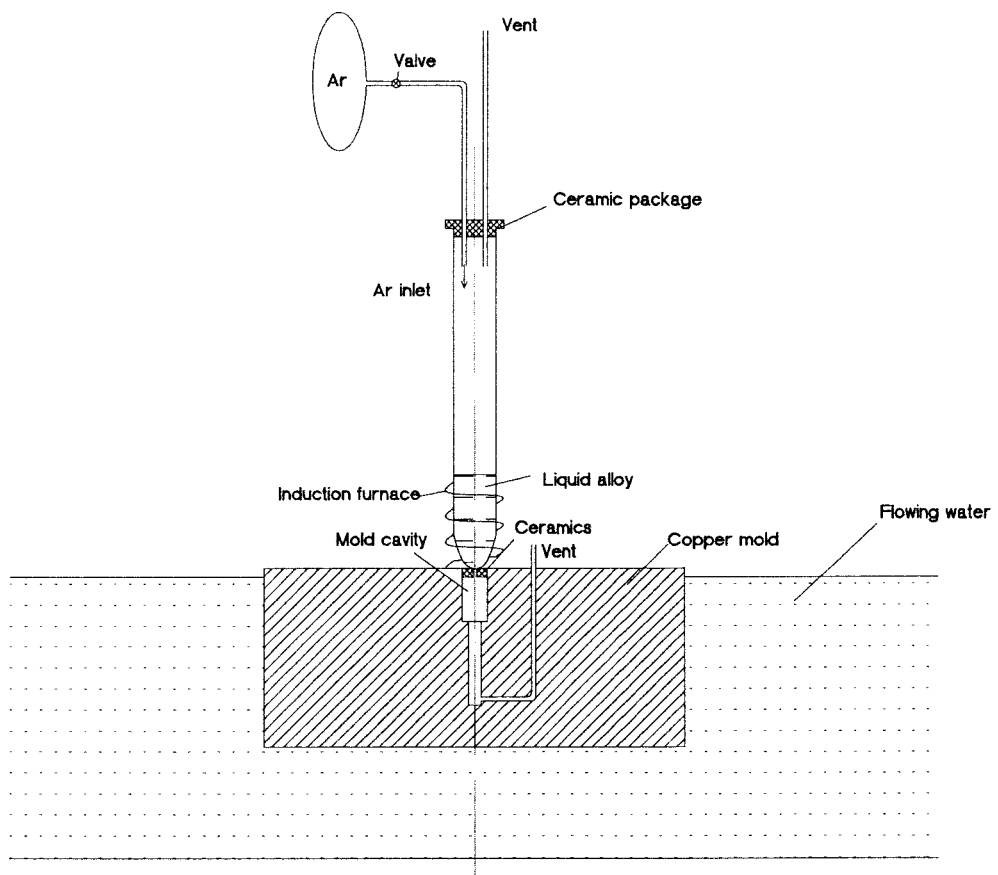


Figure 2.15 Schematic of injection casting technique.

### 2.3.3.2 Superplastic forming (SPF)

Another way to obtain complicated geometry of bulk metallic glass is by Superplastic Forming (SPF) [7]. SPF is a net-shape processing method that decouples

rapid cooling and forming of the BMG components. Figure 2.16 [8] is a schematic time-temperature-transformation (TTT) diagram that shows the processing methods of both die casting and SPF. During die casting, the solidification takes place simultaneously with high rates of heat extraction from the mould in order to avoid the crystallization nose. This makes casting of complex parts with thin sections and large aspect ratios a challenging undertaking. Only a very careful balance of process parameters such as casting temperature, mould temperature, pressure and mold design result in good quality cast parts. In SPF, the amorphous BMG is reheated into the super cooled liquid region where the available processing window is much larger than in die casting, resulting in a better control of the process and a defect free component. In the super cooled liquid region, the BMG exists as a highly viscous liquid and increases its fluidity with increasing temperature. The viscosity of the BMG can vary between  $10^{12}$  Pa s at the glass transition temperature,  $T_g$ , down to  $10^5$  Pa s at the crystallization temperature,  $T_x$  [8]. In this temperature range, molten BMG alloys can undergo substantial plastic strain under an applied pressure. Crystallization kinetics for various BMG alloys results in processing times of the order of a few minutes to many hours which enables manufacturing of accurate net-shape components with complicated geometries. This process does not require fast cooling to avoid crystallization during cooling. Currently, components of  $Zr_{44}Ti_{11}Cu_{10}Ni_{10}Be_{25}$  (LM1b), Vit1 [8], Vit4 [9] ( $Zr_{46.8}Ti_{8.2}Cu_{7.5}Ni_{10}Be_{27.5}$ ) and  $Pt_{57.5}Cu_{14.7}Ni_{5.3}P_{22.5}$  [10] with micro features have been manufactured via SPF.

SPF can be applied as alternative forming method of the AGG web pivot if casting is not successful, especially for the expected difficulty with central micropart of pivot test piece. Important processing parameters such as pressure, temperature and time must be carefully balanced to guarantee that the undercooled liquid would fully fill mold cavity as well as avoid crystallization.

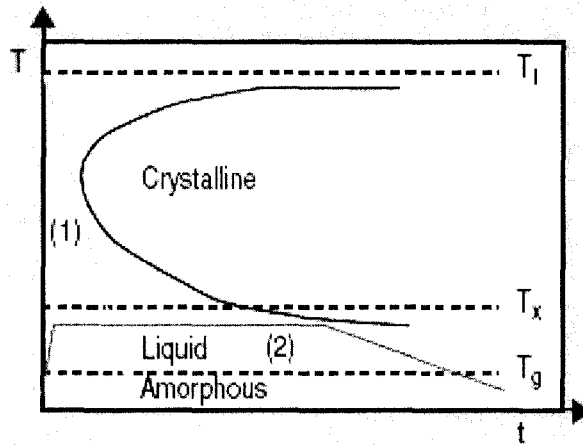


Figure 2.16 A schematic TTT diagram showing the processing methods. (1) Die casting and (2) Superplastic casting [8].

### 2.3.4 Casting of AGG pivot sample

As shown in section 2.3.2,  $\text{Cu}_{43}\text{Zr}_{43}\text{Al}_7\text{Ag}_7$  alloy is not amenable to be used in die casting process to obtain a completely amorphous cast component. Therefore, Vit1 will be used to cast the pivot component using die casting process. Because of high content of Zr and Ti (56 at % altogether) which are sensitive to oxidation, casting of the AGG pivot must be carried out in an inert atmosphere. In this section, selection of mold and coating materials, mold design and fabrication, casting procedure, result and proposed improvement for future work will be discussed in detail.

#### 2.3.4.1 Selection of mold and coating materials for casting

Basic requirements of mold material properties are as following:

- a. No reaction with alloy;
- b. Continuous service temperature is greater than  $800^\circ\text{C}$ , which is supposed to be quenching temperature of Vit1 ;
- c. Coefficient of thermal expansion (CTE) of mold material is same or greater than that of Vit1, which is  $10.1 \times 10^{-6} \text{ }^\circ\text{C}^{-1}$ .

When liquid Vit1 is quenched to solid state, and if the coefficient of thermal expansion of mold material is smaller than that for Vit1, the shrinkage of Vit1 during

solidification will be higher than that for the mold. Hence, cast piece will be stuck within the mold in the center micro flexure part of the mold as shown in Figure 2.17. In figure 2.17, the bold lines denote the areas that withstand compression stress (indicated by arrows) from the mold. Therefore, the CTE for Vit1 should be higher than that for the mold.

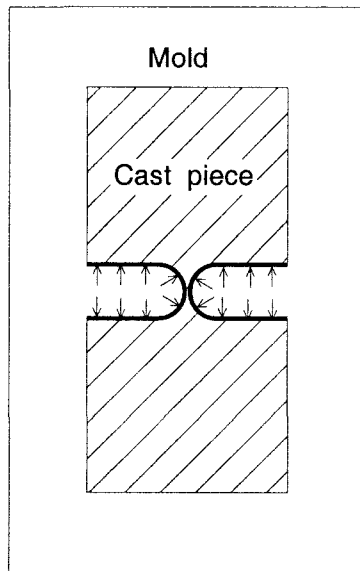


Figure 2.17 Compression stress (indicated by arrows) applied on cast piece if coefficient of mold material is less than that of mold material.

Candidates for mold materials and their respective properties are summarized in Table 2.10. Cotronics 902 is machinable alumina silicate with continuous service temperature to 1150°C and flexural strength of 96.53MPa after firing[11]. H-BN is a synthetic material with a structure similar to that of graphite, which is not wetted by most molten metals. In the hot pressed state, h-BN is readily machinable using conventional metal cutting techniques. Grade 304 is the standard austenitic "18/8" stainless steel, the most versatile and widely used material. Only stainless steel 304 possesses higher CTE than that of Vit1 alloy but it requires coating to prevent chemical bonding with Vit1. Though CTE of cotronics 902 and hexagonal boron nitride (h-BN) are less than that of Vit1, they are also selected and tested as mold material in this section for possible use in

the future. To avoid reaction of the mold surface with Vit1 alloy, a thin layer of coating of white silk aerosol boron nitride (BN) and grey BN lubricoat were applied on the mold. Except BN mold, all the other materials were prepared in two pieces. One is BN coated and the other without a coating.

To ascertain the reaction between the various selected mold surfaces as shown in Table 2.10 with  $Cu_{43}Zr_{43}Al_7Ag_7$  alloy, the alloy power with size less than 0.210mm was used. The results from these tests can be extrapolated to understand the reaction between these mold surfaces and Vit1 as well since the primary reactive elements are Cu and Zr in both cases. The candidate mold materials were prepared in cylinder shape with outer diameter (OD) 1/2"×Length (L) 1/2". A hole with 3/8" diameter and 3/8" deep was drilled for holding the molten  $Cu_{43}Zr_{43}Al_7Ag_7$  alloy powder as shown in Figure 2.18.

Table 2.10 Continuous service temperature and coefficient of thermal expansion at room temperature of candidate mold materials for die casting application.

<b>Material</b>	<b>Hexagonal –BN [12]</b>	<b>Cotronics 902</b>	<b>Stainless steel 304 [13]</b>
Coefficient of thermal expansion (CTE) $\times 10^{-6} \text{ } ^\circ\text{C}^{-1}$	1 (Parallel to press direction) 4 (Perpendicular to press direction) RT-1000°C	3.24 (RT)	17.3 (RT)
Continuous service temperature ( $^\circ\text{C}$ )	>1800 (In inert atmosphere)	1150	925



Figure 2.18 Candidate mold material for die casting BMG. From left to right: BN mold, ceramic 902(fired), white silk aerosol BN coated ceramic 902, grey BN lubricoat coated stainless steel and white silk aerosol BN coated stainless steel.

$\text{Cu}_{43}\text{Zr}_{43}\text{Al}_7\text{Ag}_7$  powder was put into the various mold cavities and the molds were stacked up in a quartz tube with ID of 14 mm and OD of 16mm as shown in Figure 2.19. A small piece of pure zirconium foil (99.9+ %) with thickness of 0.1mm was also put into the quartz tube to act as a oxygen getter. The quartz tube was evacuated to less than  $10^{-5}$  torr, then backfilled with helium at 0.5 atm. It was expected that the Zr-gettered helium atmosphere, the oxygen effect would be minimal. Subsequent to isothermal holding at  $920^{\circ}\text{C}$  for two hour, the quartz tube was quenched in water. The quenched inner surface of quartz tube and all the molds became grey and had a smooth finish. This was due to the evaporation of binding system contained in the grey BN lubricoat at higher temperature that trasports some BN and deposit on all inner surface of the quartz tube when quenched. The Zirconium foil became dark and brittle as a result of oxidation.



Figure 2.19 Experimental mold materials stacked inside the Zr-gettered He rich quartz tube. The coating used was a combination of white silk BN and grey BN lubricoat. Top to bottom: BN, Cotronics 902, white silk aerosol BN coated Cotronics 902, aerosol (white) BN coated stainless steel 304, grey BN lubricoat coated stainless steel 304.

Two more experiments were carried out with coating the molds with white silk BN layer and aerosol Alumina layer, respectively. In both these cases the problem associated with the grey BN lubricoat were eliminated. However, all aerosol coatings have organic and inorganic binders in them which interfered with the controlled atmospheres inside the quartz tube and resulted in an unsatisfactory surface finish on the BMG alloy sample due to surface reaction mechanisms.

Quenched  $\text{Cu}_{43}\text{Zr}_{43}\text{Al}_7\text{Ag}_7$  alloy samples were separated from the BN and Cotronics 902 mold with or without coating while samples stuck in stainless steel mold formed a strong bond with the mold surface and were unable to extract. Analysis of the cross section of the alloy sample fused with the steel mold revealed extensive reaction between the two.

#### **2.3.4.2 Mold design and machining**

A mold design consisting of six mold parts was assembled to form a cavity with the required dimensions of the AGG pivot piece as described in section 2.3.1. The exploded view of assembled mold is shown in Figure 2.20 and the individual mold

components shown in Figure 2.21. As shown in Figure 2.20 the mould consists of three pairs of identical parts. Considering the gap volume among small solid pieces, mold length was enlarged from 20mm to 25mm, 25% more volume to guarantee required mass can be crammed into the mold cavity. Screws and dowel pins were used to fix the mold parts together. The good alignment of the assembled mold and the two radii distance of 0.13mm depend on the fit of dowel pins with mold part 1 and 2, as shown in Figure 2.20. Due to the small size of the mold and its complexity in components, the mold was designed with tight tolerances.

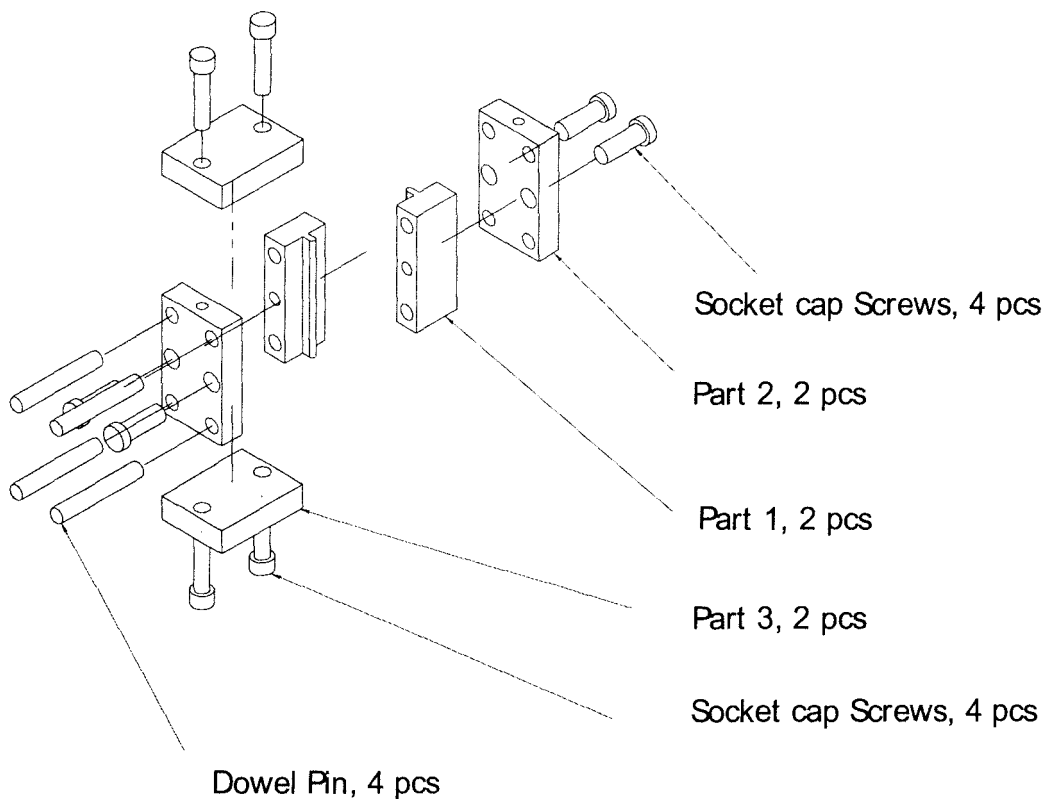


Figure 2.20 Exploded view of assembled mold used for die casting BMG.

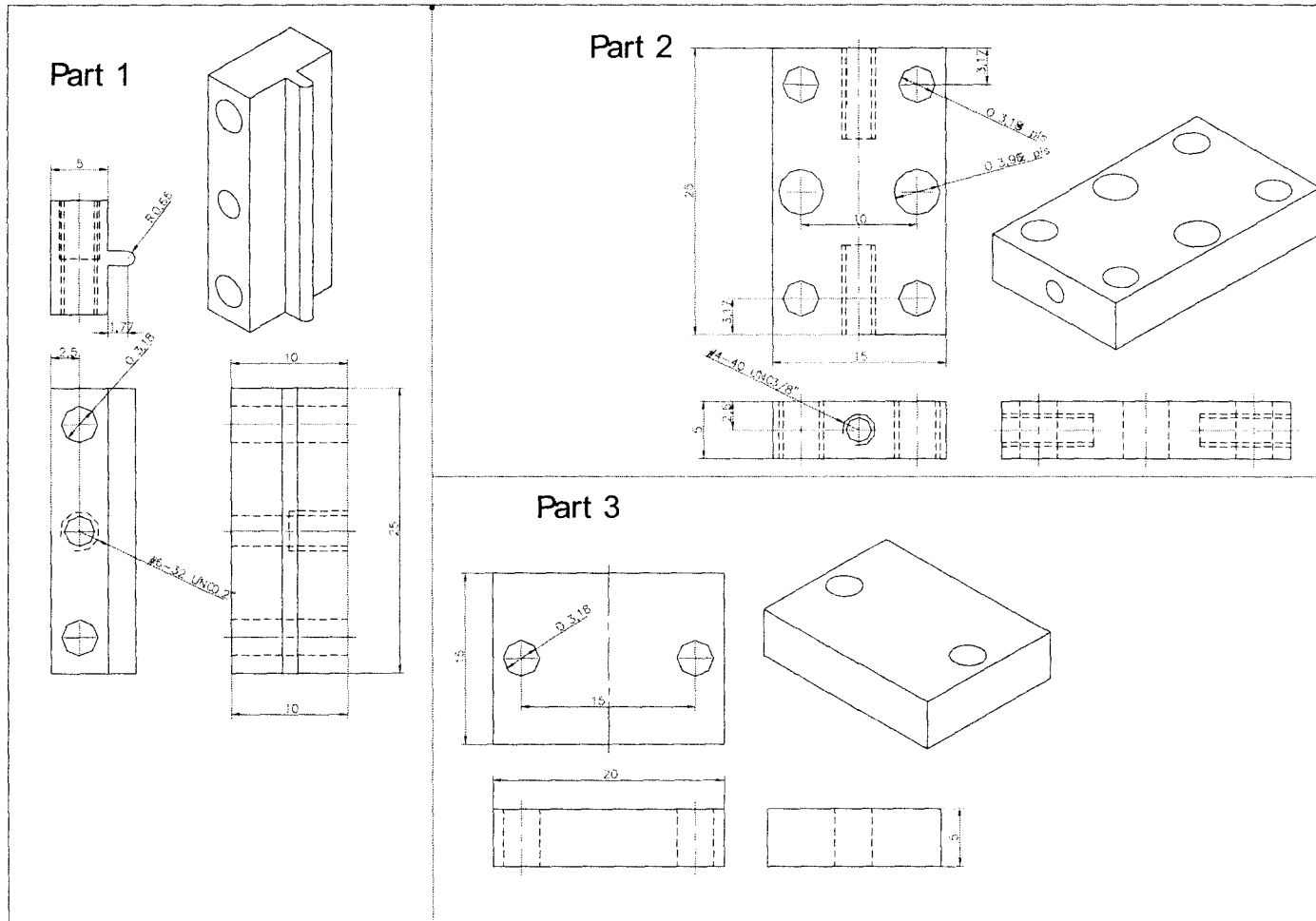


Figure 2.21 Components of the mold shown in Figure 2.20.

A piece of paper with thickness about 0.10mm is inserted into the assembled mold cavity to check the validity of the 0.13mm gap shown in Figure 2.20 as part 1. Figure 2.22 shows the machined stainless steel mold parts. Assembled mold picture is shown in Figure 2.23. Dowels pins were inserted into the open holes shown in Figure 2.23.

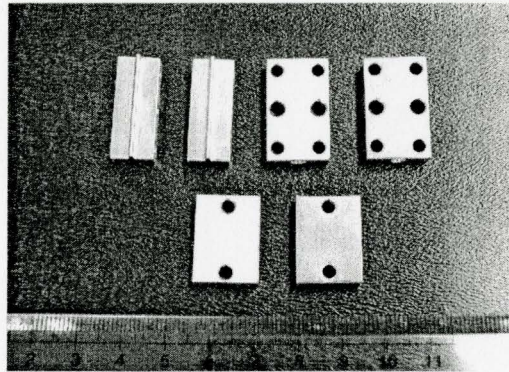


Figure 2.22 Stainless steel components of the mold shown in Figure 2.20.

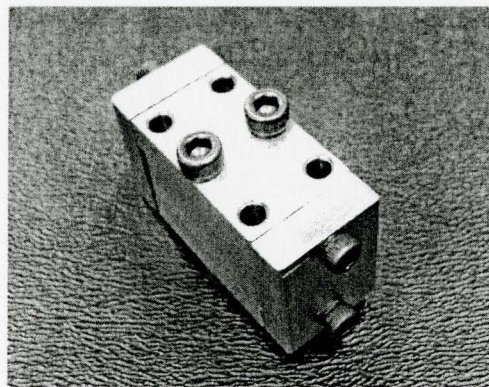


Figure 2.23 Assembled stainless steel mold for die casting BMG.

To fully prevent mold from reaction with casting alloy, electron beam-physical vapor deposition (EB-PVD) method was used to obtain compact and uniform pure alumina coating on all the mold internal surfaces. The coating was perfectly coherent with the mold material. Two sets of molds: one with a sandblasted surface, the other polished with a Dremel rotary tool with buffing wheel using high gloss polishing paste were coated with alumina in the same chamber resulting in a coating thickness of  $2\mu\text{m}$  which was verified by DEKTAK surface profile measuring system with precision of  $0.1\mu\text{m}$ .

### 2.3.4.3 Casting of Vit1 alloy

#### 2.3.4.3.1 Inert sealing process

Mold parts, screws, dowel pins and Vit1 sample were cleansed in an ultrasonic bath of acetone and then in ethanol. The calculated mass of Vit1 [14] alloy required to fill the mold cavity was determined to be 6.65g. Crystallized Vit1 rod in diameter of 10mm was crushed into small pieces with maximum size less than 4mm. Only 3.48g of Vit1 pieces could be inserted into the assembled mold cavity, 52.3% of total required mass, which shows estimated 25% more volume for Vit1 piece gap is still too low. Based on current result, the volume for holding required mass has to be at least 2.39 times of final solidified piece. The assembled mold was positioned within the quartz tube as shown in Figure 2.24 to achieve required test piece shape. Fired alumina silicate solid pieces and Inswool ceramic fiber blanket with operating temperature to 1300°C were used to guarantee that the mold was held upright as shown in Figure 2.25 (b). Considering liquid Vit1 may leak from the assembled mold gap at higher temperature, Respond 940HT, fast cure alumina adhesive was used to seal the gap on the bottom of assembled mold, which can withstand 1525°C [11]. The top small gap is left for degassing. 99.9 % zirconium pieces were sealed within the quartz tube to act as oxygen getters.

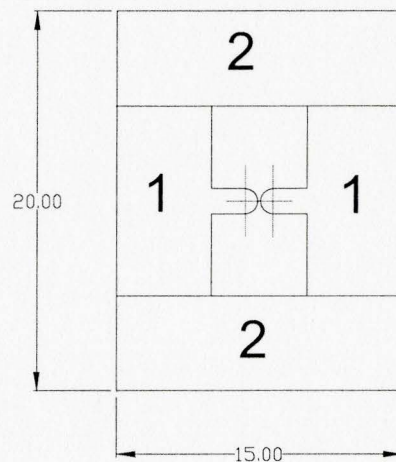


Figure 2.24 Schematic top view of mold within quartz tube.

The size of quartz tube for holding casting mold is ID: 35mm, OD: 38mm, length: 280mm. Another quartz rod with 6mm in diameter and length of 560mm was adhered to the quartz tube for easier quenching operation as shown in Figure 2.25 (a). To achieve total amorphous structure, slowest cooling rate within Vit1 alloy must be greater than its critical cooling rate, 1K/s. Helium was selected for inert atmosphere within the quartz tube to achieve a higher cooling rate. The quartz tube was evacuated to  $<4 \times 10^{-5}$  mbar and backfilled with HP plus helium with purity of 9.998% to 0.27atm. The He pressure at 800°C would be about 1 atm.

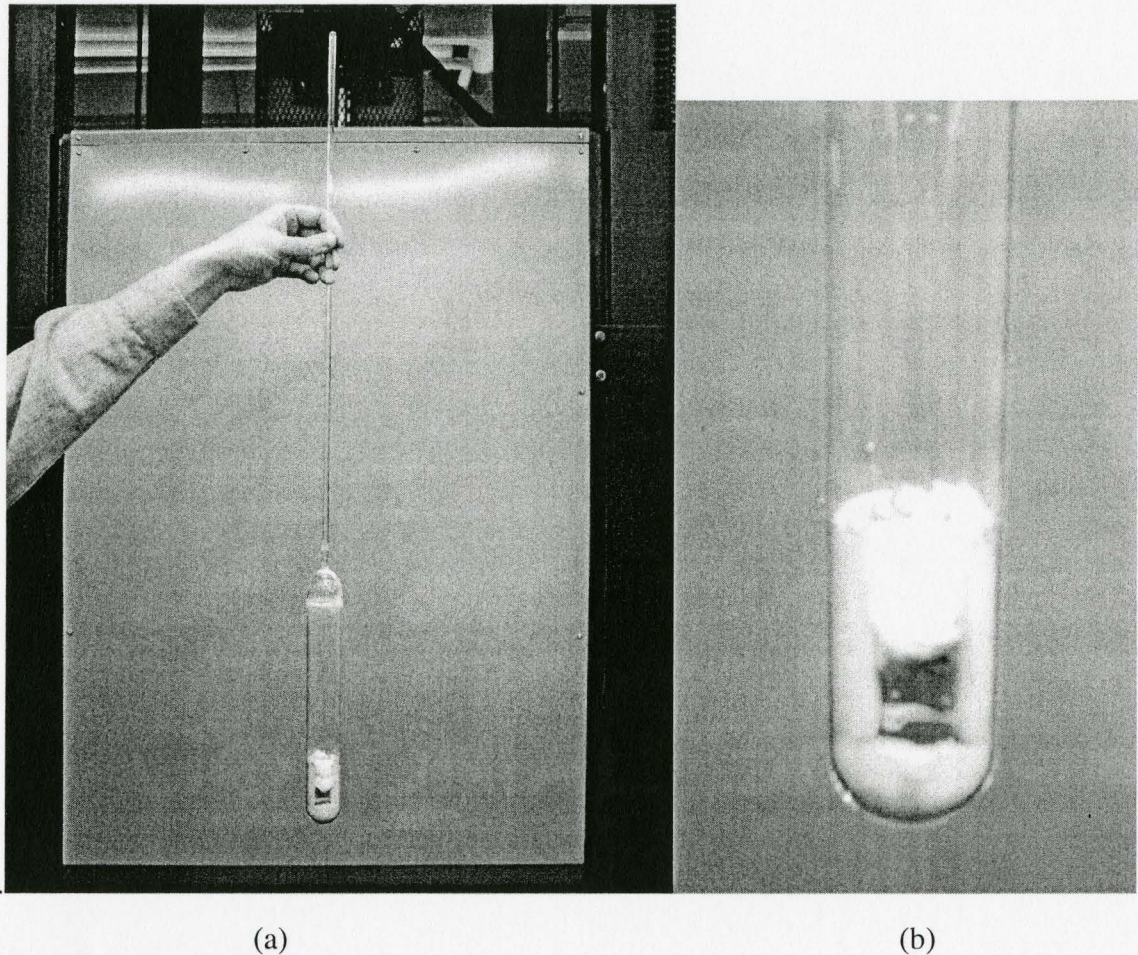


Figure 2.25 Assembled mold with Vit1 solid pieces inside sealed quartz tube.

### 2.3.4.3.2 Casting of the AGG pivot

Sealed quartz tube was heated into a furnace with cylindrical hearth. Two aluminum silicate parts were made as lids on the top of furnace to hold quartz tube vertically and for easier quenching operation as shown in Figure 2.26. Inswool ceramic fiber blanket was covered on furnace surface for better insulation. The quartz tube was slowly heated to 800°C at a heating rate of 50°C/hr, 80°C higher than its liquidus temperature at 720°C [15]. The quartz tube system was held at 800°C for 4 hours to ensure Vit1 alloy pieces were heated at this temperature. K type thermocouple with stainless steel sheath in diameter of 1.62 mm was bound with quartz tube to check furnace temperature. Before quenching the quartz tube in water, it was hit downward to the hearth bottom by hand several times in order to force the liquid alloy to enter 0.13mm gap in the mold center.

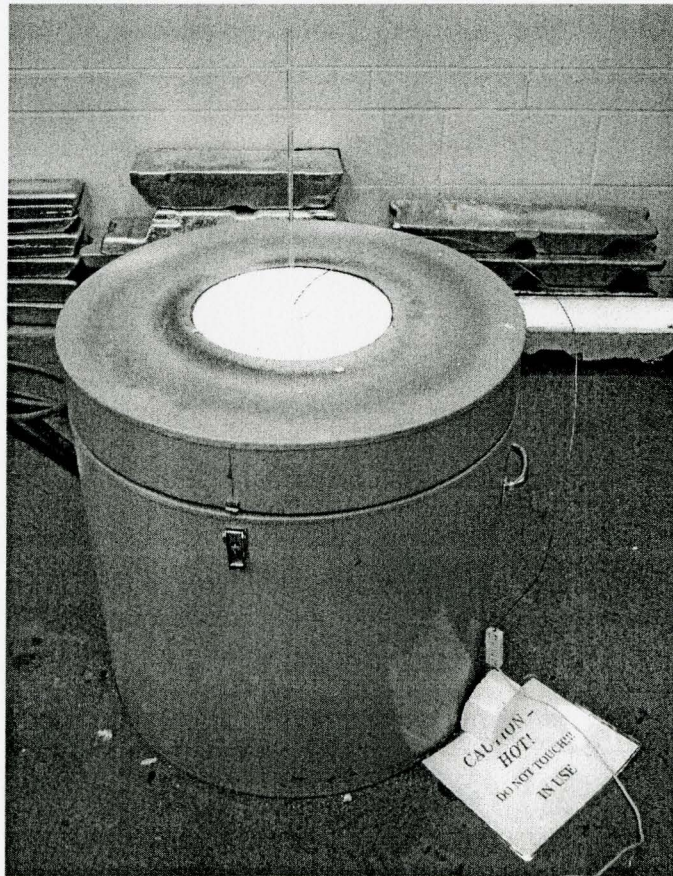


Figure 2.26 Quartz tube containing the metal mold is held inside an electric furnace.

The result shows that the quartz tube was not broken after quenching. Zirconium pieces and dowel pins are shining which shows the oxygen level is very low within the quartz tube. The as-quenched mold with Vit1 part is shown in Figure 2.27 after removing the top and bottom cap.

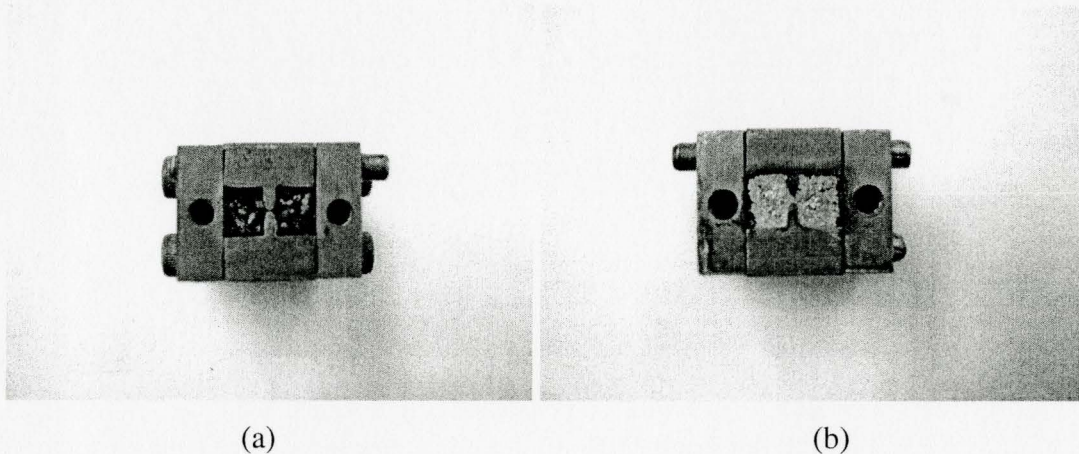


Figure 2.27 As-quenched mold with Vit1 part in it. (a) Top view and (b) Bottom view.

There is a thin layer of Vit1 formed on the mold bottom and alloy pieces retain solid shape on the mold top but adhere to each other, which shows liquid alloy pieces don't easily combine into a whole piece. The compression stress applied on liquid Vit1 pieces because of pressure head is greater on the mold bottom than on the top. Figure 2.27 (b) also shows liquid can successfully enter the 0.13mm gap which indicates it is possible to cast the AGG pivot piece by this method. To obtain a sound casting of the pivot piece, higher pressures need to be applied to within the mold cavity to ensure complete coalescence of the molten alloy pieces.

#### 2.3.4.4 Summary

1. Stainless steel 304 was selected as mold material. Uniform and compact pure alumina coating was successfully obtained on stainless steel mold by EB-PVD method.

2. Six mold parts were designed with assembled mold cavity of required size. Stainless steel 304 mold parts were obtained by milling process. Dowel pins and screws were used to assemble the mold parts together with the required cavity geometry.
3. Quenching of liquid Vit1 alloy within stainless steel mold sealed in inert atmosphere shows more pressure is required to press the liquid Vit1 pieces together to form a whole part. Quenching temperature and Vit1 mass can be increased to achieve this. Mold cavity volume should be enlarged to 2.39 times of required volume of final cast part to hold required mass.

### **2.3.5 Superplastic forming (Hot pressing) of BMG**

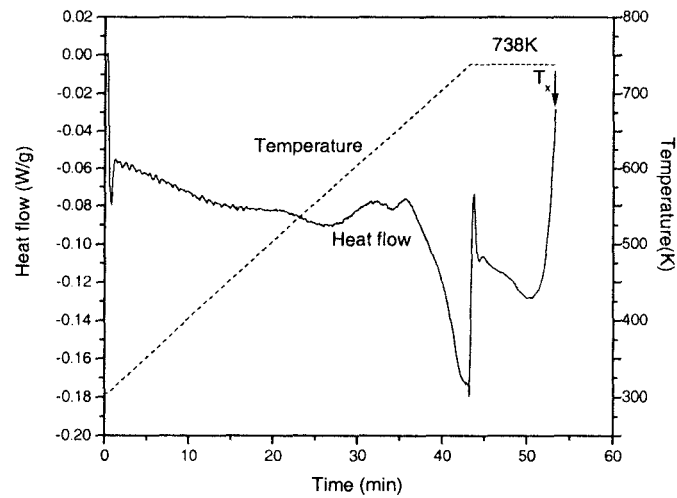
#### **2.3.5.1 Hot pressing of $\text{Cu}_{43}\text{Zr}_{43}\text{Al}_7\text{Ag}_7$ amorphous ribbons**

##### **2.3.5.1.1 Hot pressing conditions**

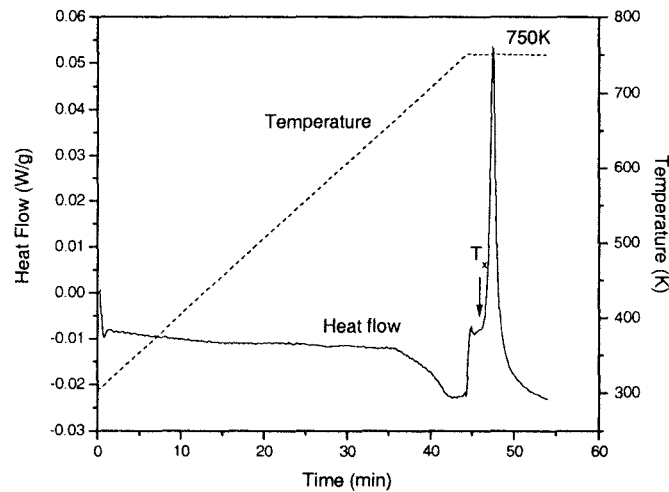
A detailed description of the SPF process is presented in section 2.3.3.2. Due to the metastable nature of metallic glass, thermal stability has to be investigated in the undercooled temperature range to find processing temperature and time to avoid phase transition, which affects the glass forming ability of superplastic forming by degradation of the viscous flow properties as well as mechanical properties. As the forming temperature is increased, the viscosity of the BMG alloy is decreased and aids the forming process. Also, the glass should not crystallize during processing which demands limited processing time. Parameters for hot pressing of  $\text{Cu}_{43}\text{Zr}_{43}\text{Al}_7\text{Ag}_7$  amorphous ribbons are found by DSC to meet the above SPF requirements.

Glass transition temperature  $T_g$  and crystallization onset temperature  $T_x$  vary with heating rate. The heating rate of hot press used for SPF is 10K/min, the temperature range for hot pressing was from  $T_g$  of 715K to  $T_x$  of 764K as shown in Table 2.9 in 2.3.2.5. The isothermal holding times for each processing temperature was determined from DSC experiments carried out on a TA Instrument DSC 910 equipment. Three test temperatures, 738K, 750K and 756K were selected. The DSC curves are shown in Figure 2.28. Time taken before crystallization is from the isothermal starting time to

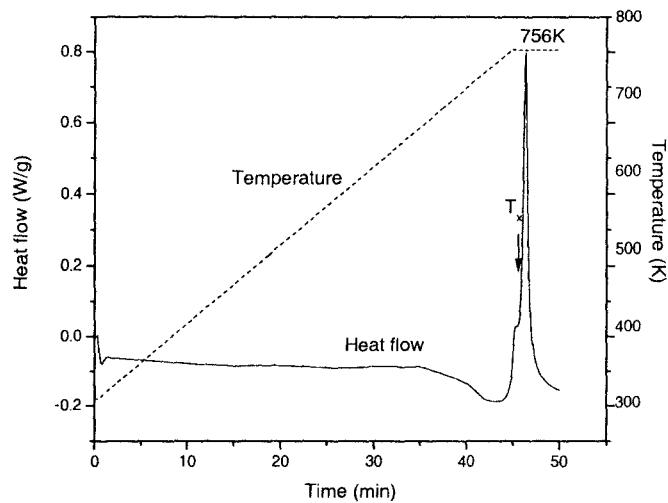
crystallization onset time, which is the maximum time period that undercooled  $\text{Cu}_{43}\text{Zr}_{43}\text{Al}_7\text{Ag}_7$  liquid pieces can retain amorphous structure without crystallization. The evaluated maximum undercooling time at isothermal temperatures of 738K, 750K and 756K were 9 min, 2.5 min and 1 min, respectively. 738K was chosen as hot pressing temperature for optimum operation conditions. As there is no available data on relationship between shear stress and shear rate for undercooled  $\text{Cu}_{43}\text{Zr}_{43}\text{Al}_7\text{Ag}_7$  alloy, a hot pressing stress of 100MPa was chosen for the experiments.



(a)



(b)



(c)

Figure 2.28 DSC curves for  $\text{Cu}_{43}\text{Zr}_{43}\text{Al}_7\text{Ag}_7$  alloy heated at constant heating rate of 10K/min and maintained at different isothermal temperatures: (a) 738K, (b) 750K and (c) 756K.

### 2.3.5.1.2 Selection of mold materials for hot pressing

The required mold material properties for hot pressing require a flexural strength of at least 100MPa at temperature range of 673-773K and greater coefficient of thermal expansion than the hot pressed alloy. The material h-BN is highly anisotropic in its mechanical properties due to the plate-like hexagonal crystals and their orientation during the hot press consolidation. The flexural strength is much lower than 100MPa parallel to pressing direction [16] which confines its use for hot pressing mold. Cotronics 902 and stainless steel 304 were selected as hot pressing mold materials. At the initial stage, hot pressing parameters were to be decided before the fabrication of web and hysteresis test pieces in complex shape. The molds were machined in cylinder as shown in Figure 2.29. Dimensions of the two sets of mold and plungers are shown in Table 2.11.

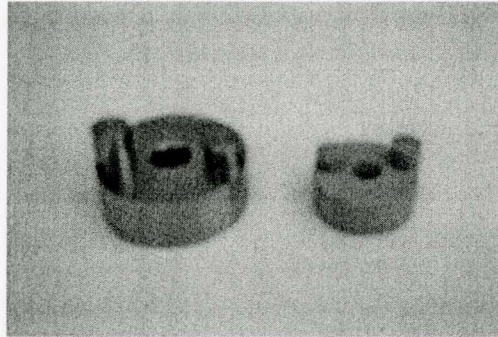


Figure 2.29 Hot pressing molds. Left: stainless steel and right: fired ceramic 902.

Table 2.11 Dimensions of molds and plungers for hot pressing

Material	Plunger 1	Plunger 2	Mold
Cotronics 902	$\Phi 8.0\text{mm} \times 4\text{mm}$	$\Phi 8.0\text{mm} \times 6\text{mm}$	ID: $\Phi 8.3\text{mm}$ OD $\Phi 25.4\text{mm}$ Height: 10mm
Stainless steel 304	$\Phi 9.22\text{mm} \times 5.03\text{mm}$	$\Phi 9.19\text{mm} \times 8.32\text{mm}$	ID: $\Phi 9.48\text{mm}$ OD: $\Phi 38.16\text{mm}$ Height: 13.13mm

Though Cotronics 902 has high compression strength of 262MPa, the flexural strength is only 96.53 MPa [17]. To test the maximum strength of cotronics 902 mold and plungers under same force condition, one set of the mold is pressed at room temperature on a small hydraulic pressing machine with the smaller plunger at bottom and the longer one on top. The top cotronics 902 plunger was broken when 500 pounds (2224.11N) load was applied at room temperature, equating pressure of 44.27MPa on it, which shows it can not be used for mold material at higher pressures. The tensile strength of stainless steel 304 can reach 137.2MPa [18] at temperature of 755K and the compression strength is higher than this value. So stainless steel 304 was chosen as mold material. White silk boron nitride was used as a barrier to prevent undercooled liquid from sticking to stainless steel molds and plungers.

### 2.3.5.1.3 Hot pressing of $\text{Cu}_{43}\text{Zr}_{43}\text{Al}_7\text{Ag}_7$ amorphous ribbons

As shown in section 2.3.2.2, amorphous  $\text{Cu}_{43}\text{Zr}_{43}\text{Al}_7\text{Ag}_7$  alloy cannot be obtained in bulk form. So melt spun amorphous ribbons will be used for hot pressing. There are methods on consolidation of amorphous metal powders into bulk form by explosive compaction [19, 20], dynamic compaction [21], high static pressure compaction [22], solid-state reaction [23] and extrusion [24] and rolling [25].

Hot pressing of  $\text{Cu}_{43}\text{Zr}_{43}\text{Al}_7\text{Ag}_7$  amorphous ribbons was carried out using 50-ton hot press within evacuated chamber backfilled with argon.  $\text{Cu}_{43}\text{Zr}_{43}\text{Al}_7\text{Ag}_7$  melt spun amorphous ribbons of  $30\mu\text{m}\times 1\text{mm}\times 4\text{mm}$  in size were given an ethanol ultrasonic wash prior to stacking into mold cavity. Heated from room temperature with heating rate of 10K/min, amorphous ribbons were kept at 738K for 3 minutes before 100MPa pressure was applied for 3min uniaxially onto the stainless steel plunger. The load was then removed and the furnace was shut off. When the mold was opened afterwards at room temperature, the alloy still remained as ribbons separate from each other as shown in Figure 2.30, which indicates the amorphous ribbons cannot be consolidated into bulk form as expected with the above test condition. The viscosity value of undercooled liquid metallic glasses at elevated temperature above  $T_g$  is found to be around  $10^8$  Pa s to  $10^9$  Pa s [2]. The large surface area/volume ratio of ribbons also requires much larger compression stress to enhance particle deformation and bonding simultaneously.

To obtain a bulk amorphous alloy of high uniform density, powder size, mold design and hot press processing parameters have to be optimized in the future.



Figure 2.30  $\text{Cu}_{43}\text{Zr}_{43}\text{Al}_7\text{Ag}_7$  alloy ribbons after hot pressing operation.

Considering that the temperature shown on the furnace read out may not represent the actual temperature of ribbons, a through hole with 2mm in diameter for K type thermocouple was obtained by electrical discharge machining (EDM) along the radial direction and on the top part of the stainless steel mold. The thermocouple tip was kept within the hole by adhering it with the mold using ceramic putty to avoid blocking the movement of the plunger. Temperature shown by the thermocouple gave the actual temperature of amorphous alloy powder within the mold cavity.

Because of the breakdown of the 50-ton hot press at McMaster University, further experiments could not be carried out. The stress limit of graphite pressing head also impedes further experiments. In the following section, previous SPF work on bulk amorphous Vit1 and Vit4 will be discussed.

#### **2.3.5.2 SPF of Vit1 and Vit4**

As candidate AGG pivot materials, Zr-Ti-Cu-Ni-Be glasses have good resistance against crystallization in the supercooled liquid state [26,27] and have excellent glass forming abilities. Previous study shows Vit1 rod can be forged into fully amorphous micropart at 673K with applied stress of 254MPa for 200s with no protection of inert

gases [28]. It was reported that Vit4 alloy is more stable than Vit1 because of lower Zr and Be levels in Vit 4 [29, 30]. Amorphous phase of Vit4 can remain sufficiently stable for 5h and 3h, respectively at 643K and 653K under small loads with newtonian flow behavior. Strain of 5 was attained at 653K with pressure of 5MPa resulting in microparts of less than 100  $\mu\text{m}$  dimensions with excellent precision [31]. Since, Vit4 has much lower flowing stress than Vit1, the requirements for related facilities, such as mold material, maximum compression stress of press, etc. are much lower and easily attainable with the hot press at McMaster University. So Vit4 is a better candidate material than Vit1 for net shape manufacturing of AGG pivot part by SPF.

### 2.3.5.3 Summary

1. Experiments of DSC on  $\text{Cu}_{43}\text{Zr}_{43}\text{Al}_7\text{Ag}_7$  alloy amorphous ribbons show that maximum undercooling time at isothermal temperatures of 738K, 750K and 756K are 9 min, 2.5 min and 1 min, respectively with constant heating rate of 10K/min.
2.  $\text{Cu}_{43}\text{Zr}_{43}\text{Al}_7\text{Ag}_7$  melt spun amorphous ribbons can not be consolidated with uniaxial compression stress of 100MPa at 738K for 3 minutes.
3. Vit1 and Vit4 alloy rod will be used for superplastic forming of AGG pivot piece. Vit4 is a better candidate material than Vit1 for SPF because of more thermal stability, lower flowing stress and much broader processing window in the low viscous state.

## References

- [1] Bob Smith, Rio Tinto exploration, Gradiometer stage 1b/1c report, P.ii.
- [2] B. V. Tryggvason, Geophysical Research Abstracts, **5**, 02913 (2003).
- [3] S. J. Thorpe, P. Borges, S. Shankar, Y. Li, K.A. Carroll and B. French, MMO project # NM40340, Progress report #1.
- [4] H. J. Paik, J. Appl. Phys., **47**, 1168 (1976).
- [5] K. A. Carroll, personal communication with Gedex Corporation, 6 May 2005.
- [6] M.F. Ashby and A. L. Greer, Scripta Materialia, **54**, 321 (2006).
- [7] Jan Schroers, JOM, 35 May (2005).
- [8] R. Busch, JOM, **52(7)**, 39 (2000).
- [9] Th. Zumkley, S. Suzuki, M. Seidel, S. Mechler and M.-P. Macht, Materials science forum, **386-388**, 541 (2002).
- [10] Y. Saotome, K. Imai, S. Shioda, S. Shimizu, T. Zhang and A. Inoue, Intermetallics **10**, 1241 (2002).
- [11] <http://www.cotronics.com/vo/cotr/pdf/902.pdf>.
- [12] <http://www.azom.com/details.asp?ArticleID=78>.
- [13] <http://www.assda.asn.au/asp/index.asp?pgid=17969>.
- [14] Ghatu Subhash, Robert J. Dowding, Laszlo J. Kecskes, Materials Science and Engineering **A334**, 33 (2002).
- [15] A. Pecker and W. L. Johnson. Appl. Phys. Lett. **63**, 2342 (1993).
- [16] <http://www accuratus.com/boron.html>.
- [17] <http://www.cotronics.com/vo/cotr/pdf/902.pdf>.
- [18] Donald Peckner and I.M. Bernstein, Handbook of stainless steel, 21-5 (1977).
- [19] C. F. Cline, and R. W. Hopper, Scr. Metall. **11**, 1137 (1977).
- [20] M. Takagi, Y. Kawamura, M. Araki, Y. Kuroyama and T. Imura, Mater. Sci. Eng., **98**, 457 (1988).
- [21] D. G. Morris, J. Mater. Sci., **17**, 1789 (1982).

- [22] Y. Kawamura, M. Takagi, M. Senoo and T. Imura, *Mater. Sci. Eng.*, **98**, 415 (1988).
- [23] R. B. Schwarz and W. L. Johnson, *Phys. Rev. Lett.*, **51**, 415 (1983).
- [24] Y. Kawamura, M. Takagi and M. Akai, *Mater. Sci. Eng.*, **98**, 449 (1988).
- [25] P.H. Shingu, *Mater. Sci. Eng.* **97**, 137 (1988).
- [26] W. L. Johnson, *MRS Bulletin*, **24**, 2-56 (1999).
- [27] A. Inoue, *Bulk Amorphous Alloys*, *Materials Science Foundations*, **4**, Trans Tech Publications, Zürich (1998).
- [28] G. Wang, J. Shen, J.F. Sun, Y.J. Huang, J. Z. Zou, Z.P. Lu, Z.H. Stachurski, B.D. Zhou, *J. of non-crystalline solids*, **351**, 209 (2005).
- [29] A. Wiedemann, J. M. Liu, *Sol. State Comm.* **100**, 331 (1996).
- [30] S. Schneider, P. Thiagarajan, U., Geyer, W.L. Johnson: in *MRS Symp. 295*, MRS Pittsburgh, PA, USA, Proc., (1997).
- [31] Th. Zumkley, S. Suzuki, M. Seidel, S. Mechler and M.-P. Macht, *Materials Science Forum*, **386-388**, 541 (2002).

## **Chapter 3 Theoretical Model for Predicting Glass Forming Ability of Metallic Glasses**

### **3.1 Glass Forming Ability (GFA)**

Glass Forming Ability (GFA) is defined as the ability for a given alloy to form an amorphous component when cooled from liquid state, which is indicated by the critical size or critical cooling rate of metallic glasses. Critical size is the maximum value for a given alloy to achieve total amorphous structure which can be ascertained by x-ray or high-resolution transmission electron microscope (HTEM). It follows that alloys exceeding critical size must include some amount of detectable crystalline phases. Different metallic glasses have quite different critical size, which ranges from micrometers to centimeters as shown in Appendix B. Since critical size of metallic glasses can only be obtained by experiments and this value depends on specific experimental parameters, comparison of GFA of different materials by this value is not accurate and can only be used as a reference under the same experimental method. Another indicator of GFA is critical cooling rate, which is the minimum cooling rate within the whole alloy piece to guarantee the full glassy phase. There are experiments on Zr-Ti-Cu-Ni-Be [1,2,3] and Pd-Cu-Ni-P alloy [4,5] which gave the critical cooling rates. One method is measuring the continuous cooling curve by casting the molten alloy into a wedge-shape copper mold. The absence of the recalescence in the entire solidification

process indicates no crystalline phase forms at corresponding position. Although this method gave the instant critical cooling rate at specific position, the heat transfer condition was not specified. Another method is cooling the molten alloy at constant cooling rates by using differential thermal analyzer. If no exothermic peak is observed, the resulting structure is amorphous. The obtained value by this method is actually an average one for the whole sample (normally in mg weight level) in the absence of flux medium under no control over the heat flow direction. As phase formation during the solidification process is directly related to how heat is extracted, it is essential to consider how amorphous structure can be achieved under uni-directional solidification and thus the underlying mechanism can possibly be disclosed.

Obviously, the larger the critical size and lower the critical cooling rate, the higher GFA. In 1995, X.H. Lin and W. L. Johnson [6] proposed a simple equation estimating the critical cooling rate by relating it to critical size which is known through experiment. Despite a convenient method, inherently it is an average cooling rate from melting temperature  $T_m$  to glass transition temperature  $T_g$  rather than instant critical cooling rate.

### 3.1.1 Summary of popular parameters used to indicate the GFA of a BMG

Various GFA indicators have been proposed and listed as following.

- Reduced glass transition temperature  $T_{rg}=T_g/T_l$ . This parameter describes the kinetic ability to avoid crystallization during cooling and predicts that alloys forming deep eutectic reactions are preferable for glass formation upon cooling a liquid. Generally alloys having higher  $T_{rg}$  exhibit better GFA [7]. Where  $T_g$  is glass transition temperature and  $T_l$  is liquidus temperature.
- Supercooled liquid region  $\Delta T_x = T_x - T_g$ , predicts the stability of glassy phase, where  $T_x$  is the onset crystallization temperature. This parameter is often used as a parameter that describes the superplastic formability of BMGs.
- $\gamma$  parameter=  $T_x/(T_l + T_g)$  [8]. It predicts stability of liquid and kinetic ability to resist crystallization, which is obtained by simple additive assumption of

devitrification tendency of a glass and suppression of crystallization during solidification.

- $\Delta T^* = [T_m^{mix} - T_i] / T_m^{mix}$ , predicts the stability of liquid phase [9]. Where  $T_m^{mix} = \sum_i^n n_i \cdot T_m^i$ .  $n_i$  is mole fraction and  $T_m^i$  is the melting point of constituent i.
- $\sigma$  parameter [10] =  $\Delta T^* \times P'$ . Where  $P' = \frac{X_B}{X_B + X_C} \left| \frac{(V_B - V_A)}{V_A} \right| + \frac{X_C}{X_B + X_C} \left| \frac{(V_C - V_A)}{V_A} \right|$

It predicts the stability of liquid and atomic size configuration and can only be used for ternary alloy system.  $X_i$  represents concentration of solution i.  $V_i$  represents atomic volume of solution i.

Although the above empirical GFA indicators present some guidelines for alloy design, they do not show a consistent trend [11,12] and related value of parameters  $T_b$ ,  $T_x$ , and  $T_g$  can only be obtained after the alloy is developed. Development of new BMGs with precise composition still largely depends on repeated adjustment of alloy compositions [13,14,15]. Also, as discussed above, quantitative relationship between GFA and heat transfer conditions failed to be derived so far, which is most important in practical manufacturing process.

### 3.1.2 Review of prior art - Identifying the best GFA alloys by competitive growth principle approach

Ma et al [16] proposed a strategy for pinpointing the best glass-forming alloys, which applies competitive-growth principle [17] and treats glass as a competing phase during solidification. The criterion of achieving amorphous structure is that glass transition temperature,  $T_g$  should be higher than the growth tip temperature,  $T_i^x$  of all the possible crystalline phases at the same growth rate,  $V$ . For example, lets consider the simplest system such as a binary alloy. Let the possible crystalline phases be  $\alpha$ ,  $\beta$  and the eutectic phases. The solid growth tip temperature of these phases is a function of temperature gradient  $G$ , growth rate  $V$ , diffusion coefficient  $D$  of solute in the liquid. Neglecting the effects of  $G$  at high  $V$ , Ma et al [16] developed the composition range

possessing the best GFA which explained the phenomenon that the optimum GFA are often at an off-eutectic composition in binary alloy systems such as Al-Ge, Ca-Mg, Ca-Al and Ca-Zn. Reflected from phase diagrams, the glass-forming region is enclosed by composite-forming regions. Thus, by examining the structure transition of composite-forming regions, the optimum composition region can be ascertained for a given alloy. Though the equations for pinpointing the best glass-forming alloys were given, the authors still use it as a rule qualitatively rather than quantitatively. Furthermore, the applied expression of tip temperature relating to growth rate actually is at quasi-steady state, while for actual fast solidification process, the crystalline phases grow under unsteady state conditions.

### **3.2 Objective of the Present Model**

The objective is to develop a predictive model to ascertain a relationship among alloy composition, critical size and heat transfer parameters under uni-directional heat conduction conditions through competitive growth principle, which will provide exact solutions for the critical size of the cast component using BMG alloy attainable under feasible casting conditions presently available. The instant critical cooling rate indicating GFA of a particular alloy can also be derived. It will vastly reduce the time spent on the design of the component and materials used for the component. Before presenting the model development, related fundamental concepts will be explained in subsequent sections.

### **3.3 Development of Theoretical Model to Predict GFA**

#### **3.3.1 Competitive growth principle**

##### **3.3.1.1 Concepts**

Tammann and Botschwar [17] observed differences in growth rate among the various crystalline phases as a function of temperature and found that those phase with the highest growth rate,  $V$  for a given undercooling  $\Delta T$ , developed and the other phases were suppressed. This criterion is analogous to stating that the observed structures have a

minimum extent of undercooling for a given growth rate. It is a very similar principle to that of bifurcation theory in mathematical physics, but has not been rigorously justified.

### 3.3.1.2 Applications

This theory is applied to calculate the coupled zone, which is defined as the range of conditions (generally composition and undercooling values) that produces a wholly eutectic structure, i.e. without primary crystals not taking into account the planar-cellular eutectic transition [18]. Figure 3.1 [19] shows the darked area is coupled zone in a phase diagram of binary alloy, which can be skewed (a) or symmetric (b). The coupled zone (V-C diagram) and growth rate relationship of various competing phases, primary phases  $\alpha$ ,  $\beta$  and eutectic phase are shown in Figure 3.2 [19].

The half width of symmetric zone(eutectic range)  $\Delta C = C_E - C_\infty$  is found by equating dendrite tip temperature  $T_D$  to eutectic tip temperature  $T_I$ , where  $C_E$  is the eutectic composition and  $C_\infty$  is the average alloy composition.

$$\text{Dendrite undercooling } \Delta T_D = T_I - T_D = \frac{GD}{V} + BV^{\frac{1}{2}} \quad (3.1)$$

$$\text{Eutectic undercooling } \Delta T_E = T_E - T_I = AV^{\frac{1}{2}} \quad (3.2)$$

Where  $T_I$  is the alloy liquidus temperature,  $T_E$  is the eutectic equilibrium temperature,  $G$  is the temperature gradient and  $V$  is the growth rate,  $A$  and  $B$  are constants. Subtracting Equation 3.2 from 3.1, we get,

$$T_I - T_E = \frac{GD}{V} + (B - A)V^{\frac{1}{2}} \quad (3.3)$$

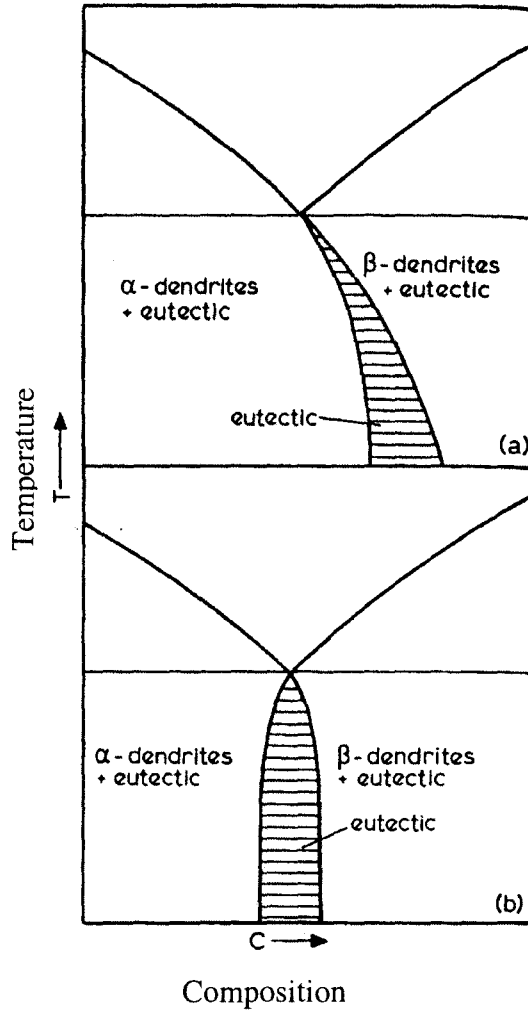


Figure 3.1 Two type of coupled zone in a binary eutectic reaction: (a) Skewed zone (b) Symmetric zone [19].

And since  $T_1 - T_E = m(C_\infty - C_E)$ , where  $m$  is the liquidus slope of one phase. Replacing the left side in Equation 3.3, we get,

$$\Delta C = C_E - C_\alpha = -\frac{1}{m} \left[ \frac{GD}{V} + (B - A)V^{\frac{1}{2}} \right] \quad (3.4)$$

Equation (3.1) and (3.2) are derived under quasi-steady state directional solidification conditions. The derivation of these equations will be presented in following sections.

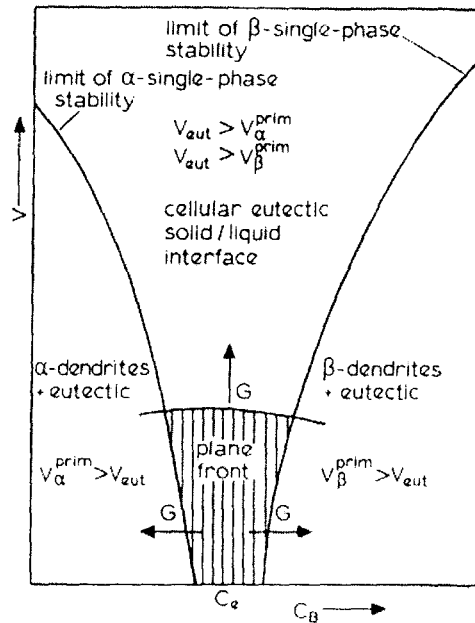


Figure 3.2 Coupled zone (V-C diagram) and growth rate relationship of various competing phases

### 3.3.2 Strategy of developing the model

As discussed in chapter 1, glass formation is actually a kinetic process of avoiding crystallization when liquid alloy is cooled from  $T_1$  to  $T_g$ . For a binary alloy, the possible alloy composition to form amorphous structure is close to eutectic composition, where primary and eutectic phases can possibly form as shown in calculating eutectic composition range (coupled zone) in section 3.3.1.2.

In the case of an amorphous alloy, when we apply the competitive growth principle, we consider that the amorphous phase is also one of the competing phases in growth. For example, in a binary alloy system, the possible amorphous phase competes to grow along with the three possible crystalline phase regions: primary  $\alpha$ , primary  $\beta$  and eutectic region. The suppression of all crystalline phases during solidification and the growth of exclusive amorphous phase occur when the growth velocity of the solid-liquid interface is greater than or equal to the critical growth velocity of the amorphous phase,  $V_g$  for a given undercooling,  $\Delta T$  for the liquid.

The criterion for achieving amorphous structure is as follows:

For the same interface undercooling  $\Delta T = T_l - T_g$ , i.e. same interface temperature  $T_g$ , growth rate of glassy phase  $V_g$  is greater than growth rate of all possible crystalline phases,  $V_i^x$ .

$$V_g \geq V_i^x \quad (3.5)$$

where  $V_i^x = V_l^\alpha$ ,  $V_l^\beta$  or  $V_l^{eu}$  (tip growth rate of  $\alpha$ ,  $\beta$  and eutectic phase, respectively).

A flow chart defining the steps involved in predicting formation of BMG is shown in Figure 3.3.

Once the relationships between tip temperature and  $V$ ,  $G$ ,  $D$  are found, as  $T_i^x$  is related with  $C_i^x$  by  $m$ , composition range for best GFA can be derived.

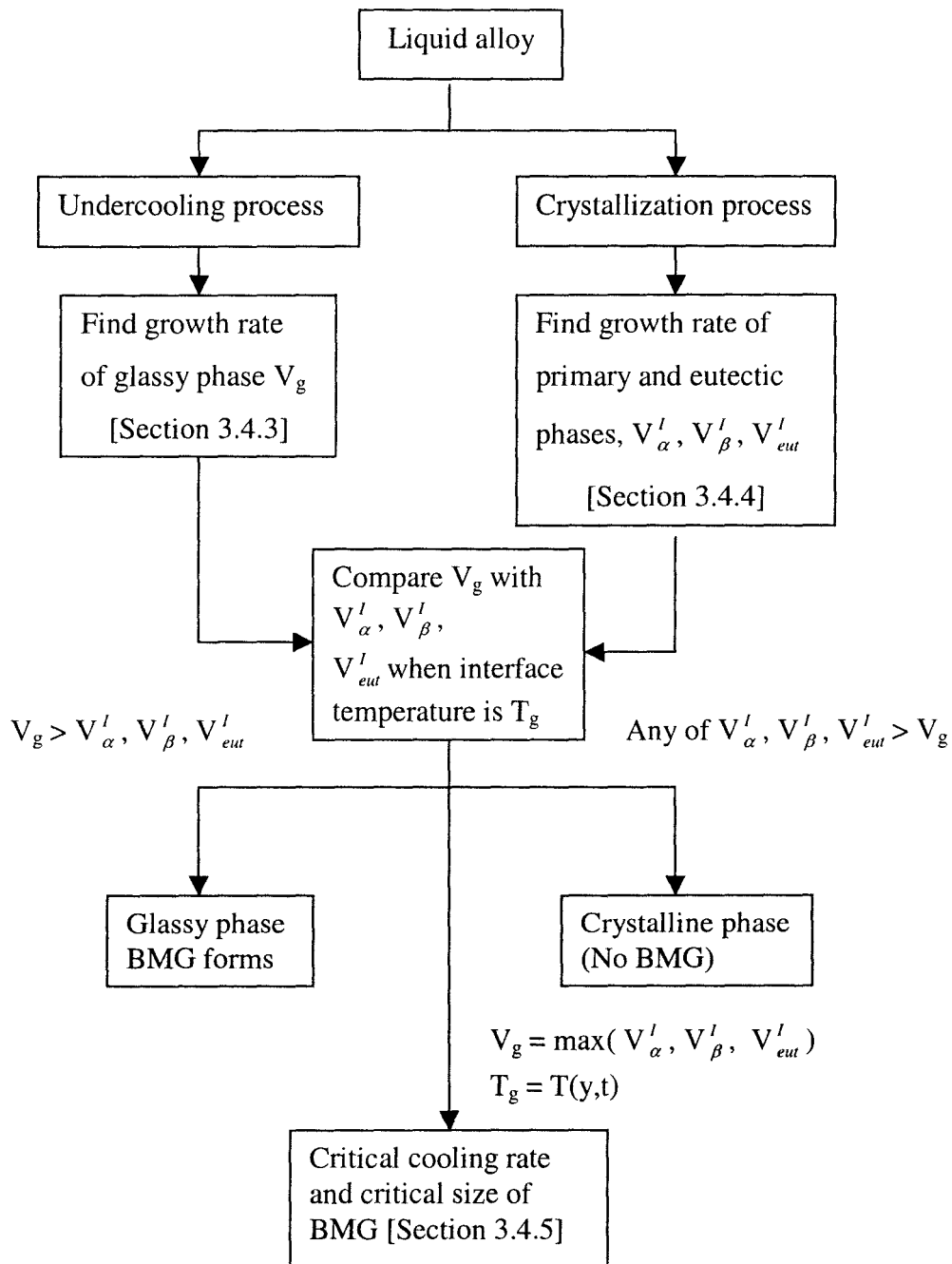


Figure 3.3 Process flow for predicting GFA of BMG

Let's consider the simplest one direction heat conduction in plate (Cartesian coordinates) for a binary alloy, two cases will be discussed during solidification process. Initially, the binary liquid at liquidus temperature,  $T_l$  occupies a volume that is infinite in

positive  $y$  direction. Heat is extracted uni-directionally along negative  $y$  direction from the semi-infinite volume at  $y=0$ . The planes perpendicular to  $y$  direction are all well insulated, as shown in Figure 3.4.

The boundary conditions are:

$$-k \frac{\partial T(0,t)}{\partial y} = h(T(0,t) - T_w) \quad (\text{heat balance at } y = 0) \quad (3.6)$$

$$\frac{\partial T(\infty,t)}{\partial y} = 0 \quad (3.7)$$

Where  $T_w$  represents constant temperature of substrate at  $y=0$ .

Initial condition is:

$$T(y,0)=T_1 \quad (3.8)$$

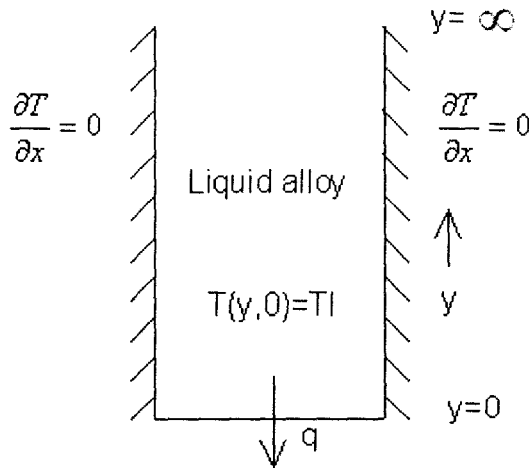


Figure 3.4 Uni-directional heat conduction.

Two cases are considered here under the same heat transfer conditions.

**Case 1:** Assuming no crystalline phases can be formed above  $T_g$ , the glassy phase is thus obtained as shown in Figure 3.5 (a). The equations to illustrate this process are presented in section 3.4.3.

**Case 2:** Assuming crystalline phases can be formed above  $T_g$ , the solidified phases are obtained as shown in Figure 3.5 (b). The local growth conditions are calculated for both eutectic and primary phases  $\alpha$  and  $\beta$ , respectively. The equations to illustrate this process are presented in section 3.4.4.

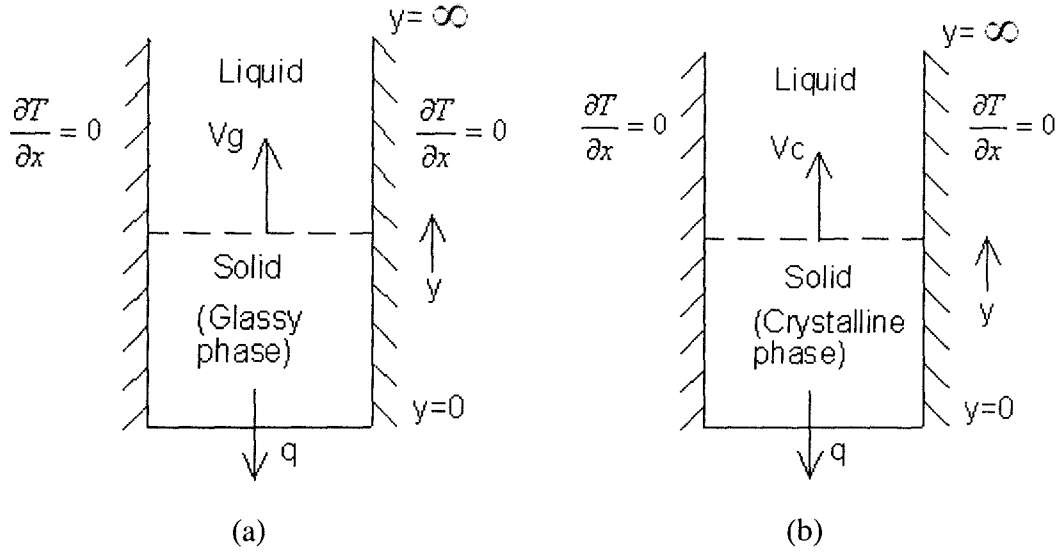


Figure 3.5 Uni-directional heat conduction from liquid bottom. (a) Solid is glassy phase; (b) Solid is crystalline phase.

### 3.3.3 Developing tip temperature $T_g$ -growth rate $V_g$ relationship for solidified amorphous structure

During the cooling process from the liquidus temperature  $T_l$ , no phase transformation occurs and the liquid is continuously undercooled till amorphous solid is finally formed at  $T_g$ , where exothermic heat flow shown in DSC curve is caused by change of physical parameters such as heat capacity etc. rather than latent heat of fusion.

Assume liquid is isotropic and homogeneous, the governing equation is:

$$\frac{\partial(\rho C_p T)}{\partial t} = -\frac{\partial q_y}{\partial y} \quad (3.9)$$

where  $q_y = -k \frac{\partial T}{\partial y}$ .  $\rho$ ,  $C_p$  and  $k$  are functions of temperature.

Boundary conditions and initial condition are the same as equations (3.6), (3.7) and (3.8).

Temperature  $T(y, t)$  can be derived though equations (3.6) to (3.9).

Growth rate of glassy phase can be derived as

$$V_g = \frac{\partial T(y, t) / \partial t}{\partial T(y, t) / \partial y} \Big|_{T=T_g} \quad (3.10)$$

### 3.3.4 Developing undercooling-growth rate relationship of crystalline phases (single phase & eutectic, equations)

Since  $\frac{\alpha}{D} = 10^4$  ( $\alpha$  is the thermal diffusivity and  $D$  is mass diffusivity), rate of heat transfer is much larger than the rate of mass transfer. The crystallization process is mass transfer controlled.

#### 3.3.4.1 Quasi-steady state directional solidification of primary phases $\alpha$ and $\beta$

M. H. Burden and J. D. Hunt proposed approximate analytical solutions for non-isothermal dendrites which grow under an imposed temperature gradient [20].

The governing equation is 
$$\frac{1}{D} \frac{\partial C}{\partial t} = \frac{\partial^2 C}{\partial y^2} \quad (3.11)$$

By coordinating transformation,  $V$  is the growth rate of primary phases.

$y' = y - Vt$ , where  $x'$  is the distance to the tip of crystalline phases.

Using coordinates moving with the dendrite tip, as

$$\frac{\partial C}{\partial t} = \frac{\partial C}{\partial y'} \frac{\partial y'}{\partial t} + \frac{\partial C}{\partial \tau} \frac{\partial \tau}{\partial t}$$

and  $\frac{\partial \tau}{\partial t} = 1$  and  $\frac{\partial x'}{\partial t} = -v$ ,

Combining above equations with Eq. (3.10)

$$\frac{\partial C}{\partial t} = -v \frac{\partial C}{\partial y'} + \frac{\partial C}{\partial \tau} = D \frac{\partial^2 C}{\partial y'^2} \quad (3.12)$$

At quasi-steady state,  $\frac{\partial C}{\partial \tau} = 0$

Thus governing equation (3.12) takes the form

$$D \frac{d^2 C}{dy'^2} + v \frac{dC}{dy'} = 0 \quad (3.13)$$

Where  $D$  is the liquid diffusion coefficient.

Boundary conditions are:

(1) The continuity of matter equation at the interface leads to

$$\left(\frac{dC}{dy'}\right)_{y'=0} = -\frac{v}{D_L} C_l (1-k) \quad (3.14)$$

Where  $c_l$  is the composition at the tip and  $c_l > c_0$ , liquid concentration at infinity,

$$\text{equilibrium partition ratio } k = \frac{C_S^*}{C_L^*}$$

$$(2) \lim_{y' \rightarrow \infty} C = C_0 \quad (3.15)$$

Undercooling  $\Delta T = \Delta T_D + \Delta T_\sigma + \Delta T_K$

Where  $\Delta T = T_1 - T_l$ , total undercooling,  $T_1$  is the interface temperature.

$\Delta T_D = m(C_0 - C_l)$ , undercooling due to the local concentration in the liquid at Liquid/solid interface.

$\Delta T_\sigma = \theta (R_1^{-1} + R_2^{-1})$ , undercooling due to the Gibbs-Thompson effect acting at curved interfaces.

$\Delta T_K$  is kinetic undercooling and small enough to be neglected comparing to  $\Delta T_D$  and  $\Delta T_\sigma$ .

Final form of  $\Delta T$  is as following:

$$\Delta T = \frac{GD}{V} - \frac{mVR}{D} (1-k) C_\infty + \frac{2\theta}{R} \quad (3.16)$$

$$\text{Where } \frac{dT_l}{dy} = G = m \frac{dC_l}{dy} = m \frac{d\bar{C}}{dy}$$

$R$  is the radius of curvature,  $m$  is liquidus slope.  $\bar{C}$  is the composition averaged across the interface,  $G$  is the temperature gradient.

Differentiating eq.(3.15) with respect to  $R$  at constant  $V$  gives the minimum of  $\Delta T$  (Minimum undercooling condition is assumed)

$$\Delta T = T_l - T_1 = \frac{GD}{V} + 2^{\frac{3}{2}} [-mV(1-k)C_0\theta]^{\frac{1}{2}} / D^{\frac{1}{2}} \quad (3.17)$$

Where  $\theta$  is Gibbs-Thompson coefficient.

Thus, analytical equation of tip temperature  $T_1$  relating to growth rate  $V$  and temperature gradient  $G$  is derived under quasi-steady state. The growth rate of primary phases  $\alpha$  and  $\beta$ ,

$V'_\alpha$  and  $V'_\beta$ , when tip temperature is  $T_I$  under quasi-steady state can be found from following equation

$$T_l - T_I = \frac{GD}{V'} + 2^{\frac{3}{2}} [-mV'(1-k)C_0\theta]^{\frac{1}{2}} / D^{\frac{1}{2}} \quad (3.18)$$

Where  $V'$  represents the growth rate of primary phases  $\alpha$  or  $\beta$  when tip temperature is  $T_I$ .

### 3.3.4.2 Unsteady-state directional solidification of primary phases $\alpha$ and $\beta$

Using coordinates moving with the tip,

The governing equation is

$$D \frac{\partial^2 C}{\partial y'^2} + V \frac{\partial C}{\partial y'} = \frac{\partial C}{\partial \tau} \quad (3.19)$$

Same as equation (3.11) using coordinates moving with the dendrite tip.

Boundary conditions are as follows:

(1) Considering continuity of mass at the liquid/solid interface,

$$\left( \frac{\partial C(0,t)}{\partial y'} \right)_{y'=0} = -\frac{V}{D_L} C_l (1-k) \quad (3.20)$$

$$(2) C(\infty, t) = C_0 \quad (3.21)$$

$$\text{Initial condition: } C(y', 0) = C_0 \quad (3.22)$$

If curvature effects and kinetic undercooling are ignored, then

$$\Delta T = T_l - T_I = \Delta T_D = m (C_0 - C_l) \quad (3.23)$$

Interface temperature  $T_I$  involving  $V$ ,  $G$ ,  $m$ ,  $D$ ,  $k$  can be derived from equations (3.19) to (3.23) by numerical method. Growth rate of primary phases  $\alpha$  and  $\beta$ ,  $V'_\alpha$  and  $V'_\beta$ , when tip temperature is  $T_I$  under un-steady state can be found by equating  $T_I$  with  $T_g$ .

### 3.3.4.3 Quasi-steady state directional solidification of lamellar eutectic phase

For quasi-steady state growth with the coordinate system moving with velocity  $V$  in the  $y$  direction, K.A. Jackson & J.D. Hunt proposed the analytical solution [21]

The diffusion equation is,

$$\frac{\partial^2 C}{\partial y^2} + \frac{V}{D} \frac{\partial C}{\partial y} = 0 \quad (3.24)$$

Which is the governing equation.

Boundary conditions are

$$(1) C=C_E + C_\infty \text{ at } y=\infty \quad (3.25)$$

$$(2) \frac{\partial C}{\partial x}=0 \text{ at } x=0 \text{ and } x= S_\alpha + S_\beta \quad (3.26)$$

$C_\infty$  is the difference between the eutectic composition and actual composition far from the interface.

Conservation of mass at the interface leads to

$$\left(\frac{\partial C}{\partial y}\right)_{y=0} = -\frac{(1-k^\alpha)C(x,0)}{D} \quad 0 \leq x \leq S_\alpha \quad (3.27)$$

$C(x,0)$  is the composition at the interface

$$\left(\frac{\partial C}{\partial y}\right)_{y=0} = -\frac{(1-k^\beta)C(x,0)}{D} \quad S_\alpha \leq x \leq S_\alpha + S_\beta \quad (3.28)$$

$$\Delta T = \Delta T_c + \Delta T_\sigma = m[C_E - C(x)] + a/r(x) \quad (3.29)$$

Where  $m$  is the slope of the liquidus and  $C(x)$  is the composition of the interface at  $x$ . “ $a$ ” is a constant given by the Gibbs-Thompson relationship and  $r(x)$  is the local curvature of the interface.

The final form of relationship between undercooling  $\Delta T$  and growth rate  $V$  is

$$\frac{\Delta T^2}{V} = 4m^2 a^L Q^L = K_e \quad (3.30)$$

Where  $K_e$  is a constant as  $m$ ,  $a^L$  and  $Q^L$  are constants, which can be found from experiments. So growth rate of eutectic phase is

$$V'_{eut} = \frac{(T_l - T_g)^2}{K_e^2} \quad (3.31)$$

### 3.3.4.4 Unsteady state directional solidification of lamellar eutectic phase

The diffusion equation is

$$\frac{\partial^2 C}{\partial y^2} + \frac{V}{D} \frac{\partial C}{\partial y} = \frac{\partial C}{\partial t} \quad (3.32)$$

which is the governing equation.

The same boundary conditions and conservation of matter at the interface as quasi-steady state are applied here as shown in equations (3.25) to (3.28),

Initial condition is

$$C(y,0) = C_E + C_\infty \quad (3.33)$$

Undercooling

$$\Delta T = \Delta T_c = m[C_E - C(x)] \quad (3.34)$$

Interface temperature can be found by equations (3.24) to (3.28), (3.33) and (3.34) by numerical method. The growth rate of eutectic phase under unsteady state can be found by equating  $T_I$  to  $T_g$ .

### 3.3.5 Apply competitive growth principle and find the instant critical cooling rate and critical size

Equating  $V_g$  to the maximum  $V_\alpha^I$ ,  $V_\beta^I$ ,  $V_{eut}^I$  and with the equation  $T(y,t) = T_g$  derived from section 3.4.3, the critical size of metallic glass formation  $y_c$  can be derived. Time taken to get metallic glass  $t_c$  can also be found. The corresponding critical cooling

rate  $\dot{C} = \left. \frac{\partial T(y,t)}{\partial t} \right|_{y=y_c, t=t_c}$  is for metallic glass formation which indicates the GFA.

### 3.5 Summary

1. The relationships between growth rate and tip temperature of glassy phase and crystalline phases were developed under uni-directional heat conduction conditions. For crystalline phases, both quasi-steady state and unsteady state are considered.
2. GFA indicators for metallic glasses - critical cooling rate and critical size could be obtained by applying competitive growth principle to the developed growth rate –

tip temperature relationship. Glassy phase will be achieved if growth rate of glassy phase is the maximum one among all possible phases  $\alpha$ ,  $\beta$ , eutectic and glassy phase when tip temperature of them are at glass transition temperature  $T_g$ .

## References

- [1] Y.J. Kim, R. Busch, W. L. Johnson, A. J. Rulison and W. K. Rhim: Appl. Phys. Lett. **65**, 2136 (1994).
- [2] Theodore A. Waniuk, Jan Schroers, and William L. Johnson: Appl. Phys. Lett. **78**, 1213 (2001).
- [3] J. Schroers and W. L. Johnson, Mater. Trans., JIM **41**, 1530 (2000).
- [4] A. Inoue, N. Nishiyama, Materials Science and Engineering A **226-228**, 401 (1997).
- [5] Nobuyuki Nishiyama and Akihisa Inoue, Materials Transactions JIM **38(5)**, 464 (1997).
- [6] X. H. Lin and W. L. Johnson, J. Appl. Phys. **78 (11)**, 6514, 1995.
- [7] David Turnbull, Contemp. Phys. **10(5)**, 473 (1969).
- [8] Z. P. Lu and C. T. Liu, Acta Mater. **50**, 3501 (2002).
- [9] I. W. Donald and H. A. Davies, J. Non-Cryst. Solids **30**, 77 (1978).
- [10] E. S. Park, W. T. Kim, and D. H. Kim, Appl. Phys. Lett. **86**, 018507 (2005).
- [11] B. Zhang, M. X. Pan, D. Q. Zhao, and W. H. Wang, Appl. Phys. Lett. **85**, 61 (2004).
- [12] E. S. Park and D. H. Kim, Appl. Phys. Lett. **86**, 201912 (2005).
- [13] A. Inoue, W. Zhang, T. Zhang and K. Kurosaka, Acta Mater. **49**, 2645 (2001).
- [14] F. Q. Guo, S. J. Poon and G. J. Shiflet, Appl. Phys. Lett. **84**, 37 (2004).
- [15] Jan Schroers and William L. Johnson, Appl. Phys. Lett. **84**, 3666 (2004).
- [16] D. Ma, H. Tan, D. Wang, Y. Li and E. Ma, Appl. Phys. Lett. **86**, 191906 (2005).
- [17] G. Tammann and A. A. Botschwar, Z. Anorg. Chem. **157**, 27 (1926).
- [18] M. H. Burden and J.D. Hunt, J. Cryst. Growth **22**, 328 (1974).
- [19] W. Kurz and D.J. Fisher, International Metals Reviews **5and 6**, 177 (1979).
- [20] M. H. Burden and J.D. Hunt, J. Cryst. Growth **22**, 109 (1974).
- [21] K.A. Jackson & J.D. Hunt, Transactions of the Metallurgical Society of AIME **236**, 1129 (1966).

## **Chapter 4 Critical Heat Flux and Instant Critical Cooling Rate of Bulk Metallic Glass under Uni-Directional Heat Conduction Conditions**

### **4.1 Introduction**

Most of the critical cooling rates of BMGs reported in literature only reflect an average value for a bulk sample with little or no control over the heat flow direction as discussed in chapter 3. Further, past researchers do not explicitly quantify the critical relationships among heat flux, cooling rate and thickness of amorphous layer. In this chapter, a uni-directional solidification setup will be presented to find instant critical cooling rates and critical heat flux of BMGs. The effect of various heat transfer conditions upon the thickness of the amorphous layer can be quantified. Microstructure characterization and X-ray diffraction will be used to evaluate the amorphous and crystalline layers.

### **4.2 Experiment Setup**

The one-dimensional (1-D) heat conduction experiment setup is schematically illustrated in Figure 4.1. A cylindrical ceramic crucible is packed with solid alloy pieces at room temperature and surrounded by induction coil which functions as a medium to transfer energy from a high-frequency generator to electrical conductors within it. Argon is introduced from the mold top to minimize alloy oxidation. The aluminum cooling

block with flowing water in it on the crucible bottom is used to quickly extract heat when the liquid alloy attains the expected temperature, which is detected by thermocouples at different sites along the depth direction in the cylindrical cavity. 1-D heat conduction is achieved by having good insulation on the mold top and circumferential side and fast cooling on the mold bottom. By adjusting speed of flowing water, various heat transfer conditions can be achieved and therefore different thickness of amorphous layers can be obtained. The critical heat flux and critical instant cooling rate as a function of solidification time can be experimentally evaluated by analyzing temperature change during cooling process recorded by data logger combining with resulted amorphous and crystallization layers ascertained by diffraction techniques.

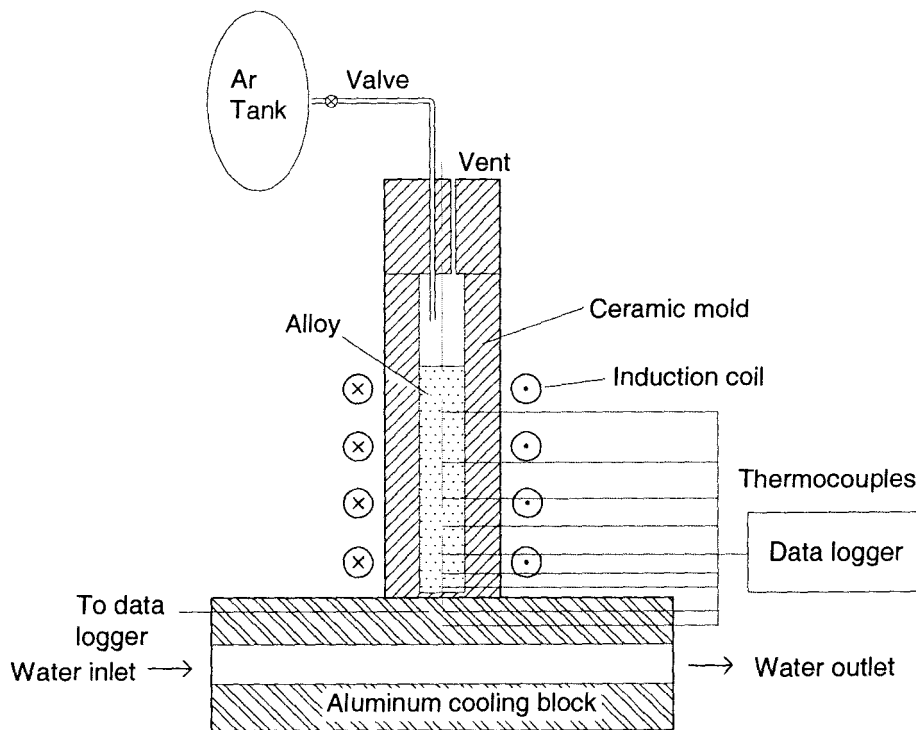


Figure 4.1 Schematic of instant critical cooling rate setup under 1-D heat condition.

#### 4.2.1 Crucible and thermocouples

Aluminum alloy will be used to examine the above experiment setup because it is much cheaper than metallic glasses. The crucible design is shown in Figure 4.2.

Cotronics 902, i.e. machinable alumina silicate was used as crucible material for continuous service temperature of 1150 °C\* which can avoid reaction with liquid alloy at high temperature. Cotronics rod with OD of 25.4mm was machined into ID of 11mm and height of 69mm cylinder with 1mm thickness solid base on the crucible bottom. 20mm height of solid cotronics 902 lid was sealed on the top of the cylindrical mold to minimize heat loss from mold top. To minimize the alloy oxidation, two-whole ceramic tube in OD of 0.166 in” was adhered to the lid to introduce HP+ grade high purity argon (99.998%) into crucible cavity and vent of 0.065” diameter for gas outlet. Eight K type thermocouples of 1.62mm diameter each with 304 stainless steel sheaths were introduced along radial direction to the center of mold cavity. The thermocouples were separated from each other by specific distances. Thermocouples towards the bottom of the cavity were closer to each other as compared to the ones away from the bottom of the cavity. A schematic of the setup is shown in Figure 4.2. 11.56g Al-7.45wt%Si alloy plates in diameter of 10.5mm and different thicknesses were put between thermocouples in the mold cavity resulting in a total estimated liquid height about 50mm. Welded tip of the two thermocouple wires with 0.254mm in diameter is about 0.3mm.

---

\*<http://www.cotronics.com/vo/cotr/pdf/902.pdf>

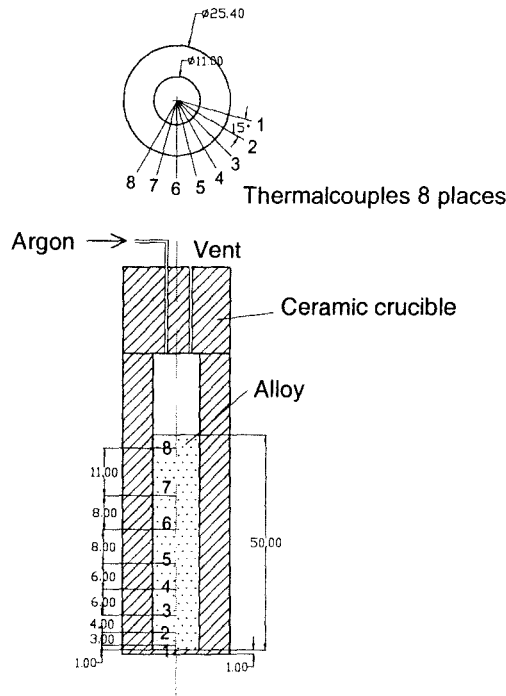
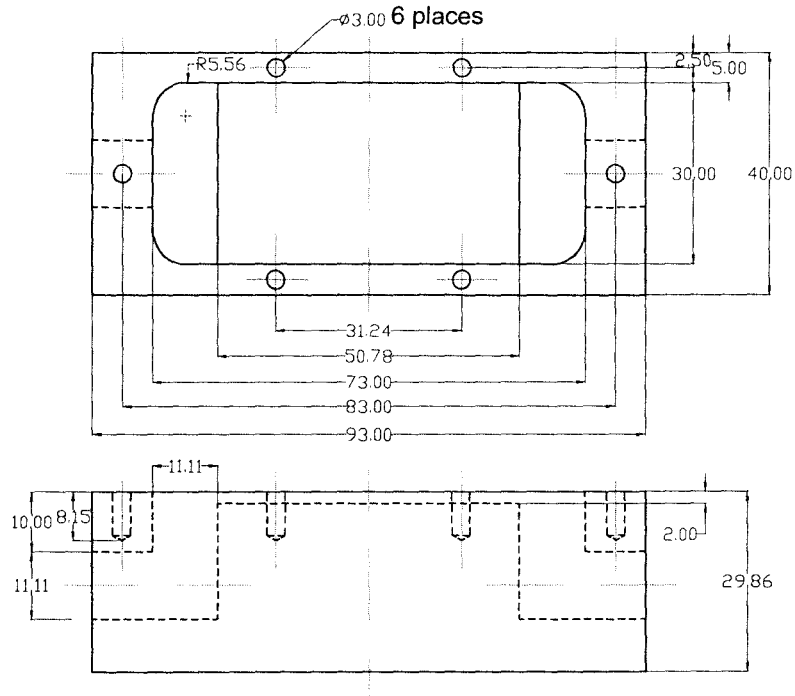


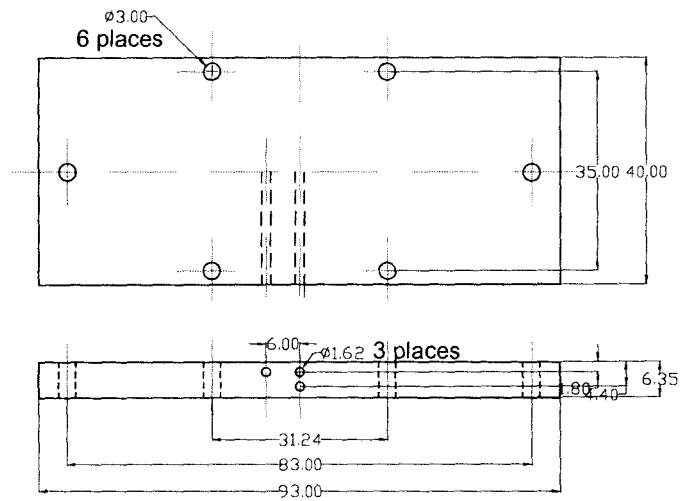
Figure 4.2 Thermocouple positions within mold cavity.

#### 4.2.2 Aluminum cooling block

Figure 4.3 shows drawing of aluminum cooling block which includes two parts: plate 'b' and block 'a'. To guarantee uniform heat transfer condition on the mold bottom surface, a 2mm thick rectangular cavity in size of 30mm×83mm was machined on top part of block 'a'. Cooling water (cold) was introduced into this cavity at a steady state steady flow condition. A control valve located at the exit of the aluminum block adjusted the flow velocity of the cooling water. 6.35mm thickness aluminum plate was fixed onto block 'a' and the gap between them was sealed by silicon sealant to avoid water leakage. Top surface is brought into a tight contact with the bottom surface of heated ceramic crucible once liquid alloy reaches the expected temperature. Three blind holes with 1.62 mm in diameter was drilled in plate 'a' to record temperature changes within the cooling block along the axis of the cylindrical mold and normal to the direction of heat extraction from the mold cavity during solidification process.



(a)



(b)

Figure 4.3 Drawing of aluminum cooling block consisting of two parts: (a) block with cavity for cooling water flow and (b) top plate to seal the cooling channel.

Figure 4.4 shows the ceramic mold with thermocouple setup and coil for the experiment. Figure 4.5 shows the machined aluminum cooling block with hose attached on it.

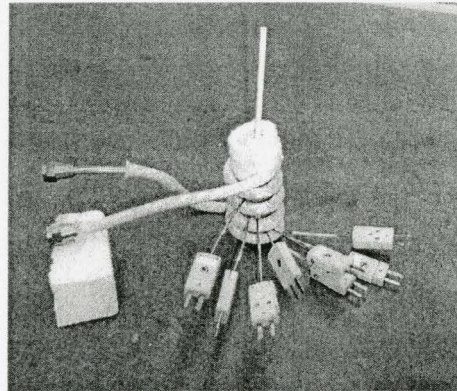


Figure 4.4 Ceramic mold with thermocouples and coil.

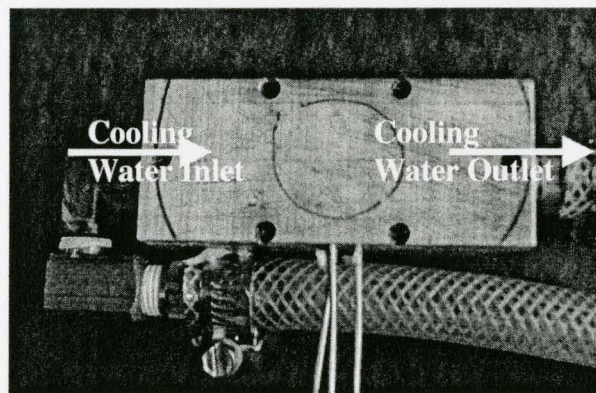


Figure 4.5 Aluminum cooling block used for uni-directional heat extraction.

### 4.3 Exploratory Experiments on Al-7.45 wt%Si Alloy

#### 4.3.1 Equipments and experiment procedure

Figure 4.6 shows the experimental setup to achieve uni-direction solidification in the ceramic crucible. The data logger used was National Instrument SCXI 1100. TA instruments' Dwyer LPM Air flow regulator was used to regulate the Ar gas flow. Induction heating generator was 20kW LEPEL T-20-3-DF3-TL with frequency range of 200 – 450 kHz. Four turns cylindrical work coil with inner diameter of 80mm and height of 50mm was made of copper tubing with OD of 1/4" and wall thickness of 0.03".

The experiment procedure was as follows:

1. After assembling all equipments shown in Figure 4.6, argon pressure was set at 3 psi with a volume flow rate of 2.5 l/min for 10 min before heating the crucible. City water flow was maintained at 20 L/min. The top surface of the cooling block was initially 20mm away from the bottom of induction coil. Data logger and computer temperature was always switched on during the whole experiment to record temperature values at 0.01 s intervals.
2. To prevent electrical interference from affecting the temperature value, induction furnace is switched off when checking the molten alloy temperature.
3. When the molten temperature reached 800 °C, argon flow was switched off and the aluminum cooling block was lifted up to obtain a firm contact with the base of the ceramic crucible. The temperatures from all thermocouples were continuously recorded and monitored.

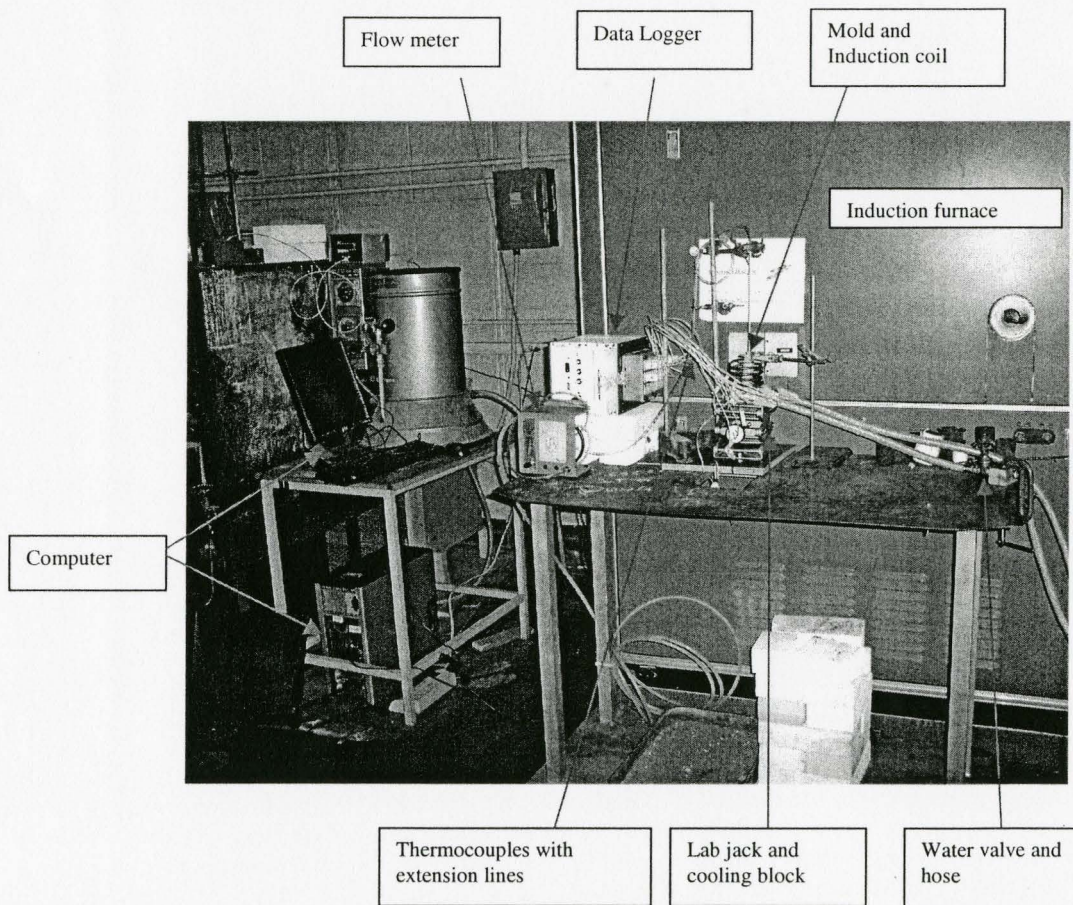


Figure 4.6 Assembled equipments for uni-directional solidification.

### 4.3.2 Results and discussion

Experiments on Al-7.45 wt%Si alloy showed that with the present setup of the crucible dimensions and the induction coil dimension, the alloy temperature could not exceed 120 °C after one hour of heating. The reason is that the coupling between alloy and induction coil was not sufficient to impart the energy required to the alloy for melting. A new induction coil with inner diameter of 30mm and height of 50mm was made of copper tubing with an OD of 1/4” and a wall thickness of 0.03”. But again the maximum alloy temperature reached was around 200°C after one hour of heating which shows the coupling is still not sufficient enough to melt the aluminum alloy. As the induction heating parameters are fixed and could not be adjusted, both the size of work coil and crucible had to be redesigned to achieve better coupling.

Since the heating of the work-piece is a function of the intensity of the induced current and the current is a function of the intensity of the electro-magnetic field, the flux density at the surface of the work decreases proportionally to the square of the coupling. Therefore the application of the above two solutions can increase the induced current within work piece by having stronger magnetic field on the work piece surface. But decreasing coupling distance increases heat loss along radial direction. Hence, coupling has to be optimized to balance melting of alloy and obtain uni-directional heat conduction from the crucible bottom.

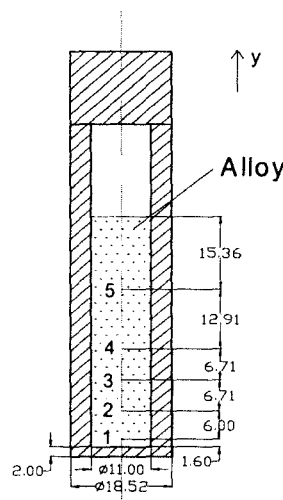


Figure 4.7 Mold dimension and thermocouple positions within mold cavity.

An induction coil with an OD of 1/8" and a coil turn distance of 6mm, uni-directional solidification experimental result of Al-7.45 wt%Si alloy was obtained by using new mold dimension and thermal couple positions as shown in Figure 4.7. When cooling block touched the mold bottom surface, data logger was switched on immediately to record temperature data of the liquid Al alloy. Temperature-time curves at different thermocouple positions were shown in Figure 4.8. Solidification began at about 610 °C and ended at 560 °C. Data from the thermocouple embedded in the Al cooling block at a depth of 1.8 mm from the top is also shown in Figure 4.8. Temperature gradient curves of the liquid alloy prior to solidification are shown in Figure 4.9. With the increase of solidification time and distance away from the mold bottom, temperature gradient decreases. In Figure 4.9, it can be observed an optimum height of at least 60 mm of the liquid metal is required to achieve a zero heat flux condition at infinity as stated in boundary condition in Equation 3.7. Hence it is recommended that the liquid height be increased to about 70 mm in subsequent experiments with the setup shown in Figure 4.7. This will ensure the validity of the boundary condition shown in our theoretical model in Chapter 3 (refer to Equation 3.7). Hence, the results of the exploratory experiment with Al-7.45 wt%Si alloy shows that the governing equation and the boundary conditions proposed in the theoretical model in section 3.3.2 are valid. Uni-directional experiments with the set-up shown in Figure 4.7 with a molten alloy height of at least 70 mm can be used to verify the theoretical model for BMG alloys.

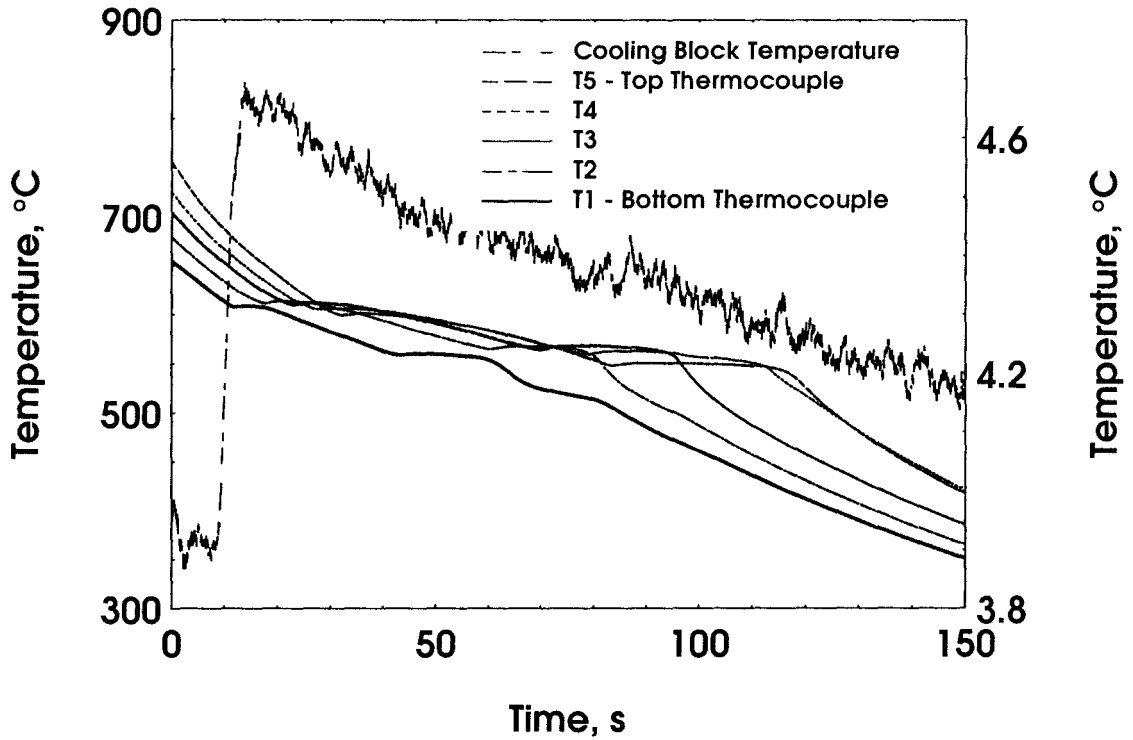


Figure 4.8 Temperature-time curves at different thermocouple positions during solidification process.

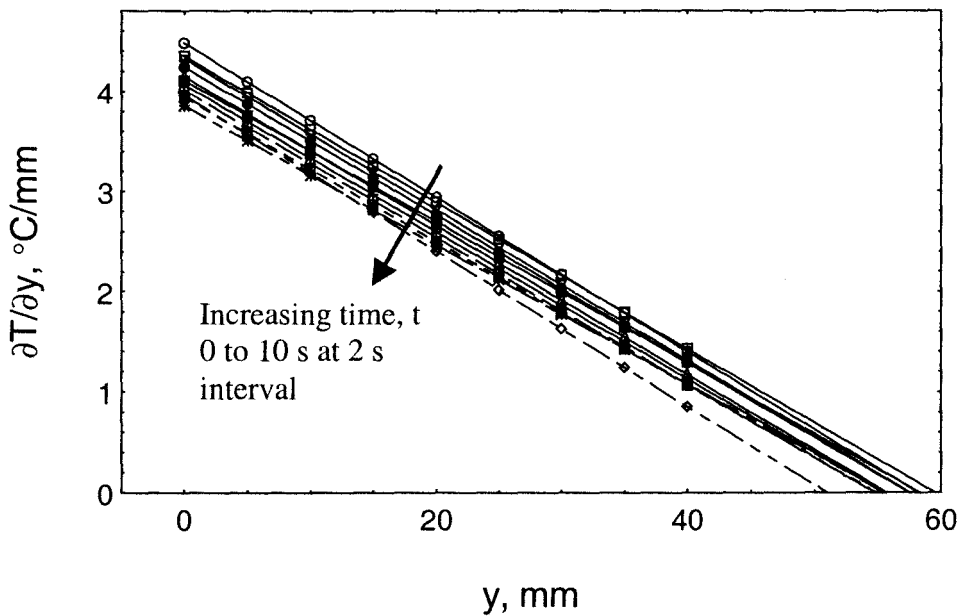


Figure 4.9 Temperature gradient curves during solidification process.

#### 4.4 Summary

1. A one-dimensional solidification setup was presented in this chapter to find critical relationships among heat flux, cooling rate and thickness of amorphous layer of BMGs.
2. Experiment on Al-7.45%Si alloy shows slow induction heating of the alloy caused by poor coupling of work coil and work piece. A new work coil with more turns and decreasing the coupling distance between work coil and work piece to increase intensity of the induced current on the work-piece would solve this problem.
3. Results of the exploratory experiments show that the proposed experimental setup shown in Figure 4.7 can be used to achieve uni-directional solidification conditions to validate the theoretical model with the assumed boundary conditions shown in section 3.3.2 of Chapter 3.

## Chapter 5 Summary and Future Work

There were two phases to this thesis work.

- Phase 1.** Investigate the feasibility of net shape manufacturing of the pivot assembly for Airborne Gravity Gradiometer (AGG) with Bulk Metallic Glass (BMG) alloy.
- Phase 2.** Understanding Glass Forming Ability (GFA) of BMG alloys to enable prediction of critical thickness of cast part under given heat transfer conditions during solidification.

GEDEX Corporation, Mississauga, ON, Canada is presently developing an advanced AGG device to enable superior detection capabilities in mineral and petroleum exploration by achieving a resolution of  $1 \text{ Eo/Hz}^{1/2}$  in detection. Further, GEDEX Corporation aims to develop the AGG device to function at ambient temperatures in lieu of the current devices which function at cryogenic temperatures of 4 K. In this project, two BMG alloy databases were developed, one based on properties (Appendix A) and the other castability (Appendix B). Subsequent to a thorough understanding of the mechanism of AGG, critical property requirements for the AGG pivot assembly were outlined. Suitable BMG alloys were identified to manufacture the pivot assembly by net shape manufacturing techniques and two alloys were identified as being most suitable for this purpose:  $\text{Cu}_{43}\text{Zr}_{43}\text{Al}_7\text{Ag}_7$  and *Vit1* ( $\text{Zr}_{41.2}\text{Ti}_{13.8}\text{Cu}_{12.5}\text{Ni}_{10.0}\text{Be}_{22.5}$ ). Two manufacturing routes for the pivot assembly with the two alloys were developed: *Die Casting* and *Super Plastic Forming* (SPF). Although, our attempts to manufacture the pivot assembly were

not entirely successful due to lack of advanced facilities at McMaster University, comprehensive and viable manufacturing procedures were drafted, established and verified.

Presently, the development of BMG materials and determination of the critical cooling rate and part size is not a scientific method based on strong fundamental understanding, but rather, an ad-hoc empirical estimate of suitable alloy compositions based on experience in the area of research. The primary reason is the lack of a clear understanding of the Glass Forming Ability (GFA) of BMG materials. Phase 2 of this project presented the current level of understanding of GFA of BMG, developed a theoretical model to enable a fair prediction of the GFA of BMG alloys and developed experiment techniques and procedures to verify theoretical model for binary BMG alloys. In the theoretical model a relationship between growth rate of the solid-liquid interface during solidification and the extent of melt undercooling under uni-direction solidification conditions were presented. Competitive growth principle was applied to ascertain the critical size and critical cooling rate of binary alloys under given heat transfer conditions. The solution for the model will be evaluate by numerical techniques in the future with parameter input from the experiments and literature. A viable uni-directional solidification experimental setup to understand and control the heat transfer conditions during uni-directional solidification of BMG alloys was designed and developed. Owing to the lack of any such prior art, preliminary exploratory experiments were carried out to identify and optimize the critical experiment parameters. A detailed procedural lay out of the experiment setup and technique has been presented in this thesis. The future outcome of these experiments will quantify relationship among heat flux, cooling rate and thickness of amorphous layer during solidification. Real time temperature data coupled with evaluation of heat flux via solutions to inverse heat conduction problems, and microstructure and X-Ray diffraction analysis of the solidified part will be carried out to achieve this goal. The experiments and the model will enable better prediction capabilities of GFA of BMG alloys.

In summary, this thesis has laid a strong foundation to introduce long-term research initiatives on Bulk Metallic Glass systems at the Centre for Solidification and

Master's Thesis - Yuelu Li McMaster - Mechanical Engineering  
Thermal Processing (CSTP) at McMaster University. Detailed procedures to develop novel techniques to manufacture BMG alloys have been developed. Carrying out the proposed experimental plan and verifying the theoretical model will enable a quantum leap in our understanding of the GFA of BMG alloys.

## Appendices

### Appendix A: Bulk Metallic Glass Properties Database. (Collaborated with Paul Borges and Dr. Steve Thorpe)

Material	Young's Modulus (GPa)	Elastic Limit (MPa)	UTS (MPa)	Maximum Elastic Deflection (%)	Loss Coefficient ( $Q^{-1}$ )	LCTE (m/m/°C)	Fatigue (MPa)
Niobium at RT	125 [1,2,3]	550 [4]	585 [4]	0.55	2.00E-07 [15]	7.10E-06	75 [7]
Niobium at -196 °C	125 [12]	772 [12]	862 [12]	0.77	7.00E-07 [15]	4.00E-06 [13]	
Niobium at -253 °C	125 [12]	1150 [12]	1175 [12]	1.15	9.00E-09 [15]	2.00E-07 [13]	
Titanium at RT	115	586	662	0.51	4.00E-05 [15]	8.60E-06	54
Titanium at -196 °C	115 [16]	637 [17]	810 [17]	0.55	2.90E-07 [15]	3.20E-06 [19]	
<b>Mg Based BMGs</b>							
Mg <sub>85</sub> Ni <sub>10</sub> Y <sub>5</sub>	40.3 [24]	640 [24]	640 [24]	1.6 [24]			
Mg <sub>80</sub> Ni <sub>15</sub> Y <sub>5</sub>	46.4 [24]	830 [24]	830 [24]	1.8 [24]			
Mg <sub>85</sub> Y <sub>10</sub> Cu <sub>5</sub>	44.1 [24]	800 [24]	800 [24]	1.8 [24]			
Mg <sub>80</sub> Ce <sub>10</sub> Ni <sub>10</sub>	49.5 [24]	750 [24]	750 [24]	1.5 [24]			
Mg <sub>80</sub> Y <sub>10</sub> Cu <sub>10</sub>	46 [27]	820 [27]	820 [27]	1.8 [27]			
Mg <sub>82.5</sub> Ni <sub>12.5</sub> Y <sub>5</sub>	44 [31]	610 [31]	610 [31]	1.4 [31]			
Mg <sub>75</sub> Ni <sub>15</sub> Y <sub>10</sub>	61 [31]	850 [31]	850 [31]	1.4 [31]			
Mg <sub>85</sub> Cu <sub>10</sub> Y <sub>5</sub>	41 [31]	740 [31]	740 [31]	1.8 [31]			
Mg <sub>65</sub> Cu <sub>20</sub> Y <sub>10</sub> Zn <sub>5</sub>	74 [111]	881 [74]	881 [74]	1.6 [111]			
Mg <sub>81</sub> Ni <sub>12</sub> Ce <sub>7</sub>	53.9 [75]		585 [75]	1.5 [75]			

Mg <sub>65</sub> Cu <sub>25</sub> Gd <sub>10</sub>	56 [82]	834 [82]	834 [82]	1.5 [82]	
Mg <sub>65</sub> Cu <sub>20</sub> Gd <sub>10</sub> Ni <sub>5</sub>	59 [82]	850 [82]	904 [82]	1.5 [82]	
Mg <sub>65</sub> Cu <sub>25</sub> Er <sub>10</sub>	44	742 [83]	742 [83]	1.7 [83]	
Mg <sub>55</sub> Cu <sub>30</sub> Y <sub>15</sub>	32 [84]	565 [84]	565 [84]	1.8	
Mg <sub>65</sub> Cu <sub>25</sub> Y <sub>10</sub>	69 [111]	823 [111]	823 [111]	1.4 [111]	
Mg <sub>84</sub> Ni <sub>12.5</sub> Y <sub>3.5</sub>					1.00E-03 [132]
Mg <sub>83</sub> Ni <sub>13</sub> Y <sub>4</sub>					5.00E-04 [149]
Mg <sub>81</sub> Ni <sub>12</sub> Y <sub>7</sub>					7.50E-04 [149]
Mg <sub>65</sub> Ni <sub>20</sub> Nd <sub>15</sub>					
Mg <sub>75</sub> Ni <sub>10</sub> Gd <sub>10</sub> Cu <sub>5</sub>	54	800 [170]	874 [170]	1.55 [170]	
Mg <sub>70</sub> Cu <sub>15</sub> Gd <sub>10</sub> Ni <sub>5</sub>	55	820 [170]	854 [170]	1.55 [170]	
Mg <sub>70</sub> Cu <sub>20</sub> Gd <sub>10</sub>	55 [170]	810 [170]	810 [170]	1.45	
Mg <sub>75</sub> Cu <sub>15</sub> Gd <sub>10</sub>	54 [170]	730 [170]	730 [170]	1.35	
Mg <sub>65</sub> Cu <sub>15</sub> Y <sub>10</sub> Ag <sub>10</sub>			861 [112]		
Mg <sub>65</sub> Cu <sub>15</sub> Y <sub>10</sub> Ag <sub>5</sub> Pd <sub>5</sub>	59 [81]	770	770 [81]	1.3 [81]	7.50E-04 [129]
Mg <sub>65</sub> Cu <sub>15</sub> Er <sub>10</sub> Ag <sub>10</sub>	39	814 [83]	814 [83]	2.1 [83]	
Mg <sub>65</sub> Y <sub>10</sub> Ni <sub>7.5</sub> Cu <sub>7.5</sub> Zn <sub>5</sub> Ag <sub>5</sub>	49 [165]	851 [165]	851 [165]	1.8 [165]	
Mg <sub>65</sub> Cu <sub>15</sub> Gd <sub>10</sub> Ag <sub>5</sub> Pd <sub>5</sub>	61	765 [110]	817 [110]	1.25 [110]	
Mg <sub>65</sub> Cu <sub>15</sub> Ag <sub>10</sub> Gd <sub>8</sub> Y <sub>2</sub>	72 [112]	864	956 [112]	1.2 [112]	
Mg <sub>65</sub> Cu <sub>20</sub> Gd <sub>10</sub> Ag <sub>5</sub>	50	850 [169]	909 [169]	1.7 [169]	
Mg <sub>65</sub> Cu <sub>15</sub> Gd <sub>10</sub> Ag <sub>10</sub>	54	935 [169]	935 [169]	1.7 [169]	

## Ln Based BMGs

La <sub>55</sub> Al <sub>25</sub> Ni <sub>20</sub>	33.8 [30]	515 [30]	515 [30]	1.5 [30]	4.00E-03 [123]
La <sub>50</sub> Al <sub>30</sub> Ni <sub>20</sub>	41.3 [30]	715 [30]	715 [30]	1.7 [30]	
La <sub>50</sub> Al <sub>35</sub> Ni <sub>15</sub>	41.1 [30]	715 [30]	715 [30]	1.7 [30]	
La <sub>45</sub> Al <sub>35</sub> Ni <sub>20</sub>	46.3 [30]	720 [30]	720 [30]	1.6 [30]	
La <sub>45</sub> Al <sub>45</sub> Ni <sub>10</sub>	52.3 [30]	795 [30]	795 [30]	1.5 [30]	

La <sub>55</sub> Al <sub>35</sub> Cu <sub>10</sub>	42.7 [28]	880 [28]	880 [28]	2.1 [28]	
La <sub>50</sub> Al <sub>30</sub> Cu <sub>20</sub>	37.7 [28]	750 [28]	750 [28]	2 [28]	
La <sub>55</sub> Al <sub>25</sub> Cu <sub>20</sub>	31.9 [28]	600 [28]	600 [28]	1.9 [28]	
La <sub>50</sub> Al <sub>25</sub> Cu <sub>25</sub>	29 [28]	535 [28]	535 [28]	1.8 [28]	
La <sub>55</sub> Al <sub>25</sub> Cu <sub>10</sub> Ni <sub>5</sub> Co <sub>5</sub>	47.5 [87]				2.00E-03 [129]
La <sub>62</sub> Al <sub>14</sub> (Cu, Ni) <sub>24</sub>	30.5	549 [88]	549 [88]	1.8 [88]	
La <sub>55</sub> Al <sub>25</sub> Ni <sub>10</sub> Cu <sub>10</sub>					
Y <sub>56</sub> Al <sub>24</sub> Co <sub>20</sub>					
Nd <sub>60</sub> Fe <sub>30</sub> Al <sub>10</sub>					
Nd <sub>70</sub> Fe <sub>20</sub> Al <sub>10</sub>					
Nd <sub>60</sub> Cu <sub>20</sub> Ni <sub>10</sub> Al <sub>10</sub>					
Nd <sub>60</sub> Fe <sub>20</sub> Al <sub>10</sub> Cu <sub>10</sub>					
Nd <sub>60</sub> Al <sub>15</sub> Ni <sub>10</sub> Cu <sub>10</sub> Fe <sub>5</sub>					
Nd <sub>61</sub> Cu <sub>15</sub> Al <sub>11</sub> Ni <sub>8</sub> Co <sub>5</sub>					
Pr <sub>60</sub> Fe <sub>30</sub> Al <sub>10</sub>					
Pr <sub>55</sub> Fe <sub>30</sub> Al <sub>12</sub> Cu <sub>3</sub>					
Pr <sub>60</sub> Cu <sub>20</sub> Ni <sub>10</sub> Al <sub>10</sub>	37.2 [167]				
Pr <sub>60</sub> Cu <sub>16</sub> Al <sub>10</sub> Ni <sub>10</sub> Fe <sub>4</sub>					
Nd <sub>60</sub> Fe <sub>20</sub> Co <sub>10</sub> Al <sub>10</sub>	54.1 [167]				
La <sub>66</sub> Al <sub>14</sub> Cu <sub>10</sub> Ni <sub>10</sub>	35.7 [167]				
Ce <sub>70</sub> Al <sub>10</sub> Cu <sub>10</sub> Ni <sub>10</sub>	30.3 [167]				
Ce <sub>65</sub> Al <sub>10</sub> Ni <sub>10</sub> Cu <sub>10</sub> Nb <sub>5</sub>					
Y <sub>36</sub> Al <sub>24</sub> Sc <sub>20</sub> Co <sub>20</sub>					
Y <sub>36</sub> Al <sub>24</sub> Sc <sub>20</sub> Co <sub>10</sub> Ni <sub>10</sub>					
Dy <sub>46</sub> Al <sub>24</sub> Co <sub>18</sub> Y <sub>10</sub> Fe <sub>2</sub>	64.2 [167]				
Gd <sub>36</sub> Al <sub>24</sub> Co <sub>20</sub> Y <sub>20</sub>	62.2 [167]				
Ti Based BMGs					
Ti <sub>50</sub> Cu <sub>20</sub> Ni <sub>20</sub> Zr <sub>10</sub>	62.5 [26]	1660 [26]	1660 [26]	2.6 [26]	

$Ti_{50}Zr_{20}Ni_{20}Cu_{10}$	77.4 [26]	1497 [26]	1497 [26]	2 [26]	
$Ti_{60}Ni_{20}Zr_{10}Cu_{10}$	58.3 [26]	1360 [26]	1360 [26]	2.5 [26]	
$Ti_{50}Cu_{40}Zr_{10}$	59.7 [26]	1483 [26]	1483 [26]	2.6 [26]	
$Ti_{60}Zr_{15}Ni_{15}Cu_{10}$	78 [40]	1480 [40]	1480 [40]	1.9	
$Ti_{20}Zr_{20}Hf_{20}Ni_{20}Cu_{20}$	104 [102]	1768	1920 [102]	1.7 [102]	
$Ti_{45}Cu_{45}Zr_5Ni_5$	110 [171]	1850 [171]	1926 [171]	1.7 [171]	
$Ti_{50}Cu_{40}Zr_5Ni_5$			2020 [171]		
$Ti_{42.5}Cu_{42.5}Zr_{10}Ni_5$			2115 [171]		
$Ti_{50}Ni_{25}Cu_{25}$	93 [108]	1800 [108]	1800 [108]	1.9	2.00E-03 [148]
$Ti_{50}Cu_{25}Ni_{22}Sn_3$	98 [108]	2050 [108]	2050 [108]	2.1	
$Ti_{50}Cu_{25}Ni_{20}Sn_5$	102 [108]	2050 [108]	2050 [108]	2	
$Ti_{50}Cu_{23}Ni_{20}Sn_7$	105 [108]	2200 [108]	2200 [108]	2.1	
$Ti_{50}Ni_{24}Cu_{20}Sn_3Si_2B_1$	110 [80]		2100 [80]		
$Ti_{65}Be_{18}Cu_9Ni_8$		2100 [106]			
$Ti_{60}Be_{18}Cu_9Ni_8Zr_5$		2090 [106]			
$Ti_{55}Be_{18}Zr_{10}Cu_9Ni_8$		2070 [106]			
$Ti_{50}Be_{18}Zr_{15}Cu_9Ni_8$		2043 [106]			
$Ti_{45}Cu_{25}Ni_{15}Be_7Zr_5Sn$	128	2300 [79]	2480 [79]	1.8 [79]	
<sup>3</sup> $Ti_{40}Zr_{25}Be_{18}Cu_9Ni_8$	94	1700 [79]	1810 [79]	1.8 [79]	
$Ti_{40}Zr_{29}Be_{16}Cu_8Ni_7$	96 [92]	1893 [92]	1921 [92]	2 [92]	
$Ti_{53}Ni_{18}Cu_{15}Al_7Zr_3Si_3$	90	1800 [107]	1950	2 [107]	

$B_1$			[107]				
$Ti_{53}Ni_{18.5}Cu_{15}Al_7Zr_3S$	81	2200 [107]	2200	2.7 [107]			
$i_3B_{0.5}$			[107]				
$Ti_{50}Cu_{25}Ni_{15}Be_7Sn_3$	106	1900 [79]	2170 [79]	1.8 [79]			
<b>Zr Based BMGs</b>							
$Zr_{60}Cu_{18}Al_{10}Ni_9Co_3$	97 [29]	1390 [29]	1510 [29]	1.4 [29]		3.40E-05	
						[151]	
$Zr_{55}Al_{20}Co_{20}Cu_5$	92 [32]	1960 [32]	1960 [32]	2.1 [32]			
$Zr_{65}Cu_{15}Al_{10}Ni_{10}$	80 [33]	1570 [53]	1570 [53]	2 [53]	2.00E-02 [128]	3.67E-05	
						[138]	
$Zr_{70}Ni_{20}Al_{10}$	61 [35]	1335 [35]	1335 [35]	2.1 [35]			
$Zr_{65}Ni_{25}Al_{10}$	64.5 [35]	1520 [35]	1520 [35]	2.4 [35]			
$Zr_{65}Ni_{20}Al_{15}$	70.5 [35]	1640 [35]	1640 [35]	2.3 [35]			
$Zr_{60}Ni_{25}Al_{15}$	72.6 [35]	1715 [35]	1715 [35]	2.4 [35]	1.00E-02 [128]		
$Zr_{60}Al_{20}Ni_{20}$	78.2 [35]	1720 [35]	1720 [35]	2.2 [35]			
$Zr_{55}Cu_{30}Al_{10}Ni_5$	81 [41]	1700 [57]	1700 [57]	2.3 [36]	1.00E-03 [129]	1.13E-05	1100
						[136]	[153]
$Zr_{60}Cu_{20}Al_{10}Ni_{10}$	84 [36]	1790 [36]	1790 [36]	2.2 [36]		2.98E-05	
						[138]	
$Zr_{55}Co_{25}Al_{20}$	114 [38]	2050 [37]	2200 [38]	2.1 [38]			
$Zr_{50}Cu_{40}Al_{10}$	105 [45]	2000 [45]	2000 [45]	1.9			752
							[145]
$Zr_{65}Cu_{17.5}Ni_{10}Al_{7.5}$	92 [58]	1570 [46]	1528 [46]	1.9	2.50E-04 [161]	9.00E-06	
						[58]	
$Zr_{65}Cu_{27.5}Al_{7.5}$	93 [58]					8.00E-04	
						[58]	
$Zr_{60}Al_{15}Cu_{15}Ni_{7.5}Co_2$	91 [58]					1.00E-05	
						[58]	

Zr <sub>57.5</sub> Cu <sub>20</sub> Al <sub>12.5</sub> Ni <sub>10</sub>		1600 [59]	1600 [59]				
Zr <sub>55</sub> Cu <sub>20</sub> Al <sub>15</sub> Ni <sub>10</sub>	90 [60]	1850 [59]	1850 [59]	2.1			
Zr <sub>54.4</sub> Cu <sub>25.6</sub> Al <sub>12</sub> Fe <sub>8</sub>		1690 [77]					
Zr <sub>58</sub> Cu <sub>22</sub> Al <sub>12</sub> Fe <sub>8</sub>	76	1710 [77]		2.25 [77]			
Zr <sub>61.6</sub> Cu <sub>18.4</sub> Al <sub>12</sub> Fe <sub>8</sub>		1560 [77]					
Zr <sub>63.7</sub> Cu <sub>17.15</sub> Ni <sub>9.8</sub> Al <sub>7.35</sub> W <sub>2</sub>	91.5 [90]	1600 [90]	1764 [90]	1.7			
Zr <sub>53.9</sub> Cu <sub>29.4</sub> Al <sub>9.8</sub> Ni <sub>4.9</sub> W <sub>2</sub>	92.2 [90]	1800 [90]	1980 [90]	2			
(Zr <sub>55</sub> Cu <sub>30</sub> Al <sub>10</sub> Ni <sub>5</sub> ) <sub>98.5</sub> S i <sub>1.5</sub>	87 [51]	1830 [51]	1830 [51]	2 [51]			
Zr <sub>69.5</sub> Cu <sub>12</sub> Ni <sub>11</sub> Al <sub>7.5</sub>					0.001 [124]		
Zr <sub>50</sub> Cu <sub>30</sub> Al <sub>10</sub> Ni <sub>10</sub>							865 [145]
Zr <sub>48</sub> Cu <sub>45</sub> Al <sub>7</sub>							
Zr <sub>66</sub> Ni <sub>26</sub> Al <sub>8</sub>							
Vitreloy I: Zr <sub>41.2</sub> Be <sub>22.5</sub> Ti <sub>13.8</sub> Cu <sub>12.5</sub> Ni <sub>10.0</sub>	96 [9]	1900 [9]	1900 [9]	1.98	1.00E-03 [147]	9.26E-06 [142]	703 [146]
Liquidmetal Alloy II [34]	79 [34]	1450 [34]	1450 [34]	2 [34]			
Zr <sub>48</sub> Be <sub>24</sub> Cu <sub>12</sub> Nb <sub>8</sub> Fe <sub>8</sub>	95.7 [89]	1600 [89]	1600 [89]	1.7			
Zr <sub>46.75</sub> Be <sub>27.5</sub> Ni <sub>10</sub> Ti <sub>8.25</sub> Cu <sub>7.5</sub>					1.00E-03 [130]		
Zr <sub>44</sub> Be <sub>25</sub> Ti <sub>11</sub> Cu <sub>10</sub> Ni <sub>10</sub>							
Zr <sub>58</sub> Cu <sub>20</sub> Al <sub>10</sub> Ni <sub>10</sub> Ti <sub>2</sub>	85 [36]	1850 [36]	1850 [36]	2.2 [36]			
Zr <sub>60</sub> Cu <sub>20</sub> Pd <sub>10</sub> Al <sub>10</sub>	80 [42]		1750 [42]	2.2 [42]			
Zr <sub>53</sub> Cu <sub>20</sub> Al <sub>12</sub> Ni <sub>10</sub> Ti <sub>5</sub>	89 [42]		1820 [42]	2.2 [42]			
Zr <sub>65</sub> Pd <sub>10</sub> Ni <sub>10</sub> Al <sub>7.5</sub> Cu <sub>7.5</sub>	85 [86]	1640 [86]	1640 [86]	2 [86]			
Zr <sub>55</sub> Co <sub>25</sub> Al <sub>20-x</sub> Nb <sub>x</sub> (x	98 [44]	1960	2100 [44]	2 [44]			

= 0, 2.5 and 5 at. %)							
Zr <sub>65</sub> Pd <sub>17.5</sub> Ni <sub>10</sub> Al <sub>7.5</sub>	86.1 [46]	1594 [46]	1698 [46]	1.9			
Zr <sub>57</sub> Cu <sub>20</sub> Al <sub>10</sub> Ni <sub>8</sub> Ti <sub>5</sub>	68 [47]	1700 [47]	1700 [47]	2.5			
Zr <sub>57</sub> Cu <sub>15.4</sub> Ni <sub>12.6</sub> Al <sub>10</sub> Ni <sub>5</sub> (Vit 106)	84.7	1200	1200	1.4		3.00E-05 [139]	
Zr <sub>52.5</sub> Cu <sub>17.9</sub> Ni <sub>14.6</sub> Al <sub>10</sub> Ti <sub>5</sub> (Vit 105)	88.6 [52]	1760 [50]	1760 [50]	2	2.50E-04 [125]	1.20E-05 [133]	907 [144]
Zr <sub>60</sub> Cu <sub>15</sub> Al <sub>10</sub> Ni <sub>10</sub> Ti <sub>5</sub>	100 [54]	1752 [54]	1752 [54]	1.8			
Zr <sub>54.5</sub> Cu <sub>20</sub> Al <sub>10</sub> Ni <sub>8</sub> Ti <sub>7.5</sub>	110 [56]	1765 [56]	1766 [56]	1.7 [56]			
Zr <sub>57.5</sub> Cu <sub>20</sub> Al <sub>10</sub> Ni <sub>10</sub> Ti <sub>2</sub>		1750 [59]	1750 [59]				
<sup>5</sup> Zr <sub>55</sub> Cu <sub>20</sub> Al <sub>12.5</sub> Ni <sub>10</sub> Ti <sub>2</sub>		1750 [59]	1750 [59]				
<sup>5</sup> Zr <sub>52.5</sub> Cu <sub>20</sub> Al <sub>15</sub> Ni <sub>10</sub> Ti <sub>2</sub>	92 [60]	1800 [59]	1800 [59]	2			
<sup>5</sup> Zr <sub>57.5</sub> Cu <sub>20</sub> Ni <sub>10</sub> Al <sub>7.5</sub> Ti <sub>5</sub>	79 [60]	1550 [59]	1550 [59]	2			
Zr <sub>55</sub> Cu <sub>20</sub> Al <sub>10</sub> Ni <sub>10</sub> Ti <sub>5</sub>	86 [60]	1600 [59]	1600 [59]	1.9			
Zr <sub>55</sub> Cu <sub>20</sub> Ni <sub>10</sub> Ti <sub>7.5</sub> Al <sub>7.5</sub>		1600 [59]	1600 [59]				
Zr <sub>52.5</sub> Cu <sub>20</sub> Al <sub>10</sub> Ni <sub>10</sub> Ti <sub>7</sub>	85 [60]	1630 [59]	1630 [59]	1.9			
<sup>5</sup> Zr <sub>50</sub> Cu <sub>20</sub> Al <sub>12.5</sub> Ni <sub>10</sub> Ti <sub>7</sub>		1800 [59]	1800 [59]				
<sup>5</sup> Zr <sub>58</sub> Cu <sub>25</sub> Al <sub>12</sub> Nb <sub>5</sub>		1550 [76]	1550 [76]				
Zr <sub>60</sub> Cu <sub>15</sub> Pd <sub>10</sub> Al <sub>10</sub> Fe <sub>5</sub>	81 [86]	1701	1750 [86]	2.1 [86]			
Zr <sub>63</sub> Cu <sub>14</sub> Al <sub>10</sub> Ni <sub>10</sub> Nb <sub>3</sub>	97	1949 [91]	1867 [91]	2 [91]			
Zr <sub>65</sub> Cu <sub>12.5</sub> Ni <sub>10</sub> Al <sub>7.5</sub> Pd <sub>5</sub>					2.00E-04 [126]		
Zr <sub>60</sub> Cu <sub>20</sub> Al <sub>10</sub> Ni <sub>8</sub> Ti <sub>2</sub>						1.10E-05 [133]	
Zr <sub>59</sub> Cu <sub>20</sub> Al <sub>10</sub> Ni <sub>8</sub> Ti <sub>3</sub>	78 [165]	1610 [165]	1710 [165]	2.1			790 [155]

Zr <sub>65</sub> Cu <sub>12.5</sub> Ni <sub>10</sub> Al <sub>7.5</sub> Ag	84 [61]	1650 [61]	1650 [61]	1.95 [61]	
<sup>5</sup> Zr <sub>59</sub> Cu <sub>18</sub> Al <sub>10</sub> Ni <sub>8</sub> Ta <sub>5</sub>	85	1700 [164]	1700 [66]	2 [164]	
Zr <sub>52.5</sub> Cu <sub>15</sub> Be <sub>12.5</sub> Al <sub>10</sub> Ni <sub>10</sub>	80	1750 [53]	1750 [53]	2.2 [53]	
Zr <sub>37</sub> Be <sub>20.25</sub> Ti <sub>12.5</sub> Cu <sub>11.2</sub> Al <sub>10</sub> Ni <sub>9</sub>	119 [49]	1820 [49]	1820 [49]	1.5	
Zr <sub>60</sub> Cu <sub>22</sub> Al <sub>10</sub> Au <sub>8</sub>	53 [86]	1740 [86]	1740 [86]	3.3	
Zr <sub>35</sub> Cu <sub>17.9</sub> Hf <sub>17.5</sub> Ni <sub>14.6</sub> Al <sub>10</sub> Ti <sub>5</sub>	93 [98]	1900 [98]	1960 [98]	2	
Zr <sub>55</sub> Cu <sub>45</sub>	102 [116]	1750 [116]	1880 [116]	1.7	
Cu Based BMGs					
Cu <sub>47</sub> Ti <sub>34</sub> Zr <sub>11</sub> Ni <sub>8</sub>	109 [62]	2102 [62]	2186 [62]	2.1 [62]	2.00E-03 [160]
Cu <sub>47</sub> Ti <sub>33</sub> Zr <sub>11</sub> Ni <sub>8</sub> Fe <sub>1</sub>	102 [62]	2008 [62]	2088 [62]	2.4 [62]	
Cu <sub>55</sub> Zr <sub>30</sub> Ti <sub>10</sub> Co <sub>5</sub>	130 [71]	2200 [71]	2310 [71]	1.8 [71]	
Cu <sub>54</sub> Zr <sub>22</sub> Ti <sub>18</sub> Ni <sub>6</sub>	105	2100 [78]	2100 [78]	2 [78]	
(Cu <sub>0.6</sub> Zr <sub>0.3</sub> Ti <sub>0.1</sub> ) <sub>97.5</sub> Fe <sub>2.5</sub>	115 [104]	1820 [104]	2030 [104]	1.5 [104]	
(Cu <sub>0.6</sub> Zr <sub>0.3</sub> Ti <sub>0.1</sub> ) <sub>96</sub> Co <sub>4</sub>	107 [104]	1640 [104]	1920 [104]	1.7 [104]	
(Cu <sub>0.6</sub> Zr <sub>0.3</sub> Ti <sub>0.1</sub> ) <sub>94</sub> Ni <sub>6</sub>	115 [104]	1600 [104]	1960 [104]	1.2 [104]	
Cu <sub>47</sub> Ti <sub>33</sub> Zr <sub>11</sub> Ni <sub>8</sub> Si <sub>1</sub>	118.6 [66]	1900 [66]	2087 [66]	1.8 [66]	
Cu <sub>47</sub> Ti <sub>33</sub> Ni <sub>8</sub> Zr <sub>7</sub> Nb <sub>4</sub> Si <sub>1</sub>	116.7 [66]	2000 [66]	2170 [66]	1.9 [66]	
(Cu <sub>0.6</sub> Zr <sub>0.3</sub> Ti <sub>0.1</sub> ) <sub>93</sub> Nb <sub>4</sub> Ni <sub>3</sub>	109 [105]	1900 [105]	2043 [105]	1.7	
(Cu <sub>0.6</sub> Zr <sub>0.3</sub> Ti <sub>0.1</sub> ) <sub>91</sub> Nb <sub>5</sub>	116 [105]	1900 [105]	2035	1.6	

Ni <sub>4</sub>			[105]	
(Cu <sub>0.6</sub> Zr <sub>0.3</sub> Ti <sub>0.1</sub> ) <sub>90</sub> Ni <sub>5</sub>	117 [105]	1900 [105]	2032	1.6
Nb <sub>5</sub>			[105]	
Cu <sub>42.5</sub> Ti <sub>41.5</sub> Ni <sub>7.5</sub> Hf <sub>5</sub> Zr <sub>2.5</sub> Si <sub>1</sub>	103 [93]	2040 [93]		2
Cu <sub>55</sub> Zr <sub>30</sub> Ti <sub>10</sub> Ni <sub>5</sub>				1.30E-05 [162]
Cu <sub>45</sub> Ti <sub>42.5</sub> Zr <sub>7.5</sub> Ni <sub>5</sub>			2068 [171]	
Cu <sub>55</sub> Zr <sub>30</sub> Ti <sub>10</sub> Pd <sub>5</sub>	118 [63]	2200 [63]	2270 [63]	1.9
Cu <sub>60</sub> Zr <sub>30</sub> Ti <sub>10</sub>	124 [99]	1780 [68]	2000 [68]	1.6
Cu <sub>60</sub> Ti <sub>25</sub> Zr <sub>15</sub>			1720 [65]	
Cu <sub>60</sub> Zr <sub>20</sub> Ti <sub>20</sub>	110 [101]	1745 [101]	2000 [101]	1.6
Cu <sub>60</sub> Zr <sub>22</sub> Ti <sub>18</sub>	115 [67]		1460 [65]	
Cu <sub>60</sub> Zr <sub>25</sub> Ti <sub>15</sub>			1670 [65]	
Cu <sub>60</sub> Hf <sub>25</sub> Ti <sub>15</sub>	134 [99]	1920 [68]	2130 [68]	1.6
Cu <sub>60</sub> Zr <sub>20</sub> Hf <sub>10</sub> Ti <sub>10</sub>	122 [69]	1780 [99]	1990 [69]	1.4 [69]
Cu <sub>60</sub> Hf <sub>15</sub> Ti <sub>15</sub> Zr <sub>10</sub>	127 [99]	1910 [99]	2030 [99]	1.5
Cu <sub>60</sub> Hf <sub>30</sub> Ti <sub>10</sub>	119 [72]	1995 [72]	2120 [72]	1.7
(Cu <sub>0.6</sub> Hf <sub>0.25</sub> Ti <sub>0.15</sub> ) <sub>96</sub> Nb <sub>4</sub>	130 [73]		2405 [73]	
(Cu <sub>0.6</sub> Hf <sub>0.25</sub> Ti <sub>0.15</sub> ) <sub>92</sub> Nb <sub>8</sub>	126 [73]		2305 [73]	
(Cu <sub>0.6</sub> Zr <sub>0.3</sub> Ti <sub>0.1</sub> ) <sub>99</sub> Nb <sub>1</sub>	118 [103]	1800 [103]	2235 [103]	1.8 [103]
(Cu <sub>0.6</sub> Zr <sub>0.3</sub> Ti <sub>0.1</sub> ) <sub>98</sub> Nb <sub>2</sub>	120 [103]	1800 [103]	2250 [103]	1.9 [103]
(Cu <sub>0.6</sub> Zr <sub>0.3</sub> Ti <sub>0.1</sub> ) <sub>97</sub> Nb <sub>3</sub>	120 [103]	1900 [103]	2100 [103]	1.9 [103]

$(\text{Cu}_{0.6}\text{Zr}_{0.3}\text{Ti}_{0.1})_{99}\text{Ta}_1$	119 [103]	1925 [103]	2250 [103]	2 [103]
$(\text{Cu}_{0.6}\text{Zr}_{0.3}\text{Ti}_{0.1})_{98}\text{Ta}_2$	123 [103]	2025 [103]	2250 [103]	2.1 [103]
$(\text{Cu}_{0.6}\text{Zr}_{0.3}\text{Ti}_{0.1})_{97}\text{Ta}_3$	123 [103]	2000 [103]	2100 [103]	2.1 [103]
$\text{Cu}_{51}\text{Ti}_{37}\text{Zr}_{12}$				1.00E-03 [160]
$\text{Cu}_{50}\text{Zr}_{42.5}\text{Ti}_{7.5}$	88 [166]	1700 [166]	1798 [166]	1.9
$\text{Cu}_{50}\text{Ti}_{40}\text{Zr}_{10}$	86 [166]	1700 [166]	1810 [166]	2
$\text{Cu}_{50}\text{Hf}_{42.5}\text{Al}_{7.5}$	128 [94]		2370 [94]	
$\text{Cu}_{52.5}\text{Hf}_{40}\text{Al}_{7.5}$	125 [94]		2345 [94]	
$\text{Cu}_{50}\text{Hf}_{45}\text{Al}_5$	121 [94]		2260 [94]	
$\text{Cu}_{50}(\text{Zr}_{0.75}\text{Hf}_{0.25})_{45}\text{Al}_5$	107 [113]	2000 [113]	2000 [113]	1.8
$\text{Cu}_{50}(\text{Zr}_{0.5}\text{Hf}_{0.5})_{45}\text{Al}_5$	115 [113]	2000 [113]	2025 [113]	1.7
$\text{Cu}_{50}(\text{Zr}_{0.25}\text{Hf}_{0.75})_{45}\text{Al}_5$	120 [113]	2100 [113]	2175 [113]	1.8
$\text{Cu}_{50}\text{Zr}_{45}\text{Al}_5$	102 [113]	1885 [39]	1885 [113]	1.8
$\text{Cu}_{52.5}\text{Zr}_{42.5}\text{Ga}_5$	105 [115]	1900 [115]	1940 [115]	1.8
$\text{Cu}_{55}\text{Zr}_{40}\text{Ga}_5$	109 [115]	1950 [115]	2025 [115]	1.8
$\text{Cu}_{52.5}\text{Zr}_{40}\text{Ga}_{7.5}$	111 [115]	2100 [115]	2130 [115]	1.9
$\text{Cu}_{57.5}\text{Zr}_{40}\text{Ga}_{2.5}$	105 [115]	1800 [115]	1910 [115]	1.7

$\text{Cu}_{55}\text{Zr}_{40}\text{Al}_5$	115 [39]	2150 [117]	2210 [39]	1.9	
$\text{Cu}_{52.5}\text{Zr}_{42.5}\text{Al}_5$	111 [117]		2115 [117]		
$\text{Cu}_{55}\text{Hf}_{40}\text{Al}_5$	122 [117]	2275 [117]	2275 [117]	1.9	
$(\text{Cu}_{0.6}\text{Zr}_{0.3}\text{Ti}_{0.1})_{98}\text{Y}_2$	115 [69]	2000 [69]	2030 [69]	1.7 [69]	
$\text{Cu}_{54}\text{Zr}_{27}\text{Be}_{10}\text{Ti}_9$	146 [100]	2180 [100]	2500 [70]	1.5 [70]	
$(\text{Cu}_{0.6}\text{Zr}_{0.3}\text{Ti}_{0.1})_{92.5}\text{Be}_7$	145 [100]	2090 [100]	2380 [100]	1.4	
$\text{Cu}_{64}\text{Zr}_{36}$	92.3 [95]	2000 [95]	2000 [95]	2.2	
$\text{Cu}_{66}\text{Hf}_{34}$	108 [97]	2100 [97]	2100 [97]	1.8 [97]	
$\text{Cu}_{60}\text{Zr}_{40}$	107 [116]	1920 [116]	1920 [116]	1.8	1.00E-03 [131]
$\text{Cu}_{60}\text{Hf}_{40}$	120 [116]	2100 [116]	2245 [116]	1.8	
$\text{Cu}_{55}\text{Hf}_{45}$	121 [116]	2200 [116]	2260 [116]	1.8	
$\text{Cu}_{64.5}\text{Zr}_{35.5}$					
$\text{Cu}_{50}\text{Zr}_{30}\text{Ti}_{10}\text{Pd}_{10}$	125 [63]		2160 [63]		
$\text{Cu}_{55}\text{Zr}_{30}\text{Ti}_{10}\text{Ag}_5$	112 [64]	2070 [64]	2100 [64]	1.8 [64]	
$\text{Cu}_{55}\text{Zr}_{30}\text{Ti}_{10}\text{Au}_5$	127 [64]	2230 [64]	2230 [64]	1.7 [64]	
$\text{Cu}_{45}\text{Hf}_{45}\text{Al}_5\text{Ag}_5$	119 [96]		2200 [96]		
$\text{Cu}_{45}\text{Hf}_{45}\text{Al}_5\text{Au}_5$	125 [114]	2300 [114]	2330 [114]	1.8	
$\text{Cu}_{45}\text{Hf}_{45}\text{Al}_5\text{Pd}_5$	124 [114]	2250 [114]	2310 [114]	1.8	
$\text{Cu}_{45}\text{Hf}_{45}\text{Al}_5\text{Pt}_5$	124 [114]	2315 [114]	2315 [114]	1.9	
$\text{Cu}_{55}\text{Zr}_{30}\text{Ti}_{10}\text{Pd}_5$	118 [63]	2100 [63]	2270 [63]	1.8	3.40E-05 [140]

$\text{Cu}_{43}\text{Zr}_{43}\text{Al}_7\text{Ag}_7$	103	1850 [173]	1850 [173]	1.8 [173]			
$\text{Cu}_{55}\text{Hf}_{25}\text{Ti}_{15}\text{Pd}_5$						1.20E-05 [162]	
$\text{Cu}_{50}\text{Hf}_{35}\text{Ti}_{10}\text{Ag}_5$	124 [168]	1990 [168]	2180 [168]	1.6			
<b>Hf Based BMGs</b>							
$\text{Hf}_{35}\text{Cu}_{17.9}\text{Zr}_{17.5}\text{Ni}_{14.6}$ $\text{Al}_{10}\text{Ti}_5$	99 [98]	1975 [98]	2035 [98]		2		
$\text{Hf}_{26.25}\text{Zr}_{26.25}\text{Cu}_{17.9}\text{Ni}_1$ $4.6\text{Al}_{10}\text{Ti}_5$	95 [98]	1935 [98]	2000 [98]		2		
$\text{Hf}_{50}\text{Cu}_{30}\text{Ni}_{10}\text{Al}_{10}$	118 [122]	2420	2420 [122]	2.1 [122]			
$\text{Hf}_{50}\text{Cu}_{24}\text{Al}_{10}\text{Ni}_8\text{Zr}_3\text{G}$ $\text{a}_3\text{Ti}_2$						2.70E-05 [139]	
<b>Pd Based BMGs</b>							
$\text{Pd}_{42.5}\text{Cu}_{30}\text{P}_{20}\text{Ni}_{7.5}$	102 [121]	1710 [121]	1710 [121]	2 [118]			
$\text{Pd}_{79}\text{Si}_{10}\text{Cu}_6\text{P}_5$	82 [119]	1475 [119]	1575 [119]	1.8			
$\text{Pd}_{40}\text{Ni}_{40}\text{P}_{20}$	103 [158]	1400 [120]	1400 [120]	1.4		1.30E-05 [141]	
$\text{Pd}_{40}\text{Cu}_{30}\text{P}_{20}\text{Ni}_{10}$	106 [121]	1640 [120]	1640 [120]	1.5	3.00E-04 [129]	1.70E-05 [150]	410 [163]
$\text{Pd}_{35}\text{Cu}_{30}\text{P}_{20}\text{Pt}_{15}$	83 [120]	1410 [120]	1410 [120]	1.7			

$\text{Pd}_{37.5}\text{Cu}_{30}\text{P}_{20}\text{Ni}_{12.5}$	108 [121]	1734 [121]	1734 [121]	1.6	
$\text{Pd}_{50}\text{Cu}_{20}\text{P}_{20}\text{Ni}_{10}$	104 [121]	1550 [121]	1610 [121]	1.5	4.40E-05 [137]
$\text{Pd}_{45}\text{Cu}_{20}\text{P}_{20}\text{Ni}_{15}$	108 [121]	1600 [121]	1630 [121]	1.5	
$\text{Pd}_{40}\text{Cu}_{20}\text{Ni}_{20}\text{P}_{20}$	110 [121]	1700 [121]	1736 [121]	1.5	
$\text{Pd}_{43}\text{Cu}_{27}\text{P}_{20}\text{Ni}_{10}$					1.30E-05 [152]
$\text{Pd}_{77}\text{Si}_{17}\text{Cu}_6$	93	1440 [172]	1570	1.5	
Ca Based BMGs					
$\text{Ca}_{57}\text{Cu}_{24}\text{Mg}_{19}$	38 [109]	545 [109]	545 [109]	1.4	
Ca-(33-35%)Al					
$\text{Ca}_{56.5}\text{Al}_{28.5}\text{Mg}_{10}\text{Cu}_5$					
$\text{Ca}_{56.5}\text{Al}_{28.5}\text{Mg}_{10}\text{Ag}_5$					
$\text{Ca}_{60}\text{Mg}_{25}\text{Ni}_{15}$					
$\text{Ca}_{65}\text{Zn}_{20}\text{Mg}_{15}$					
Au Based BMGs					
$\text{Au}_{46}\text{Cu}_{29}\text{Si}_{20}\text{Ag}_5$					
$\text{Au}_{52}\text{Cu}_{29.2}\text{Si}_{16.5}\text{Pd}_{2.3}$					
$\text{Au}_{49}\text{Cu}_{26.9}\text{Si}_{16.3}\text{Ag}_{5.5}\text{Pd}_{2.3}$					
$\text{Au}_{77.8}\text{Ge}_{13.8}\text{Si}_{8.4}$					
Pt Based BMGs					

$Pt_{60}Cu_{20}P_{20}$	
$Pt_{57.5}P_{22.5}Cu_{14.7}Ni_{5.3}$	
$Pt_{42.5}Cu_{27}P_{21}Ni_{9.5}$	
$Pt_{60}P_{22}Cu_{16}Co_2$	
Sc Based BMGs	
$Sc_{36}Al_{24}Co_{20}Y_{20}$	85.2 [167]

## REFERENCES

- [1] T. E. Tietz and J. W. Wilson, "Behavior and Properties of Refractory Metals", Stanford University Press, 1965.
- [2] K. A. Gschneider, Jr. Solid State Physics 16, 1964, p. 275.
- [3] H. A. Wriedt and R. A. Oriani, Scripta Metallurgica 8, 1974, p. 203-208.
- [4] A. L. Mincher and W. F. Sheeley, Transactions of the Metallurgical Society of AIME 221, 1961, p. 19-25.
- [5] F. F. Schmidt and H. R. Ogden "The Engineering Properties of Columbium and Columbium Alloys" DMIC Report 188, Batelle Memorial Institute - Defence Metals Information Center, 1963, p. A-83.
- [6] G. Elssner and G. Horz, Journal of the Less-Common Metals, 21, 1970, p. 383-393.
- [7] J. F. Enrietto, G. M. Sinclair and C. A. Wert, "Mechanical Behavior of Columbium Containing Oxygen", p. 503-519 in Columbium Metallurgy (D. L. Douglass F. W. Kunz etc.) Interscience Publishers, N. Y. 1961.
- [8] N. Igata, H. Murakami and N. Kuramochi. Scripta Metallurgica v 13 n 7, 1979, p. 627-629.
- [9] R. D. Conner, A. J. Rosakis, W. L. Johnson and D. M. Owen, Scripta Materialia 37, 1997, p. 1373-1378.

- [10] A. Pecker and W. L. Johnson. *Appl. Phys. Lett.* v 63, 1993, p. 2342-2344.
- [11] J. Xue, Q. Zhou, H. Suzuki and S. Misawa, *Journal of Low Temperature Physics*, Vol 121, Nos. 3/4, 2000, p. 127-136.
- [12] M. I. Bychkova, P. F. Koshelev, P. N. Nikitin and V. V. Katkova, *Metal Science and Heat Treatment*, v 25, n 9-10, Sep-Oct. 1983, p. 707-709.
- [13] V. P. Lebedev, A. A. Mamalui, V. A. Pervakov, N. S. Petrenko, V. P. Popov and V. I. Khotkevich, *Ukr. Fiz. Zh.* v 14 (5), 1969, p. 746-750.
- [14] *ASM Handbook*, Vol. 2, 1990, p. 1144.
- [15] P. J. Veitch, J. Ferreira, D. G. Blair and N. Linthorne, *Cryogenics* v 27, n 10, Oct. 1987, p. 586-588.
- [16] P. F. Koshelev, V. S. Mikheev and P. N. Nikitin, *Metal Science and Heat Treatment*, v 14, n 1-2, Jan-Feb, 1972, p. 111-113.
- [17] V. N. Kovaleva and V. A. Moskalenko, *Cryogenics* v 29, n 10, Oct. 1989, p. 1002-1005.
- [18] E. W. Collings and J. C. Ho, *Phys Rev. B Solid State*, v 2, n 2, July 15, 1970, p. 235-244.
- [19] H. W. Altman, T. Rubin and H. L. Johnston "Coefficient of Thermal Expansion of Solids at Low Temperature III. The Thermal Expansion of Pure Metals, with data for Aluminum, Nickel, Titanium, and Zirconium", Ohio State University, Cryogenic Laboratory Rept. OSU-TR-264-27, 10 pp., 1954.
- [20] *ASM Handbook*, Vol. 2, 1990, p. 597.
- [21] J. Petit, M. Quintard, P. Mazot and J. de Fouquet, *Proceedings of the Society of Photo-Optical Instrumentation Engineers*, v 2, 1975, p. 407-414.
- [22] M. Doner and H. Conrad, *Met. Trans.* v. 4, 1973, p. 2809.
- [23] H. A. Buhler and H. W. Wagener, *Bänder Bläche Rohre*, v. 6, 1965, p. 677.
- [24] A. Inoue, T. Masumoto, *Materials Science & Engineering A: Structural Materials: Properties, Microstructure and Processing*, v A133, n pt 1, Mar 15, 1991, *Structural Materials: Properties, Microstructure and Processing*, p. 6-9.

- [25] A. Inoue, T. Masumoto, *Journal of Alloys and Compounds*, v 207-08, Jun, 1994, p. 340-348.
- [26] K. Amiya, N. Nishiyama, A. Inoue, T. Masumoto, *Materials Science & Engineering A: Structural Materials: Properties, Microstructure and Processing*, v 179-80, n pt 1, May 1, 1994, p. 692-696.
- [27] A. Inoue, T. Masumoto, *Materials Science & Engineering A: Structural Materials: Properties, Microstructure and Processing*, v A173, n 1-2, Dec 20, 1993, *Advances in Solidification Processes*, p. 1-8.
- [28] A. Inoue, H. Yamaguchi, T. Zhang and T. Masumoto, *Materials Transactions JIM*, v 30, n 2, Feb, 1990, p. 104-109.
- [29] A. Inoue, T. Zhang and T. Masumoto, *Materials Transactions, JIM*, v 36, n 3, Mar, 1995, p. 391-398.
- [30] A. Inoue, T. Zhang and T. Masumoto, *Materials Transactions, JIM*. V30 (1989), p. 965.
- [31] S. G. Kim, A. Inoue and T. Masumoto, *Materials Transactions, JIM*. V31 (1990), p. 929.
- [32] T. Zhang and A. Inoue, *Materials Science and Engineering A*, v 375-377, n 1-2 SPEC. ISS., Jul 15, 2004, p. 432-435.
- [33] Y. Kawamura, H. Kato, A. Inoue and T. Masumoto, *Materials Science & Engineering A*, v 219, n 1-2, Nov 30, 1996, p. 39-43.
- [34] Dr. Riccardo DeSalvo website, <http://www.ligo.caltech.edu/~desalvo/>
- [35] A. Inoue, T. Zhang and T. Masumoto, *Materials Transactions, JIM*, v 31, n 3, Mar, 1990, p. 177-183.
- [36] A. Inoue, M. Onuki, Y. Takano and T. Yamaguchi, *Materials Transactions*, v 42, n 4, 2001, p. 678-681.
- [37] T. Zhang and A. Inoue, *Materials Transactions*, v 43, n 2, February, 2002, p. 267-270.
- [38] T. Wada, T. Zhang and A. Inoue, *Materials Transactions*, v 43, n 11, November, 2002, p. 2843-2846.
- [39] A. Inoue and W. Zhang, *Materials Transactions*, v 43, n 11, November, 2002, p. 2921-2925.
- [40] L. Wang, L. Ma and A. Inoue, *Materials Transactions*, v 43, n 9, September, 2002, p. 2346-2349.
- [41] A. Leonhard, M. Heilmaier, J. Eckert and L. Schultz, *Materials Research Society Symposium - Proceedings*, v 554, 1999, p. 137-142.
- [42] A. Inoue, *Intermetallics*, v 8, n 5-6, May-Jun, 2000, p. 455-468.

- 
- [43] C. Fan and A. Inoue, *Applied Physics Letters*, v 77, n 1, Jul 3, 2000, p. 46-48.
- [44] S. Pang, T. Zhang, K. Asami and A. Inoue, *Journal of Materials Research*, v 18, n 7, July, 2003, p. 1652-1658.
- [45] Y. Yokoyama, K. Fukaura and A. Inoue, *Materials Science and Engineering A*, v 375-377, n 1-2 SPEC. ISS., Jul 15, 2004, p. 427-431.
- [46] H. Kato, J. Saida and A. Inoue, *Scripta Materialia*, v 51, n 11, November, 2004, p. 1063-1068.
- [47] L. Q. Xing, D. M. Herlach, M. Cornet, C. Bertrand, J. Dallas, M. Trichet and J. Chevalier, *Materials Science & Engineering A: Structural Materials: Properties, Microstructure and Processing*, v A226-22, Jun 15, 1997, p. 874-877.
- [48] R. D. Conner, H. Choi-Yim and W. L. Johnson, *Journal of Materials Research*, v 14, n 8, Aug, 1999, p. 3292-3297.
- [49] X. Rao, P. C. Si, J. N. Wang, Z. Xu, S. Xu, W. M. Wang and W. H. Wang, *Materials Letters*, v 50, n 5-6, September, 2001, p. 279-283.
- [50] C. T. Liu, M. F. Chisholm and M. K. Miller, *Intermetallics*, v 10, n 11-12, November, 2002, p. 1105-1112.
- [51] K. Q. Qiu, A. M. Wang, H. F. Zhang, B.Z. Ding and Z. Q. Hu, *Intermetallics*, v 10, n 11-12, November, 2002, p. 1283-1288.
- [52] Z. Bian, M. X. Pan, Y. Zhang and W. H. Wang, *Applied Physics Letters*, v 81, n 25, Dec 16 2003, 2002, p. 4739-4741.
- [53] X. Xiao, S. Fang, L. Xia, W. Li, Q. Hua, Y. Dong, *Journal of Alloys and Compounds*, v 351, n 1-2, Mar 10, 2003, p. 324-328.
- [54] G. He, W. Loser, J. Eckert and L. Schultz, *Materials Science and Engineering A*, v 352, n 1-2, Jul 15, 2003, p. 179-185.
- [55] D. Xu, G. Duan, W. L. Johnson and C. Garland, *Acta Materialia*, v 52, n 12, Jul 12, 2004, p. 3493-3497.
- [56] J. Eckert, U. Kuhn, J. Das, S. Scudino and N. Radtke, *Advanced Engineering Materials*, v 7, n 7, July, 2005, p. 587-596.
- [57] A. Inoue and T. Zhang, *Materials Transactions, JIM*, v 36, n 9, Sep, 1995, p. 1184-1187.
- [58] H. Kimura, M. Kishida, T. Kaneko, A. Inoue, T. Masumoto, *Materials Transactions, JIM*, v 36, n 7, Jul, 1995, p. 890-895.
- [59] T. Zhang and A. Inoue, *Materials Transactions, JIM*, v 39, n 8, Aug, 1998, p. 857-862.
- [60] T. Zhang and A. Inoue, *Materials Transactions, JIM*, v 39, n 12, Dec, 1998, p. 1230-1237.

- 
- [61] A. Inoue, T. Zhang, M. W. Chen and T. Sakurai, *Materials Transactions, JIM*, v 40, n 12, Dec, 1999, p. 1382-1389.
- [62] M. Calin, J. Eckert and L. Schultz, *Scripta Materialia*, v 48, n 6, March, 2003, p. 653-658.
- [63] D. V. Louzguine, A.R. Yavari and A. Inoue, *Philosophical Magazine*, v 83, n 26, Sep 11, 2003, p. 2989-3003.
- [64] D. V. Louzguine, H. Kato and A. Inoue, *Science and Technology of Advanced Materials*, v 4, n 4, Jul 1, 2003, p. 327-333.
- [65] A. Concustell, M. Zielinska, A. Revesz, L. K. Varga, S. Surinach and M.D. Baro, *Intermetallics*, v 12, n 10-11.
- [66] E. S. Park, D. H. Kim, T. Ohkubo and K. Hono, *Journal of Non-Crystalline Solids*, v 351, n 14-15, May 15, 2005, p. 1232-1238.
- [67] A. Concustell, G. Alcala, S. Mato, T.G. Woodcock, A. Gebert, J. Eckert and M.D. Baro, *Intermetallics*, v 13, n 11, November, 2005, p. 1214-1219.
- [68] A. Inoue, W. Zhang, T. Zhang and K. Kurosaka, *Acta Materialia*, v 49, n 14, Aug 16, 2001, p. 2645-2652.
- [69] A. Inoue, W. Zhang, T. Zhang and K. Kurosaka, *Journal of Non-Crystalline Solids*, v 304, n 1-3, June, 2002, p. 200-209.
- [70] A. Inoue, W. Zhang, T. Zhang, K. Kurosaka and D. V. Louzguine, *Journal of Metastable and Nanocrystalline Materials*, v 15-16, *Proceedings of the 9th International Symposium on Metastable Mechanically Alloyed and Nanocrystalline Materials (ISMANAM-2002)*, 2003, p. 3-10.
- [71] D. V. Louzguine and A. Inoue, *Philosophical Magazine Letters*, v 83, n 3, March, 2003, p. 191-196.
- [72] A. Inoue, W. Zhang, T. Zhang and K. Kurosaka, *Journal of Materials Research*, v 16, n 10, October, 2001, p. 2836-2844.
- [73] C. Qin, W. Zhang, K. Asami, N. Ohtsu and A. Inoue, *Acta Materialia*, v 53, n 14, August, 2005, p. 3903-3911.
- [74] Y. K. Xu and J. Xu, *Scripta Materialia*, v 49, n 9, November, 2003, p. 843-848.
- [75] A. Inoue, K. Ohtera, M. Kohinata, T. Masayoshi, A.P Tsai and T. Masumoto, *Journal of Non-Crystalline Solids*, v 117-18, n pt 2, Feb 1, 1990, p. 712-715.
- [76] C. Fan, C. Li and A. Inoue, *Journal of Non-Crystalline Solids*, v 270, n 1-3, May, 2000, p. 28-33.

- 
- [77] K. Jin and J. F. Loffler, *Applied Physics Letters*, v 86, n 24, Jun 13, 2005, p. 241909.
- [78] H. J. Kim, J. K. Lee, S. Y. Shin, H. G. Jeong, D. H. Kim and J. C. Bae, *Intermetallics*, v 12, n 10-11 SPEC. ISS., October/November, 2004, p. 1109-1113.
- [79] Y. C. Kim, W. T. Kim and D. H. Kim, *Materials Science and Engineering A*, v 375-377, n 1-2 SPEC. ISS., Jul 15, 2004, p. 127-135.
- [80] T. Zhang and A. Inoue, *Materials Science and Engineering A*, v 304-306, n 1-2, May 31, 2001, p. 771-774.
- [81] K. Amiya and A. Inoue, *Materials Transactions, JIM*, v 41, n 11, Nov, 2000, p. 1460-1462.
- [82] G. Yuan and A. Inoue, *Journal of Alloys and Compounds*, v 387, n 1-2, Jan 25, 2005, p. 134-138.
- [83] W. Y. Liu, H. F. Zhang, Z. Q. Hu and H. Wang, *Journal of Alloys and Compounds*, v 397, n 1-2, Jul 19, 2005, p. 202-206.
- [84] J. Eckert, B. Bartusch and A. Gebert, *Journal of Metastable and Nanocrystalline Materials*, v 15-16, Proceedings of the 9th International Symposium on Metastable Mechanically Alloyed and Nanocrystalline Materials (ISMANAM-2002), 2003, p. 37-42.
- [85] Y. K. Xu, H. Ma, J. Xu and En Ma, *Acta Materialia*, v 53, n 6, April, 2005, p. 1857-1866.
- [86] A. Inoue, C. Fan, J. Saida and T. Zhang, *Science and Technology of Advanced Materials*, v 1, n 2, July, 2000, p. 73-86.
- [87] J. Basu, N. Nagendra, Y. Li and U. Ramamurty, *Philosophical Magazine*, v 83, n 15, May 21, 2003, p. 1747-1760.
- [88] M. L. Lee, Y. Li and C. A. Schuh, *Acta Materialia*, v 52, n 14, Aug 16, 2004, p. 4121-4131.
- [89] Y. Zhang, D. Q. Zhao, B. C. Wei, P. Wen, M. X. Pan, W. H. Wang, *Journal of Materials Research*, v 16, n 6, June, 2001, p. 1675-1679.
- [90] X. D. Hui, H. C. Kou, J. P. He, Y. L. Wang, W. Dong, G. L. Chen, *Intermetallics*, v 10, n 11-12, November, 2002, p. 1065-1069.

- [91] Y. F. Sun, S. K. Guan, B. C. Wei, Y. R. Wang, C. H. Shek, *Materials Science and Engineering A*, v 406, n 1-2, Oct 15, 2005, p. 57-62.
- [92] Y. C. Kim, J. H. Na, J. M. Park, D. H Kim, J. K. Lee and W. T Kim, *Applied Physics Letters*, v 83, n 15, Oct 13, 2003, p. 3093-3095.
- [93] C. Ma, H. Soejima, S. Ishihara, K. Amiya, N. Nishiyama and A. Inoue, *Materials Transactions*, v 45, n 11, November, 2004, p. 3223-3227.
- [94] A. Inoue and W. Zhang, *Journal of Materials Research*, v 18, n 6, June, 2003, p. 1435-1440.
- [95] D. Xu, B. Lohwongwatana, G. Duan, W. L. Johnson and C. Garland, *Acta Materialia*, v 52, n 9, May 17, 2004, p. 2621-2624.
- [96] A. Inoue and W. Zhang, *Applied Physics Letters*, v 83, n 12, Sep 22, 2003, p. 2351-2353.
- [97] G. Duan, D. Xu and W. L. Johnson, *Metallurgical and Materials Transactions A: Physical Metallurgy and Materials Science*, v 36 A, n 2, February, 2005, p. 455-458.
- [98] X. Gu, T. Jiao, L. J. Kecskes, R. H. Woodman, C. Fan, K. T. Ramesh and T. C. Huftnagel, *Journal of Non-Crystalline Solids*, v 317, n 1-2, March, 2003, p. 112-117.
- [99] A. Inoue, W. Zhang, T. Zhang and K. Kurosaka, *Materials Transactions*, v 42, n 8, Nano-Metals I, 2001, p. 1805-1812.
- [100] A. Inoue, T. Zhang, K. Kurosaka and W. Zhang, *Materials Transactions*, v 42, n 8, Nano-Metals I, 2001, p. 1800-1804.
- [101] A. Inoue, W. Zhang, T. Zhang and K. Kurosaka, *Materials Transactions*, v 42, n 6, Structure and Electronic Properties in the Pseudogap Systems, 2001, p. 1149-1151.
- [102] L. Ma, L. Wang, T. Zhang and A. Inoue, *Materials Transactions*, v 43, n 2, February, 2002, p. 277-280.
- [103] T. Zhang and A. Inoue, *Materials Transactions*, v 43, n 6, June, 2002, p. 1367-1370.
- [104] T. Zhang, T. Yamamoto and A. Inoue, *Materials Transactions*, v 43, n 12, December, 2002, p. 3222-3226.
- [105] T. Yamamoto, C. Qin, T. Zhang, K. Asami and A. Inoue, *Materials Transactions*, v 44, n 6, June, 2003, p. 1147-1152.

- [106] J. M. Park, Y. C. Kim, W. T. Kim and D. H. Kim, *Materials Transactions*, v 45, n 2, February, 2004, p. 595-598.
- [107] C. Ma, S. Ishihara, H. Soejima, N. Nishiyama and A. Inoue, *Materials Transactions*, v 45, n 5, May, 2004, p. 1802-1806.
- [108] T. Zhang and A. Inoue, *Materials Transactions, JIM*, v 39, n 10, Oct, 1998, p. 1001-1006.
- [109] K. Amiya and A. Inoue, *Materials Transactions*, v 43, n 1, January, 2002, p. 81-84.
- [110] H. Men, W. T. Kim and D. H. Kim, *Materials Transactions*, v 44, n 10, October, 2003, p. 2141-2144.
- [111] G. Yuan, T. Zhang and A. Inoue, *Materials Transactions*, v 44, n 11, November, 2003, p. 2271-2275.
- [112] E. S. Park, W. T. Kim and D. H. Kim, *Materials Transactions*, v 45, n 7, July, 2004, p. 2474-2477.
- [113] W. Zhang and A. Inoue, *Materials Transactions*, v 44, n 10, October, 2003, p. 2220-2223.
- [114] W. Zhang and A. Inoue, *Materials Transactions*, v 44, n 11, November, 2003, p. 2346-2349.
- [115] W. Zhang and A. Inoue, *Materials Transactions, Materials Transactions*, v 45, n 2, February, 2004, p. 532-535.
- [116] A. Inoue and W. Zhang, *Materials Transactions*, v 45, n 2, February, 2004, p. 584-587.
- [117] W. Zhang and A. Inoue, *Materials Transactions*, v 45, n 4, April, 2004, p. 1210-1213.
- [118] T. Wada and A. Inoue, *Materials Transactions*, v 44, n 10, October, 2003, p. 2228-2231.
- [119] L. Liu, A. Inoue and T. Zhang, *Materials Transactions*, v 46, n 2, February, 2005, p. 376-378.
- [120] K. Takenaka, T. Wada, N. Nishiyama, H. Kimura and A. Inoue, *Materials Transactions*, v 46, n 7, July, 2005, p. 1720-1724.
- [121] C. Ma and A. Inoue, *Materials Transactions*, v 43, n 12, December, 2002, p. 3266-3272.
- [122] L. Ma, L. Wang, T. Zhang and A. Inoue, *Materials Transactions*, v 43, n 9, September, 2002, p. 2357-2359.
- [123] H. Okumura, H. S. Chen, A. Inoue and T. Masumoto, *Journal of Non-Crystalline Solids*, v 130, n 3, Aug, 1991, p. 304-310.
- [124] R. Scarfone and H. R. Sinning, *Journal of Alloys and Compounds*, v 310, Sep, 2000, p. 229-232.
- [125] O. P. Bobrov, V. A. Khonik, S. N. Laptev and M. Y. Yazvitsky, *Scripta Materialia*, v 49, n 3, August, 2003, p. 255-260.

- [126] M. Hasegawa, S. Yamaura, H. Kato, K. Amiya, N. Nishiyama and A. Inoue, *Journal of Alloys and Compounds*, v 355, n 1-2, Jun 30, 2003, p. 37-41.
- [127] Y. Hiki, T. Yagi, T. Aida and S. Takeuchi, *Journal of Alloys and Compounds*, v 355, n 1-2, Jun 30, 2003, p. 42-46.
- [128] Y. Hiki, T. Yagi, T. Aida and S. Takeuchi, *Materials Science and Engineering A*, v 370, n 1-2, Apr 15, 2004, p. 302-306.
- [129] T. Yagi, T. Imai, R. Tamura and S. Takeuchi, *Materials Science and Engineering A*, v 370, n 1-2, Apr 15, 2004, p. 264-267.
- [130] P. Wen, D. Q. Zhao, M. X. Pan, W. H. Wang, J. P. Shui and Y. P. Sun, *Intermetallics*, v 12, n 10-11 SPEC. ISS., October/November, 2004, p. 1245-1249.
- [131] H. Mizubayashi, M. Matsumoto and S. Okuda, *Journal of Alloys and Compounds*, v 211-1, Sept, 1994, p. 237-240.
- [132] Y. M. Soifer, N. P. Kobelev, I. G. Brodova, A. N. Manukhin, E. Korin and L. Soifer, *Nanostructured Materials*, v 12, n 5, 1999, p. 875-878.
- [133] N. Mattern, U. Kuhn, H. Hermann, S. Roth, H. Vinzelberg and J. Eckert, *Materials Science and Engineering A*, v 375-377, n 1-2 SPEC. ISS., Jul 15, 2004, p. 351-354.
- [134] G. D. Mukherjee, C. Bansal and A. Chatterjee, *Solid State Communications*, v 104, n 11, Dec, 1997, p. 657-661.
- [135] D. Schermeyer and H. Neuhaeuser, *Materials Science & Engineering A: Structural Materials: Properties, Microstructure and Processing*, v A226-22, June 15, 1997, p. 846-850.
- [136] V. Keryvin, M. L. Vaillant, T. Rouxel and Y. Kawamura, *Scripta Materialia*, v 47, n 1, July, 2002, p. 19-23.
- [137] A. R. Yavari, N. Nikolov, N. Nishiyama, T. Zhang, A. Inoue, J. L. Uriarte and G. Heunen, *Materials Science and Engineering A*, v 375-377, n 1-2 SPEC. ISS., Jul 15, 2004, p. 709-712.
- [138] K. Hajlaoui, T. Benameur, G. Vaughan and A. R. Yavari, *Scripta Materialia*, v 51, n 9, November, 2004, p 843-848.

- [139] A. R. Yavari, A. Le Moulec, N. Nishiyama, A. Inoue, G. Vaughan, A. Kvik and W. J. F. Botta, *Journal of Metastable and Nanocrystalline Materials*, v 20-21, Metastable, Mechanically Alloyed and Nanocrystalline Materials ISMANAM-2002, 2004, p. 23-28.
- [140] A. R. Yavari, S. Pang, D. Louzguine, A. Inoue, N. Lupu, N. Nikolov and G. Heunen, *Journal of Metastable and Nanocrystalline Materials*, v 15-16, Proceedings of the 9th International Symposium on Metastable Mechanically Alloyed and Nanocrystalline Materials (ISMANAM-2002), 2003, p. 105-110.
- [141] G. Wilde, S. G. Klose, W. Soellner, G. P. Goerler, K. Jeropoulos, R. Willnecker and H. J. Fecht, *Materials Science & Engineering A: Structural Materials: Properties, Microstructure and Processing*, v A226-22, Jun 15, 1997, p. 434-438.
- [142] Q. Jing, R. P. Liu, G. Li and W. K. Wang, *Scripta Materialia*, v 49, n 2, July, 2003, p. 111-115.
- [143] C. J. Gilbert, J. M. Lippmann and R. O. Ritchie, *Scripta Materialia*, v 38, n 4, Jan 13, 1998, p. 537-542.
- [144] W. H. Peter, P. K. Liaw, R. A. Buchanan, C. T. Liu, C. R. Brooks, J. A. Horton Jr., C. A. Carmichael Jr. and J. L. Wright, *Intermetallics*, v 10, n 11-12, November, 2002, p. 1125-1129.
- [145] G. Y. Wang, P. K. Liaw, W. H. Peter, B. Yang, Y. Yokoyama, M. L. Benson, B. A. Green, M. J. Kirkham, S. A. White, T. A. Saleh, R. L. McDaniels, R. V. Steward, R. A. Buchanan, C. T. Liu and C. R. Brooks, *Intermetallics*, v 12, n 7-9 SPEC. ISS., July/September, 2004, p. 885-892.
- [146] G. Y. Wang, P. K. Liaw, A. Peker, B. Yang, M. L. Benson, W. Yuan, W. H. Peter, L. Huang, M. Freels, R. A. Buchanan, C. T. Liu, C. R. Brooks, *Intermetallics*, v 13, n 3-4, March/April, 2005, International Workshop on Ordered Intermetallics and Advanced Metallic Materials, p. 429-435.
- [147] H. R. Sinning and R. Scarfone, *Materials Science Forum*, v 343 II, 2000, p. 738-743.
- [148] S. I. Yamaura, M. Hasegawa, H. Kimura and A. Inoue, *Materials Transactions*, v 43, n 10, October, 2002, p. 2543-2547.

- [149] Y. M. Soifer, N. P. Kobelev, E. Korin, L. Soifer, D. Mogilyanskii and A. Bettelheim, Materials Research Society Symposium - Proceedings, v 644, 2001, p. L11.3.1-L11.3.6.
- [150] N. Nishiyama, M. Horino and A. Inoue, Materials Transactions, JIM, v 41, n 11, Nov, 2000, p. 1432-1434.
- [151] K. Samwer, B. Damaschke, M. Krause and P. Ryder, Materials Research Society Symposium - Proceedings, v 644, 2001, p. L12.21.1-L12.21.6.
- [152] I. R. Lu, G. P. Gorler, R. Willnecker and H. J. Fecht, Materials Research Society Symposium - Proceedings, v 644, 2001, p. L3.2.1-L3.2.6.
- [153] T. Zhang and A. Inoue, Materials Research Society Symposium - Proceedings, v 554, 1999, p. 361-366.
- [154] Y. Yokoyama, K. Fukaura and A. Inoue, TMS Annual Meeting, Science and Engineering, 2003, p. 77-90.
- [155] Z. F. Zhang, J. Eckert and L. Schultz, Journal of Materials Research, v 18, n 2, February, 2003, p. 456-465.
- [156] J. Schroers, B. Lohwongwatana, W. L. Johnson and A. Peker, Applied Physics Letters, v 87, n 6, 2005, p. 061912.
- [157] J. Schroers, W. L. Johnson, Applied Physics Letters, v 84, n 18, May 3, 2004, p. 3666-3668.
- [158] Y. He, T. Shen and R. B. Schwarz, Metallurgical and Materials Transactions A: Physical Metallurgy and Materials Science, v 29A, n 7, Jul, 1998, p. 1795-1804.
- [159] Y. Yokoyama, D. Fukaura and H. Sunada, Materials Transactions, JIM, v 41, n 6, Jun, 2000, p. 675-680.
- [160] M. Hasegawa, M. Takeuchi, H. Kato, S. Yamaura and A. Inoue, Journal of Alloys and Compounds, v 372, n 1-2, Jun 9, 2004, p. 116-120.
- [161] M. Hasegawa, K. Kotani, S. Yamaura, H. Kato, I. Kodama and A. Inoue, Journal of Alloys and Compounds, v 365, n 1-2, Feb 25, 2004, p. 221-227.
- [162] D. Louzguine, A. R. Yavari, K. Ota, G. Vaughan and A. Inoue, Journal of Non-Crystalline Solids, v 351, n 19-20, Jul 1, 2005, p. 1639-1645.

- [163] Y. Yokoyama, N. Nishiyama, K. Fukaura, H. Sunada, Y. Murakami and A. Inoue, *Materials Transactions*, v 42, n 5, 2001, p. 876-880.
- [164] T. C. Hufnagel, T. Jiao, Y. Li, L. Q. Xing and K. T. Ramesh, *Journal of Materials Research*, v 17, n 6, June, 2002, p. 1441-1445.
- [165] X. F. Pan, H. Zhang, Z. F. Zhang, M. Stoica, G. He and J. Eckert, *Journal of Materials Research*, v 20, n 10, October, 2005, p. 2632-2638.
- [166] H. Men, S. J. Pang and T. Zhang, *Materials Science and Engineering A*, v 408, n 1-2, Nov 5, 2005, p. 326-329.
- [167] X. K. Xi, S. Li, R. J. Wang, D. Q. Zhao, M. X. Pan and W. H. Wang, *Journal of Materials Research*, v 20, n 9, September, 2005, p. 2243-2247.
- [168] Z. Bian, H. Kato, C. Qin, W. Zhang and A. Inoue, *Acta Materialia*, v 53, n 7, April, 2005, p. 2037-2048.
- [169] E. S. Park, J. Y. Lee and D. H. Kim, *Journal of Materials Research*, v 20, n 9, September, 2005, p. 2379-2385.
- [170] G. Yuan, C. Qin and A. Inoue, *Journal of Materials Research*, v 20, n 2, February, 2005, p. 394-400.
- [171] H. Men, S. Pang, A. Inoue and T. Zhang, *Materials Transactions*, v 46, n 10, October, 2005, p. 2218-2220.
- [172] L. A. Davis, *Mechanical Behavior of Rapidly Solidified Materials* edited by S. M. L. Sastry and B. A. MacDonald, Publication of The Metallurgical Society, 1986, p. 284.

**Appendix B: Bulk Metallic Glass Systems Literature Review Based on Castability**

Appendix B lists the results of a thorough literature review on the globally available BMG alloy systems based on the castability issues such as critical size of casting, critical cooling rate during solidification, casting techniques and performance properties of the cast part. This is an on-going task in this project and Table B does not present an exhaustive list of BMG alloys.

Major System	Material	Hv or $\sigma^*$ (MPa)	E (GPa)	Critical Size thickness** ( $\delta$ ) or diameter ( $\phi$ ), (mm)	Critical cooling rate(K/s)	Property characteristics & Applications	Fabrication Method	
Zr-based	Zr-Al,Ti -Ni,Fe-Nb,Cu-(Be)	Zr <sub>41.2</sub> Ti <sub>13.8</sub> Cu <sub>12.5</sub> Ni <sub>10</sub> Be <sub>22.5</sub> (Vit1) [1,2]	1900	90 (101.2,96)	$\delta$ 100	1-10	High mechanical strength, high fracture toughness and corrosion resistance. Sporting goods materials	Induction melting on a water cooled silver boat under a Ti-gettered argon atmosphere, further processed by casting into copper molds under an inert gas atmosphere and by melting of several ingots together in sealed silica tubes followed by water quenching <sup>[11]</sup> Ti(99.99%),Zr(99.9%),Cu(99.999%), Ni(99.99%), and Be(99.99%) in an inductive levitation melting device under a Ti-gettered Ar atmosphere, and by quenching the molten droplet on a water-cooled Cu mol d <sup>[19]</sup>
		Zr <sub>46.75</sub> Ti <sub>8.25</sub> Cu <sub>7.5</sub> Ni <sub>14.6</sub> Be <sub>27.5</sub> (Vit2) [2]			( $\delta$ 30)			
		Zr <sub>44</sub> Ti <sub>11</sub> Cu <sub>10</sub> Ni <sub>10</sub> Be <sub>25</sub> (LM1b) [2]						Thermal expansion coefficient: 5 $\mu$ m/m/ <sup>o</sup> C
		Zr <sub>52.5</sub> Ti <sub>5</sub> Cu <sub>17.9</sub> Ni <sub>14.6</sub> Al <sub>10</sub> (Vit105) [2]						

		Zr <sub>48</sub> Nb <sub>8</sub> Cu <sub>12</sub> Fe <sub>8</sub> Be <sub>24</sub> [3]	1600	95.7	φ8			Arc melting a mixture of constituent elements in Ti-gettered argon atmosphere. The ingot was remelted in a vacuum-sealed quartz tube and quenched in water
		Zr <sub>57</sub> Nb <sub>5</sub> Cu <sub>15.4</sub> Ni <sub>12.6</sub> Al <sub>10</sub> [4]						
		Zr <sub>57</sub> Ti <sub>5</sub> Al <sub>10</sub> Cu <sub>20</sub> Ni <sub>8</sub> [4]						
		Zr <sub>65</sub> Al <sub>7.5</sub> Ni <sub>10</sub> Cu <sub>17.5</sub> [5]	1570,1.9	92	δ 15			LCTE:9.00E-06
		Zr <sub>60</sub> Al <sub>10</sub> Ni <sub>10</sub> Cu <sub>20</sub> [4]	1790,2.2	84	φ17[6]			LCTE:2.98E-05
		Zr <sub>55</sub> Al <sub>10</sub> Ni <sub>5</sub> Cu <sub>30</sub> [4]			φ 3			
		Zr <sub>48</sub> Cu <sub>45</sub> Al <sub>7</sub> [4]			φ 8			
		Zr <sub>66</sub> Al <sub>8</sub> Ni <sub>26</sub> [4]						
		Zr <sub>55</sub> Al <sub>20</sub> Co <sub>25</sub> [7]			φ2.5			
		Zr <sub>55</sub> Al <sub>20</sub> Co <sub>20</sub> Cu <sub>5</sub> [7]			φ5			Arc melting the mixtures of pure Zr, Al, Co, and Cu metals in an argon atmosphere. From the alloy ingots. Rod samples with diameters of 1–5mm and length of 50mm were prepared by copper-mold casting.
	Pd-Ni-P	Pd <sub>40</sub> Ni <sub>40</sub> P <sub>20</sub> [8]			φ 10	1(10),0.15 with B <sub>2</sub> O <sub>3</sub> flux		Induction melting a mixture of pure Ni and Cu metals and pre-alloyed Pd-P ingots in an argon atmosphere.
		Pd <sub>43</sub> Ni <sub>10</sub> Cu <sub>27</sub> P <sub>20</sub> [9]			φ5			The amorphous alloys were prepared by copper mold casting and water quenching/ Boron oxide fluxing method to purify the melt and keep it very clean to inhibit heterogeneous nucleation
Pd-based	Pd-Cu-Ni-P	Pd <sub>40</sub> Cu <sub>30</sub> Ni <sub>10</sub> P <sub>20</sub> [9]	1640	106	δ 75	0.1 with B <sub>2</sub> O <sub>3</sub> flux	Die materials	
	Pd-Cu-Si	Pd <sub>77</sub> Cu <sub>6</sub> Si <sub>17</sub> [10]	1570	93	φ1-3	100(10 <sup>3</sup> )	Pd-Cu-Si-P, Electrode material	Suction-casting
		La <sub>55</sub> Al <sub>25</sub> Ni <sub>20</sub> [11,12]	515,1.5	33.8	φ3, δ5			
		La <sub>55</sub> Al <sub>25</sub> Cu <sub>20</sub> [11,12]	600,1.9	31.9	φ3			
La-based	La-Al-TM (Ni,Co,Cu)	La <sub>55</sub> Al <sub>25</sub> Ni <sub>10</sub> Cu <sub>10</sub> [11]			δ 9	200		Water-cooled Cu molds casting
		La <sub>55</sub> Al <sub>25</sub> Ni <sub>5</sub> Cu <sub>10</sub> Co <sub>5</sub> [11]			Several centimeter	100		

Ce-based	Ce-Al-Ni-Cu [13]	$Ce_{65}Al_{10}Ni_{10}Cu_{10}Nb_5$ [14]			$\phi$ 5		Softest in elastic moduli in known BMGs	Arc melting pure Cu, Ni, Al, Nb with industrial pure Ce in a Ti-gettered argon atmosphere, the alloy ingots were remelted and suck cast into a Cu mold	
		$Y_{36}Sc_{20}Al_{24}Co_{20}$ [15]			$\phi$ 20			Alloy ingots with the nominal compositions were made by alloying high-purity elements in an arc furnace under a flowing argon atmosphere. The glassy ingot samples were then sealed in quartz tubes under a vacuum and melted in an annealing furnace, then quenched in water or simple injection casting of the alloy melt into thin-walled bass tubes	
		$Y_{36}Sc_{20}Al_{24}Co_{10}Ni_{10}$ [15]			$\phi$ 20				
Y-based		$Y_{56}Al_{24}Co_{20}$ [15]			$\phi$ 1.5				
Ca-based	Ca-Al-Mg-Cu	$Ca-(33-35\%)Al$ [16]			$\phi$ 1			High purity elements with nominal compositions were alloyed using an induction furnace under a flowing argon atmosphere. The ingots were then cast into different size cylinder-shaped cavities inside a water-cooled copper block.	
		$Ca_{56.5}Al_{28.5}Mg_{10}Cu_5$ [16]			$\phi$ 3				
	$Ca_{56.5}Al_{28.5}Mg_{10}Ag_5$ [16]			$\phi$ 3					
	Ca-Mg-Ni	$Ca_{60}Mg_{25}Ni_{15}$ [17]			$\phi$ 13				High-purity elements were alloyed in a boron nitride BN d-coated graphite crucible in a dynamic Ar atmosphere using an induction furnace. The liquid alloy was poured into a copper mold in air atmosphere.
		$Ca_{65}Mg_{15}Zn_{20}$ [17]			$\phi$ 15				
Mg-based	Mg-Cu-Ln	$Mg_{65}Cu_{25}Gd_{10}$ [11]	834,1.5	56	$\phi$ 8			High pressure die casting	
		$Mg_{65}Cu_{25}Y_{10}$ [11,18,19]	800(823), 1.4	69	$\delta$ 7				
		$Mg_{65}Ni_{20}Nd_{15}$ [11]			$\phi$ 3.5				
	Mg-Al-Cu-Ni [11]				$\delta$ 10	200			
Ti-based	Ti-Ni-Cu-Sn [24]	$Ti_{50}Ni_{15}Cu_{25}Sn_5Zr_5$ [20]	2000	100	$\phi$ 6	200		Arc melting pure Ti, Ni, Cu, Sn, Zr metals in an argon atmosphere; bulk	
		$Ti_{50}Ni_{24}Cu_{20}B_1Si_2Sn_3$ [21]	2100	110	$\phi$ 1				





based	(Cu,Ni,Fe,Co)- Al	Nd <sub>70</sub> Fe <sub>20</sub> Al <sub>10</sub> [33,34]		magnetism	Ingots of alloy were prepared by melting 99.9 at% pure Nd, Cu, Ni and Al in an arc-melting furnace under argon atmosphere. As-cast rod samples with 3 and 5mm diameters and 80mm length were produced by suction of the melt into a copper mould.
		Nd <sub>60</sub> Cu <sub>20</sub> Ni <sub>10</sub> Al <sub>10</sub> [35]	φ 5		
		Nd <sub>60</sub> Al <sub>10</sub> Cu <sub>10</sub> Fe <sub>20</sub>			
		Nd <sub>60</sub> Al <sub>15</sub> Ni <sub>10</sub> Cu <sub>10</sub> Fe <sub>5</sub> [36]	φ4	Copper mold casting	
		Nd <sub>61</sub> Al <sub>11</sub> Ni <sub>8</sub> Co <sub>5</sub> Cu <sub>15</sub>			
		Nd <sub>60</sub> Al <sub>10</sub> Fe <sub>20</sub> Co <sub>10</sub> [37]	φ3	hard magnetism	Ingots were prepared by arc melting from elemental Nd, Fe, Al and Co with a purity of 99.9% in a titanium-gettered argon atmosphere. Cylindrical specimens were prepared from the ingots by die casting into a copper mold under argon atmosphere.
		Nd <sub>57</sub> Fe <sub>20</sub> B <sub>8</sub> Co <sub>5</sub> Al <sub>10</sub> [36]	φ3		Ingots were prepared by melting the elemental constituents in an electron beam furnace under a vacuum of <math>10^{-5}</math>Pa. Cylinders were prepared by remelting the master alloy in a quartz tube and ejecting the melt into a copper mold under Ar atmosphere.
Pr-based	Pr-(Cu,Ni,Fe,Co)- Al	Pr <sub>60</sub> Fe <sub>30</sub> Al <sub>10</sub> [38]	φ 3	Hard magnetism	Arc melting with pure Pr, Cu, Ni, and Al in a Ti-gettered argon atmosphere. The ingots were remelted and suck-cast into a Cu mold under argon atmosphere to get a cylindrical rod
		Pr <sub>55</sub> Al <sub>12</sub> Fe <sub>30</sub> Cu <sub>3</sub> [38]			
		Pr <sub>60</sub> Cu <sub>20</sub> Ni <sub>10</sub> Al <sub>10</sub> [38]	φ5	Paramagnetic properties	

		$\text{Pr}_{60}\text{Al}_{10}\text{Ni}_{10}\text{Cu}_{16}\text{Fe}_4$ [39]			$\phi 5$	Diagnetism (distinct glass transition, different from other rare- earth-based BMGs)	Arc melting of pure Pr, Al, Ni, Cu, and Fe and sucked into a Cu mold under argon atmosphere
	Fe-(Al,Ga)- (P,C,B,Si)	$\text{Fe}_{72}\text{Al}_5\text{Ga}_2\text{P}_{11}\text{C}_6\text{B}_4$ [40] $\text{Fe}_{72}\text{Al}_5\text{Ga}_2\text{P}_{10}\text{C}_6\text{B}_4\text{Si}_1$ [41][42]			$\phi 1-3$		
	Fe-(Co,Ni)- (Zr,Nb,Ta,Mo,W ) -B	$\text{Fe}_{61}\text{Co}_7\text{Zr}_8\text{Mo}_5\text{W}_2\text{B}_{15}$ [6]	Hv 1360		$\delta 6$	Soft ferromagnetism Common mode choke coils	Copper-mold casting
Fe- based <sup>[24]</sup>	$(\text{Fe}_{1-x}\text{Co}_x)_{0.75}\text{B}_{0.2}\text{Si}_{0.05}$ $_{96}\text{Nb}_4$ [24]		3900- 4250	190-210	5		
		$\text{Fe}_{61}\text{Co}_7\text{Zr}_{9.5}\text{Mo}_{5-x}\text{Ni}_x\text{W}_2\text{B}_{15.5}$ ( $x =$ 0 to 4 at%) [43]			$\phi 2$		Arc melting the high purity constituents in a titanium gettered argon atmosphere. Cylindrical samples were prepared by die casting the remelted ingots into a copper mould under argon atmosphere.
Ni- based	Ni-Nb	$\text{Ni}_{59.5}\text{Nb}_{40.5}$ [44]			$\delta 2$		arc melting furnace on a water cooled copper crucible under Ar atmosphere.
		$\text{Ni}_{59.5}\text{Nb}_{33.6}\text{Sn}_{6.9}$	3100		$\delta 3$		Arc-melting a mixture of the elements having a purity of 99.7 at.% or better in a Ti gettered, high- purity argon atmosphere. Remelted under high vacuum in a quartz tube using an induction-heating coil and then injected through a nozzle into a copper mold using high-purity argon at a pressure of 2 atm for injecting the molten alloys.
		$\text{Ni}_{59.35}\text{Nb}_{34.45}\text{Sn}_{6.2}$	3800		$\delta 3$		
	Ni-Nb-Sn [63]	$\text{Ni}_{60}\text{Nb}_{36}\text{Sn}_3\text{B}_1$	3300		$\delta 3$		
	Ni-Nb-Cr-Mo-P- B [45]		2700		$\phi 1$		

	Ni-Ti-Zr-(Si,Sn) [45]		φ2	
	Ni-Nb-Ti-Zr-Co- Cu [45]		φ3	
		$Ni_{45}Ti_{20}Zr_{25}Al_{10}$	2	arc melting mixtures of ultrasonically cleansed elemental metals having a purity of 99.5 at.% or higher. The arc melting was performed in a Ti-gettered high purity Argon atmosphere. Each ingot was re-melted in the arc melter for at least three times aimed at obtaining chemical homogeneity. The alloyed ingots were then re-melted under high vacuum in a quartz tube using an induction-heating coil and then injected through a small nozzle into a copper mold using high purity argon at a pressure of 1–2 atm.
		$Ni_{40}Cu_6Ti_{16}Zr_{28}Al_{10}$	3	
		$Ni_{40}Cu_5Ti_{17}Zr_{28}Al_{10}$	4	
		$Ni_{40}Cu_5Ti_{16.5}Zr_{28.5}Al_{10}$	5	
	Ni-Ti-Zr-Al [46]			
		$Ni_{39.8}Cu_{5.97}Ti_{15.92}Zr_{27.86}Al_{9.95}Si_{0.5}$	5	
Pt-based	Pt-Cu,Ni,Co-P [47]		φ4 φ12( in copper mold)	Alloys were prepared by inductively melting the elements in quartz tubes. Subsequently, the alloy was exposed to a fluxing treatment. $B_2O_3$ was added to the alloy and heated to about 1200 K for 20 min. Samples are water quenched in various diameter quartz tubes of a wall thickness of 1 mm.
		$Pt_{60}Cu_{20}P_{20}$		
		$Pt_{57.5}Cu_{14.7}Ni_{5.3}P_{22.5}$	φ16	
		$Pt_{42.5}Cu_{27}Ni_{9.5}P_{21}$	φ20	
		$Pt_{60}Cu_{16}Co_{2}P_{22}$	φ16	
Co-based		$(Co_{0.705}Fe_{0.045}Si_{0.10}B_{0.15})_{96}Nb_4$ [48]		

\* For estimation of tensile strength:  $\sigma = 10Hv/3$

\*\*Critical sizes are gotten by copper mold casting if not specified.

---

**REFERENCES**

- [1] Wei-Hua Wang, Hai Yang Bai, J. Appl. Phys. **84(11)**, 5961 (1998).
- [2] A. Peker, W.L. Johnson, Appl. Phys. Lett. **63**, 2342 (1993).
- [3] Yong Zhang, D.Q. Zhao, B.C. Wei, P. Wen, M.X. Pan, and W.H. Wang, J. Mater. Res. **16(6)**, 1675 (2001).
- [4] A. Inoue, T. Zhang and T. Masumoto, Mater. Trans., JIM **31**, 177 (1990).
- [5] H. Kato, J. Saida and A. Inoue, Scripta Materialia, **51 (11)**, 1063 (2004).
- [6] A. Inoue, Acta mater. **48**, 279 (2000).
- [7] T. Zhang and A. Inoue, Materials Science and Engineering A, **375-377(1-2)**, SPEC. ISS., 432 (2004).
- [8] Y. He, T. Shen, Metal. & Mater. Trans. A **29A**, 1795 (1998).
- [9] Akihisa Inoue, Nobuyuki Nishiyama, Materials Science and Engineering **A226-228**, 401 (1997).
- [10] H.S. Chen: Acta Metall. **22**, 1505 (1974).
- [11] A. Inoue, T. Zhang, T. Masumoto, Mater. Tran. JIM **30**, 965 (1989).
- [12] A. Inoue, M. Tran., JIM, **30(2)**, 104 (1990).
- [13] B. Zhang, R. J. Wang, Physical Review B **70**, 224208 (2004).
- [14] B. Zhang, M. X. Pan, Appl. Phys. Lett. **85**, 61 (2004).
- [15] Faqiang Guo and S. Joseph Poon, Appl. Phys. Lett. **83**, 2575 (2003).
- [16] F. Q. Guo and S. J. Poon, Appl. Phys. Lett. **84**, 37 (2004).
- [17] E. S. Park and D. H. Kim, Appl. Phys. Lett. **86**, 201912 (2005).
- [18] A. Inoue, Mater. Trans. JIM **36**, 866 (1995).
- [19] A. Inoue, A. Kato, T. Zhang, S. G. Kim, and T. Masumoto, Mater. Trans. JIM **32**, 609 (1991).

- 
- [20] T. Zhang and A. Inoue, *Trans., JIM* **39**, 1001 (1998)
- [21] T. Zhang and A. Inoue, *Materials Science and Engineering A*, **304-306(1-2)**, 771 (2001).
- [22] Y.C. Kim, W.T. Kim and D.H. Kim, *Materials Science and Engineering A*, **375- 377(1-2)**, SPEC. ISS., 127 (2004).
- [23] Jan Schroers, *Appl. Phys. Lett.* **87**, 061912, (2005).
- [24] D. Wang and Y. Li, *Appl. Phys. Lett.* **84**, 4029 (2004).
- [25] Xu, Donghua Ph. D. dissertation, (2005-05-17) Development of novel binary and multi-component bulk metallic glasses.  
<http://resolver.caltech.edu/CaltechETD:etd-05272005-160315>.
- [26] Q. P Cao, J. F. Li and Y. H. Zhou, *Appl. Phys. Lett.* **86**, 081913 (2005).
- [27] Q. P. Cao, Y.H. Zhou, A. Horsewell and J. Z. Jiang, *J. Phys.: Condens. Matter* **15**, 8703 (2003).
- [28] A. Inoue, W. Zhang, T. Zhang, and K. Kurosaka, *Mater. Trans., JIM* **42**, 1149 (2001).
- [29] Do-Soo Sung<sup>1</sup>, O-Jib Kwon<sup>1</sup>, Eric Fleury, Ki-Bae Kim, Jae-Chul Lee, Do-Hyang Kim, and Yu-Chan Kim, *Metals and Materials International*, **10(6)**, 575 (2004).
- [30] X. H. Lin and W. L. Johnson *J. Appl. Phys.* **78(11)**, 6514 (1995).
- [31] M. Calin, J. Eckert and L. Schultz, *Scripta Materialia*, **48(6)**, 653 (2003).
- [32] G. Duan, D.H. Xu, and W. L. Johnson, *Metall. Mater. Trans. A*, **36A**, 455 (2005).
- [33] A. Inoue, T. Zhang, A. Takeuchi, and W. Zhang, *Mater. Trans., JIM* **37**, 636 (1996).
- [34] A. Inoue, T. Zhang, W. Zhang, and A. Takeuchi, *Mater. Trans., JIM* **37**, 99 (1996).
- [35] M B Tang<sup>1</sup>, D Q Zhao, M X Pan<sup>1</sup>, B C Wei and W H Wang, *J. Phys. D: Appl. Phys.* **37**, 973 (2004).
- [36] L. Q. Xing, J. Eckert, W. Looser, S. Roth, and L. Schultz, *J. Appl. Phys* **88(6)**, 3565 (2000).
- [37] Bing Chen, Wei Hua Wang, Lei Xia, Zhi Zhang, De Qian Zhao, Ming Xiang Pan, *Materials Science and Engineering A* **334**, 307 (2002).

- [38] Z. F. Zhao, *Appl. Phys. Lett.* **82**, 4699 (2003).
- [39] Y. T. Wang, M. X. Pan, D. Q. Zhao, and W. H. Wang, *Appl. Phys. Lett.* **85**, 2881 (2004).
- [40] Inoue, A., Shinohara, Y. and Gook, J. S., *Mater. Trans. JIM* **36**, 1427 (1995).
- [41] Inoue, A., Murakami, A., Zhang, T. and Takeuchi, A., *Mater. Trans. JIM* **38**, 189 (1997).
- [42] Inoue, A., *Mater. Sci. Eng.* **A226-228**, 357 (1997).
- [43] W.H. Wang, M X Pan, D Q Zhao, Y. Hu and H Y. Bai, *J. Phys.: Condens. Matter* **16**, 3719 (2004).
- [44] M. Leonhardt, W. Loeser and H.-G. Lindenkreuz, *Acta. Mater.* **47(10)**, 2961 (1999).
- [45] Donghua Xu, Gang Duan, William L. Johnson, Carol Garland, *Acta. Mater.* **52**, 3493 (2004).
- [46] Haein Choi-Yim, Donghua Xu, and William L. Johnson, *Appl. Phys. Lett.* **82**, 1030 (2003).
- [47] Jan Schroers, William L. Johnson, *Appl. Phys. Lett.* **84**, 3666 (2004).
- [48] A. Inoue, A. Murakami, A. Takeuchi, *Mater. Trans. JIM* **38**, 189 (1997).